



PH.D. PROGRAM

MEDITERRANEA UNIVERSITY OF REGGIO CALABRIA

DEPARTMENT OF CIVIL, ENERGY, ENVIRONMENT AND MATERIALS ENGINEERING (DICEAM)

PH.D. IN CIVIL, ENVIRONMENT AND SAFETY ENGINEERING

XXX CYCLE

UAV GEOMETRICAL SURVEY FOR BRIDGE STRUCTURAL ANALYSIS

PH.D. STUDENT:

Gabriele Candela

TUTOR:

Prof. Vincenzo Barrile

CO-TUTOR:

Prof. Alberto De Capua

Dott. Ing. Cristoforo Demartino

COORDINATOR:

Prof. Felice Arena

REGGIO CALABRIA, JULY 2019

GABRIELE CANDELA

**UAV GEOMETRICAL SURVEY
FOR BRIDGE
STRUCTURAL ANALYSIS**

Acknowledgement

Un ringraziamento di cuore:

Al tutor accademico Prof. Vincenzo Barrile per la sincera e sempre presente disponibilità

Ai co-tutor, Prof Alberto De Capua per il supporto costante

Dott. Ing. Cristoforo Demartino per avermi amichevolmente e professionalmente guidato

al Prof. Giorgio Monti per la fiducia e disponibilità

Ai colleghi dell'Università di Nanchino

Alla mia famiglia, in particolare a mia madre, supporto costante, ed alle persone che mi sono state vicine in questo percorso.

Cover picture:

Viadotto Musmeci, Potenza

Index

1. Introduction	7
1.1 Problem statement	7
1.2 State of the art.....	7
1.3 Methodology	8
1.4 Thesis outline.....	8
2. State of the art of UAV and application in AEC	11
2.1 Brief History of Unmanned Aerial Vehicles.....	13
2.2 UAS definition and description.....	17
2.3 UAS classification.....	26
2.4 UAV Regulation	28
2.5 Application in AEC (Architecture Engineering and Construction)	36
References.....	47
3. Three-dimensional reconstruction and segmentation using photogrammetry.....	51
3.1 Photogrammetry: Description, principles and 3d reconstruction	51
3.2 UAV in Aerial photogrammetry	57
3.3 Photogrammetric Algorithms for 3d reconstruction: SFM-MVS	57
3.4 Point cloud classification	66
References.....	74
4. Bridge system and traditional survey	77
4.1 Bridges systems: description and components.....	77
4.2 Bridge classification.....	79
4.3 Bridge's maintenance.....	88
4.4 Survey techniques for monitoring and inspection.....	90
References.....	98

5.	UAV geometrical survey of bridges	101
5.1	Methodology for aerial survey of bridges using UAV and photogrammetry.....	101
5.2	Application to Annunziata viaduct, Reggio Calabria.....	118
5.3	Application to Musmeci bridge – Potenza	135
	References.....	142
6.	Structural Application: rapid Seismic Risk assessment and form efficiency assessment.....	145
6.1	Rapid seismic risk assessment	145
6.2	Seismic risk assessment of Annunziata Bridges	156
6.3	Form efficiency evaluation of Musmeci Bridge	160
	References.....	167
7.	Conclusion and perspectives	169

1. Introduction

Today the infrastructure maintenance represents an essential and very huge problem that the developed country should face. Both in Us and Europe, during '60 -'70 years, the critical infrastructure and primary way of communication (road and railway) were built. Infrastructure project life is almost 50 years without any extraordinary maintenance operation. It is clear that today all this infrastructure, such as roads and bridges, needs a complete plan for maintenance to preserve the structural performance and prevent collapse and disaster also affecting the communication way.

1.1 Problem statement

In the infrastructure system, bridges are the most sophisticated and critical structure to analyse and the most complex to survey. The problem linked with the investigation of the existing structure is actual and needs a rapid survey to acquire information, mainly if performed on the infrastructure network. Actual survey methodologies to verify the condition of the bridges are performed through visual inspection by technician that is very expensive and time-consuming.

Rapid seismic risk assessment is fundamental to verify the condition of existing bridges and viaduct on a network system and ensure an adequate level of safety and service. Time and costs in the extensive analysis are fundamental to quickly gather information and find the most critical part of the system. For this reason, the rapid seismic assessment is oriented to the large scale and network verification, to quickly identify the vulnerable elements in the network and optimise the resources used for the analysis. Blueprints and technical information are often missing; for this reason it is necessary to acquire geometrical information to ensure an adequate level of knowledge and perform seismic analysis. In the present thesis the safety verification of the simply supported bridge typology, as the common and diffused typology in Italian road network, are presented. Also, for bridges with complex structure such as an arch or shell, the structural efficiency is verified through structural analysis.

1.2 State of the art

State of the art in terms of survey methodology and instruments is presented, as well as the description and classification of bridges and viaducts typology. The rapid growth of the new technology such as UAV (Unmanned Aerial Vehicle) and the contextual application in the field of civil engineering are simplifying the way to perform survey and reduce cost and time, allowing analysis at the macro scale. The main focus is the use of this technology as game-changer for monitoring and surveying.

State of the art in computer vision algorithms and photogrammetry techniques used for the 3d reconstruction of object starting from photographic dataset is also discussed. Also, the use of traditional survey techniques and instruments such as laser scanner, are described and compared in terms of efficiency, precision and survey times. The combined use of new instruments such as aerial survey (performed with UAV) and photogrammetric techniques are presented, highlighting the advantages compared with traditional techniques.

1.3 Methodology

The methodology used to acquire data and perform a seismic risk assessment using geometrical data derived from UAV survey is presented. A complete workflow for the aerial survey is detailed: from the acquisition phase, planning UAV flight according to photogrammetric principles to optimise the camera location, to the 3d reconstruction using computer vision algorithms and point cloud segmentation to isolate the structural bridges component. Geometrical features are then used to perform structural analysis of simply supported bridges and form efficiency assessment of arch bridges. Two different case study are then analysed to validate the methodology on two different bridges located in Italy.

1.4 Thesis outline

In this study, a methodology for a rapid seismic risk assessment using UAV (Unmanned Aerial Vehicle) aerial survey is presented. The state of art of the UAV is discussed with a focus on the application of this technology in the field of civil engineering and bridges survey.

In the third chapter, the 3d reconstruction process using photogrammetry is applied to elaborate and construct the 3d model of an acquired object.

In chapter four bridges system and bridges classification are presented with a focus on the survey methodology for the extraction of geometrical feature.

Chapter five present the methodology to perform the aerial survey using aerial survey and photogrammetry of bridges and viaduct, to automatically extract the geometrical features. The obtained data are presented on an online platform that allows the easy consultation and use of the extracted data. The methodology is applied for the survey of two different bridges as case study: a simply supported bridge and an arch bridge.

The obtained data are used in chapter six to perform a rapid seismic risk assessment of the simply supported bridge and the form efficiency verification on the arch bridge. The results are used to validate the presented methodology. Finally in the conclusions, future perspective such as network analysis and autonomous flight are discussed.

2. State of the art of UAV and application in AEC

Unmanned Aerial Vehicle (UAV), also known as “drone”, is defined as crewless aircraft (with an integrated electronic system), able to fly remotely piloted, or autonomously based on a pre-programmed flight-plans or more complex dynamic automation systems. Those systems are mainly appreciated since they can accomplish pre-defined operation with a large group of civilian and military applications without putting human life at stake. Furthermore, the absence of aircrew makes these vehicles designed to be smaller and more efficient, with advantages in terms of portability.

The name of unmanned aircraft has changed over the years, as viewed by aerial manufacturers, civil aviation and military authorities: aerial torpedoes, pilotless vehicle, radio-controlled aircraft, remotely controlled aircraft, remotely piloted vehicle; the model aircraft or “drones”, as commonly called, can be considered as a sub-category of the unmanned aircraft.

Today the commonly diffused names, are *RPAS* (Remotely Piloted Aircraft System), used worldwide from the aviation agencies, *UAS* (Unmanned Aerial System) and *UAV* (Unmanned Aerial Vehicle).

UAS (Unmanned Aerial System) is used to describe the entire operating equipment including the aircraft or UAV itself and payloads, the control station from where the aircraft is operated and the wireless data link.

UAV (Unmanned Aerial Vehicle) (the most frequent term) is the name of the aircraft that includes all classes of aeroplanes, helicopters and powered-lift aircraft, that flies to accomplish specific tasks, has a higher degree of “automatic intelligence” and is able to communicate with its controller and return mission and payload data. Even if a fault occurs, the UAV may be designed to take corrective actions automatically.







The availability of UAV often depended on the maturation of the requisite technology, and today this aviation sector’s is proliferating for two main reasons that enable the automation integration: the advancements of manned aircraft systems’ development coupled with advancements in electronic systems. Due to their essential application potential, smart autonomous aircraft have become the new focus on academic research and education. Autonomy is the possibility of a system to sense, communicate, plan, make decisions and act without human intervention. The possibility of performing autonomous and repetitive tasks constitute the added value in the UAV application and makes these systems not only a “flying payloads” but autonomous objects. Intelligence is necessary for:

- mission planning, using navigation guidance and tracking control, with optimised battery consumption

- path planning and dynamic waypoint generation accounting for changing the weather and air traffic en route
- control reconfiguration through the use of a flight control system
- taking the corrective action, in the presence of an external condition, to avoid an obstacle or evade a threat, or in the presence of an abnormal internal condition
- Interpreting data from a variety of sources to execute specific functions

Rapid advancements in the sciences of aerodynamics, materials, propulsion, flight control systems, stabilisation and navigation systems and the integration of all in-flight automation system made the fully autonomous UAV feasible in the next five to ten years and this industry highly dynamic and continuously evolving. Moreover, the implementation of the onboard computer and consequentially decision making capability using artificial intelligence will provide a complete autonomy of operation (Reg Austin, 2010).

The applications of this system are at the beginning and range from different sectors such as engineering architecture and construction, remote sensing, survey and monitoring, filming and logistics. The aviation agencies expect that by 2020 thousands of UAV will swarm in the skies with 42 % of commercial UAV that will be used in industrial inspection, 19 % in agriculture, 15% in insurance sector, a further 22% in real estate or aerial photography and 2 % in government (Federal Aviation Administration Aerospace forecast, 2016). In Europe the EASA (European Aerospace Safety Agency) in the “*Europe industry Outlook 2016*” forecast the economic impact of UAV in the different economic sector, estimating the impact by 2035 and 2050; the introduction of this technology in agriculture and delivery will have the significant economic impact as shown in Figure 1.

in EUR	2035 impact				2050 impact			
	Products	Services	Others	Total	Products	Services	Others	Total
 Agriculture	800 M€	3 200 M	500 M€	4 500 M	600 M	3 200 M	400 M	4 200 M
 Energy	<100 M	1 600 M	<100 M	1 600 M	<100 M	1 600 M	<100 M	1 600 M
 P.S.S. ¹	300 M	800 M	300 M	1 400 M	300 M	700 M	200 M	1 200 M
 Delivery	600 M	800 M	600 M	2 000 M	700 M	1 400 M	800 M	2 900 M
 Mobility	<100 M	<100 M	<100 M	<100 M	400 M	2 600 M	600 M	3 600 M
 Others	200 M	700 M	100 M	1 000 M	200 M	800 M	100 M	1 100 M

1: Public safety and security
Note: Figures rounded to EUR 50M and 1K jobs, differences in totals due to rounding. Nominal 2016 EUR

Figure 1 - Industry view of forecasted economic impact

According to *Drone Industry Insight Report 2019*, on a global basis, the industry sector that will have the major effect of enterprise application will be the Health care and Social Assistance and Art, entertainment and Recreation (Figure 2).

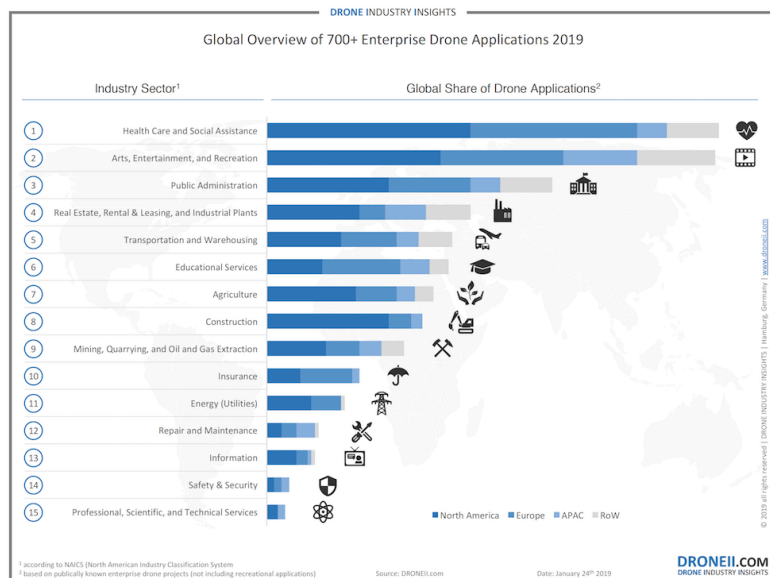


Figure 2 - Droneii Enterprise Drone Application 2019 Source: Drone Industry Insight

The only limitation for the applications of this technology at the industrial level is represented by legal/normative systems actually in the phase of definition in several countries.

2.1 Brief History of Unmanned Aerial Vehicles

The origin and evolution of Unmanned Aerial Vehicle (UAV) are closely linked with military reasons and with the technological evolution of radio communication systems, electronics and logistics of guidance and control.

The first military UAVs were deployed to enable the use of torpedoes and long-range armaments. The main idea behind the use of UAV in aviation history is entirely synthesised by the operational pattern of the “three D”, as described today: *Dangerous*, *Dirty* and *Dull*. Where *Dangerous* means that the life of the pilot may be under undue risk operationally, *Dirty* is where the environment may be contaminated by chemical, biological or radiobiological hazards precluding human exposure and *Dull* is where the task required long hours on board, making manned flight stressful and fatiguing. In the early years of aviation, the idea of flying an aircraft without a person on board had the obvious advantage of removing the risk to life and limb of these highly experimental contraptions. However, the lack of a satisfactory method to affect vehicle control limited the use of the early unmanned aircraft.

The first unmanned aircraft the “Aerial Torpedo” (Figure 3) was made by the Navy in 1916, but the two basic systems that enable the remote control were created almost twenty years before, during the late 1890s. The radio communication, invented by Nicola Tesla made possible to transmit the signal to the remote aircraft, and the gyroscope, invented by Elmer Sperry, was used for the inertial measurements onboard, allowing vehicle stabilisation. Both inventors worked initially on those systems for underwater torpedoes and guidance related systems; in particular, Nicola Tesla promoted the idea of a remotely piloted aircraft in the late 1890s to act as a flying guided bomb and in 1898 build the world’s first guided underwater torpedoes, controlled by “tele-automation”. In the same period, Elmer Sperry was developing the first practical gyroscopic guidance system, focusing on underwater torpedoes for the US Navy. This three-axis mechanical gyroscope system took inputs from the gyros and converted them to simple magnetic signals, which in turn were used to affect actuators. The slow speeds of water travel, and the weight not being as critical as in the air allowing the creation of the world first mechanical autopilot.

While those systems make possible the stabilisation and the remote control of the aircraft, as known Wright brothers developed the aeroplane control system in 1903, performing the first controlled flight. The tragedy of World War I stimulated the rapid development of the aviation sector which combined with the invention of the radio, aeroplane, and mechanical autopilot joined in the world’s first practical unmanned aircraft. The “Aerial Torpedo” was able to fly unmanned guided to a target and detonate its warhead. The aircraft characteristics can be listed as a (i) gyrostabilizer to keep the aircraft level (ii) an automatic steering gyro to keep the aircraft on a pre-set heading (iii) a barometer to indicate cruise altitude, causing the aircraft to level off, and (iv) an engine revolution counter to determine when the aircraft should cut power and dive into its target. Also, a wind-driven electrical generator was used to provide power for the gyro motors and the servomotors that moved the aerial torpedo’s flight control surface. Like the Navy, the US Army invested in an aerial bomb concept like the aerial torpedo, engaging Charles Kettering to design a lightweight biplane able to carry an explosive payload. The “Kettering Bug” (Figure 5) weighs 270 kg, was powered by 40 horsepower Ford engines and was able to carry 82 kg of payload. This system incorporated



Figure 3 - Aerial Torpedo, first unmanned aircraft of the history, WWI
Source: Cradle of aviation museum, World War I gallery

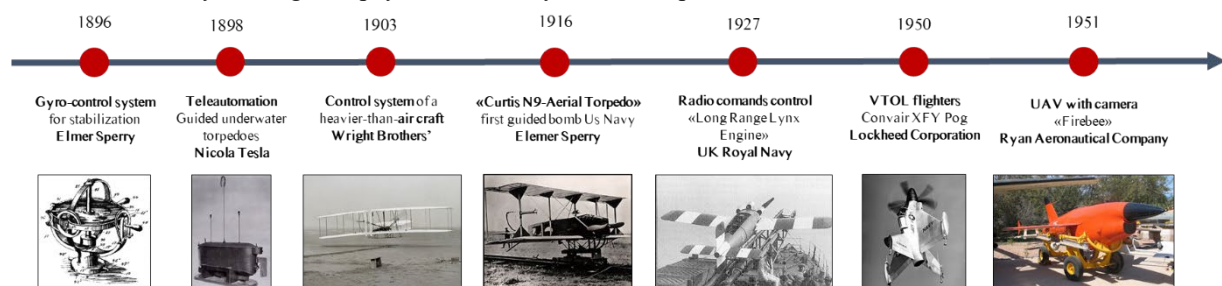


Figure 4 - Milestone in UAV evolution from the beginning to 1950



Figure 5 – “Kettering Bug”
Source: Encyclopaedia of Astrobiology,
Astronomy, and Space Flight

aerodynamic static stability features (not emphasised on manned aircraft) that increase aeroplane’s stability and paper skin incorporated into the frame to reduce cost and to highlight the dispensable nature of the aircraft.

Kettering Bug represents the first mass-produced unmanned aircraft because demonstrates, unlike the Navy Aerial Torpedo, impressive aerial performances, having flown some tests at 150 km distance and 3 km (10.000ft) altitude. During the same period, the British Army introduced in 1914 the “Aerial Target”, a radio-controlled pilotless monoplane built to prove the effectiveness of using a radio signal to guide the flying bomb to its target. The level of development achieved while constructing these three vehicles signalled the beginning of a new technological era for aviation.

After the WWI (1919-1939) research work focused primarily on employing unmanned aircraft as target drones, and during the WWII, the unmanned systems were applied as target drone or in weapon delivery cases. The unsuccessful use of this technology for reconnaissance had more to deal with imaging technologies and navigation requirements than the aircraft platform themselves. Cameras in the 1940s required relatively accurate navigation to gain the desired areas of interest, and navigation technology of the day could not compete as well as a trained pilot with a map. This changed in the post-war years with the advent of radar mapping, better radio navigation and inertial navigation, enabling the aircraft to fly autonomously to and from the target area with sufficient accuracy.

In 1927 the UK Royal Aircraft Establishment (RAE) presented the “Long-Range Gun with Lynx Engine” a monoplane capable of carrying a warhead of 114 kg over a range of 480 km and the first aircraft to introduce a measure of radio control. This program automates an existing manned aircraft. Unlike the previous machine, it was fitted with a radio control for the launch mode, after which the autopilot restrained it to fly on a pre-set course at a pre-set height to a pre-set range. Then Great Britain decided to move from “Cruise Missile” to aircraft with full-mission radio control and produced in 1934 “Queen Bee”, the first non-disposable target aircraft controlled remotely by a human pilot via radio commands. During the WWII Nazi Germany launched the first aircraft that use jet propulsion, the “V1-Buzz Bomb”.

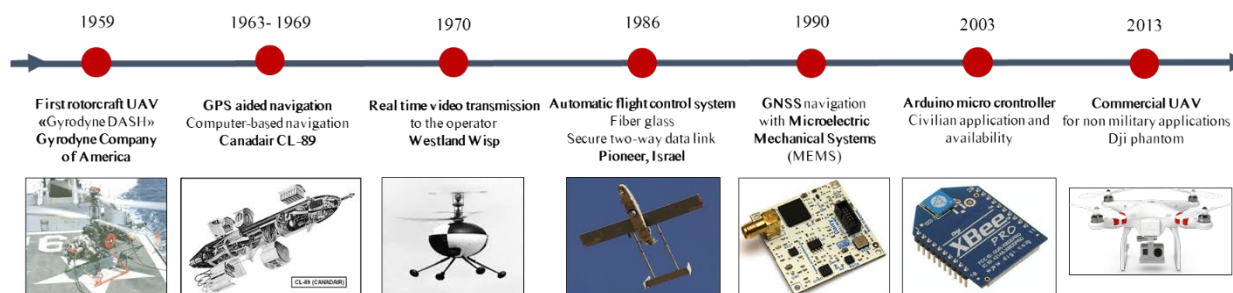


Figure 6 - Milestone in UAV evolution from 1959 to recent days

In the same period, the US Navy “Project Fox” achieved the installation of an RCA television camera on the aircraft nose. This vehicle was considered as an early experience on teleoperation control.

In 1951 the UAV began to be definitively used for reconnaissance purposes over enemy territory, the “Firebee” carried a still camera, whose photographs were developed at the base after the return of UAV; moreover, the aircraft was recovered by a parachute on returning to a suitable area for landing. This system eliminates any risks and diplomatic incidents upon the capture of the human pilot.

1959 is another important milestone in the evolution of UAV: the Drone Anti-Submarine Helicopter, “Gyrodyne DASH” was the first system that introduces the use of a rotorcraft UAV, with a specific and dedicated design conceived to carry torpedoes to attack enemy submarine.

During the cold war, the long endurance characteristics became primary research due to the importance of the surveillance mission. Moreover, lightweight computer technologies and Global Positioning System satellite network enabled the autonomous flight operation gained flight autonomy on par with the human-piloted vehicle. VTOL (Vertical Take-Off and Landing) vehicles appear in shorter range operation, and the “Westland Wisp” system was the first VTOL rotorcraft with real-time video. This machine gave insight into the advantages of a hover capability during surveillance missions.

During the 1980s with the introduction of “Canadair CL-89” the UAV surveillance and navigation system became even more advanced, providing real-time visual intelligence of enemy territory with an operating radius of 70 km and the vehicle guidance achieved by a pre-set program. In 1986 “Pioneer” aircraft, made in the joint by Israeli-US and remotely piloted via remote-control joystick on the ground, became the most frequently employed system. The fully autonomous flight was at this point technically possible (Pioneer had a range about 150 km with an altitude of 2000ft), but GPS and computer power were not yet sufficiently integrated to enable ground operators to designate waypoints on short notice. Also, imagine satellite links were not sufficiently developed at a small size to affect the transmission of data. For this reason, in the 1990s the increasing availability of low-cost computers and more precise and miniaturised GPS systems enable more precise control, freed the UAV from their dependencies on inaccurate onboard navigation systems.

The 2000s saw a much-increased use of UAV in military roles, with aircraft able to carry armament while performing military reconnaissance missions. Although potentially more extensive than military, civilian operations have not come to fruition due to the perceived difficulty in ensuring separation between manned and unmanned systems. In the next ten years from the 2000s to terrorists attack of 9/11, unmanned aircraft made slow progress, not for the



Figure 7 - DJI Phantom commercial UAV

technological barriers, but in relation with manned aircraft technologies (considered more reliable in terms of safety) and the pilots who saw UAV technology as replacing their livelihoods. After the terrorist's attack of 9/11, the argument against unmanned aircraft had finally given way to the low costs, reduced risk and the practice of a drone in performing the annoying, long and dangerous missions.

The turning point in 2003 was the introduction of the low-cost microcontroller like Arduino, that enables the commercial availability and rise of UAV systems for civilian purpose and application in the different field. From a large point of view, it can be argued that the rapid advancements in the hobbyist radio-controlled aircraft and the development of miniature automated stability and navigation systems are creating the commercial revolution of a technology that is rivalled only by computer and the mobile phone. This revolution happened so quickly that the regulatory bodies have had difficulty controlling its proliferation in many commercial industries. The timeline with a relevant milestone in the described evolution of UAV is represented in Figure 4 and Figure 6.

Today the market is dominated by the Chinese company *Dà-Jiāng* (*Grand general*) *Innovations*, better known as *DJI*, founded in Shenzhen in 2006 that manufactures a wide range of products including unmanned aerial vehicles, flying platforms, flight controllers for multi-rotors, helicopters accessories, aerial and handheld gimbals and ground stations. The Phantom model (Figure 7), released in January 2013, is the most popular product and commonly associated with the drone itself.

The next steps in the evolution of UAV and their application will be the process automation (Sebbane, 2016; Gonzalez et al., 2016) and application of artificial intelligence algorithms for flight autonomy (H. Chen, Wang, & Li, 2009; Ma'sum et al., 2013; Lu et al., 2018).

The interested reader can find detailed information on history and evolution of UAS on Garcia Carrillo and Dzul Lopez (2012).

2.2 UAS definition and description

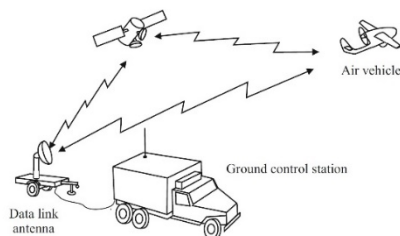


Figure 8 - Basic UAS element

The aircraft in the UAS (Unmanned Aerial System) is only a part, albeit an important part, of a more complex and complete system. In fact, the UAS consists of three essential elements (Figure 8):

- Unmanned aircraft*, carrying the payload according to the needs of the operational tasks;
- Control Station (CS)* which houses the system operators, the interfaces between the operators and the rest of the systems;
- Datalink* or system communication, usually achieved by radio transmission, which allows the communication between aircraft (and payload) and control station.

This system, that must be considered as a part of the air transportation environment with rules and regulation, comprises several sub-systems which include transport, communication, aircraft launch and recovery and aircrew. The aircraft is designed to be operated without an aircrew onboard that is replaced by an electronic intelligence and control subsystem. For this reason, the aircraft's performances, in terms of aerodynamics, is often enhanced by not having to carry the weight of equipment and structure required to accommodate the aircrew. The vehicle performances also benefit the advantageous scale effect associated with smaller aircraft. Relevant sub-systems include launch and recovery equipment (that can vary according to the UAV model), payload and the human element. Detailed information on the UAS system can be found in (Fahlstrom & Gleason, 2012; Douglas M. Marshall Richard Kurt Barnhart, 2016).

Unmanned aircraft

The aircraft is the part of the system used to transport the payload (recognised as an independent subsystem) and it is composed of the following main parts (Figure 9):

- a. **Propulsion Unit:** the props of a quadcopter rotating in the opposite direction.
- b. **Airframe:** the proper name of the UAV chassis.
- c. **Motors:** DC or AC motors that give energy to the props.
- d. **Electronic Speed Controllers:** ESCs convert DC to AC for brushless motor and also regulate the motor power supply.
- e. **Payload:** is also onboard the air vehicle, but it is recognized as an independent subsystem that often is easily interchanged with different air vehicles and uniquely designed to accomplish one or more of a variety of mission.
- f. **Landing struts:** leg is the drone rests on when it is on the ground
- g. **Electric power system:** often a LiPo battery that ensures energy with high voltage to propellers and onboard electronics.
- h. **Receiver:** that transmits the information to the flight controller.
- i. **Flight controller:** assists manual flight with autonomous function ensuring UAV stability.

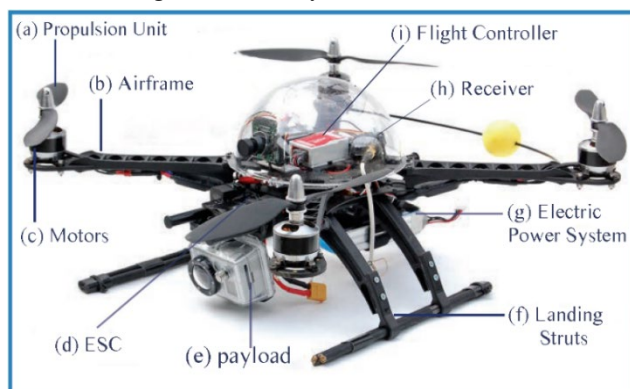


Figure 9 - UAV Main components, Quad rotor model

Control Station

The Control Station provides the facilities for human control of Unmanned vehicles in the airspace. CS can vary physically from a small size handled Remote Controller (RC) (Figure 10) to a large and self-contained facility with multiple workstations (Figure 11).



Figure 10 - UAV Remote Controller



Figure 11 - Military multiple control station

Larger military UASs require a Ground Control Station with multiple personnel to operate separate aircraft systems: at least a pilot station, with the pilot-in-command who operates the aircraft and its system and a sensor station for the operation of the sensor payload and radio communications. For smaller and less sophisticated UAV these workstations can be combined requiring only one operator.

One of the foremost goals in the future UAS operation will be the capability for one crew to operate multiple aircraft from one GCS.

Based on the distance between the UAV and the remote pilot (operating from the control station) flight operation can be categorised as (Figure 12):

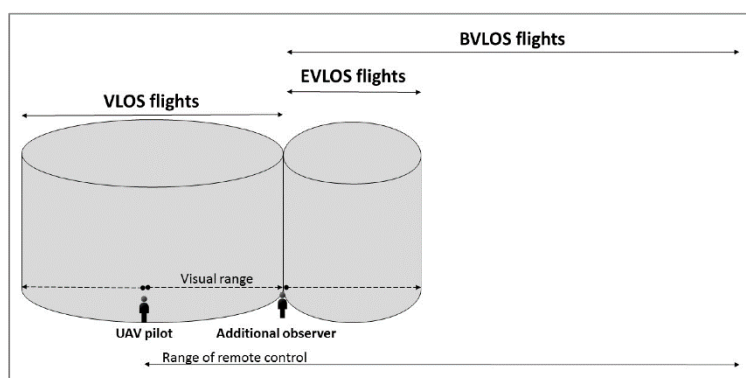


Figure 12 – Flight operation distance

- **Visual line-of-sight (VLOS)** operation: the operator is always able to see the UAV without visual aids and remains in visual contact during the entire flight.
- **Extended Visual line-of-sight (EVLOS)** operation: the operator commanding the UAV may rely on the other remote observers who

are in visual line-of-sight of the UAV. The remote observers must be able to rely on critical flight information to the operator in real-time.

- **Beyond Visual line-of-sight (BVLOS)** operation: the UAV is operated remotely based on instrumentation between the UAV and a remote ground control station. An on-board camera-based system is usually employed but not sufficient to allow BVLOS operations. Additional levels of autonomy like detect-and-avoid are installed on these systems for safety.
- **First-person view (FPV)** operation: the operator utilises onboard video cameras to provide a real-time view from the UAV and operates it based on this video stream (Figure 13).



Figure 13 - FPV operation
Source: Epson Moverio

Datalink

The datalink (Figure 14) is a crucial subsystem for any UAV because provides two-way communication, either upon demand or continuously. An uplink with a data of a few kHz provides control of the air vehicle flight path and commands to its payload. From the other side, the downlink provides both a low data-rate channel to acknowledge commands and transmit status information about the air vehicle and a high data-rate channel (1-10 MHz) for sensors data such as video and radar. There are also separate data links for some payload systems. The antennas for transmitting the data and receive commands from the ground are in the air data terminal that is part of the data link: thanks to this communication system the ground terminal transmit guidance and payload commands and receive flight and mission status information (such as telemetry, battery status) and payload sensor data (target range, real-time video streaming etc). Datalink also requires anti-jam and anti-decryption capability to ensure the complete control of the systems and avoid the external attack.



Figure 14 - External data link and air data terminal

2.2.1 Payloads and sensors

The payload is an essential component of the UAV because it enables different tasks and operation. Selection of the proper payload for the application is the first significant platform decision that must occur, and this decision should be based on the tasks to accomplish or desired information to be collected; in fact, the size and weight of payload are two of the most significant considerations when designing a UAS. Each type has different advantages and disadvantages that must be carefully weighed before the conduction of the mission, although some application will use a combination of different payload type. The payload can be related to different purpose such as surveillance, delivery, weapons, communication, aerial sensing, cargo or platform for communication to extend coverage and range of line-of-sight.

Generally, UAVs are designed around the intended payload they will employ.

In this section, payload **sensors** used for aerial mapping are presented. Sensors type can be divided into active and passive according to the source of light illumination:

1) Active sensors have their source of light of illumination, actively sends a wave and measure that backscatter reflected it;

- **Time of Flight (ToF) Camera**

Time-of-flight camera is a 3d camera with a depth sensor emit a very short infrared light pulse and each pixel of the camera sensor measure the return time. It is highly accurate 3d imaging technology able to measure distances within a complete scene in a single shot and can be used for mapping, object scanning, measure distance, indoor navigation, obstacle avoidance, gesture recognition, tracking object 3d photography and much more. Despite this type of sensor is efficient, simple, fast and delivers accurate depth information at high frame rates in a low-cost solid-state camera, it is not yet commonly diffused on UAV. The additional third dimension and the image processing can open up new way techniques in industrial inspection, automation and logistics, as well as human-computer interaction.



Figure 15 - Time of Flight Intel camera on UAV

- **Laser sensors (Lidar)**

Light detection and ranging (Lidar) use a laser beam and a receiver to measure the time delays in the reflection of the signal from the object back to the detector (Zhou, Yang, Li, & Yang, 2012). The use of Lidar on UAV requires the installation of several additional accessories to balance the aerodynamic movement and compensate the induced displacement such as Inertial Measurement Unit (IMU), GPS antenna and computer. For this reason the use of these sensors as payload on the UAV is still challenging in terms of size and weight (Colomina & Molina, 2014), but the increasing popularity of low-cost UAVs encouraged the development of miniaturized Lidar, thanks to the level accuracy compared with flying altitude in surveys (W. Zhang et al., 2016).

2) **Passive:** measure the reflected sunlight, electromagnetic spectrum (Figure 16), emitted from the sun.

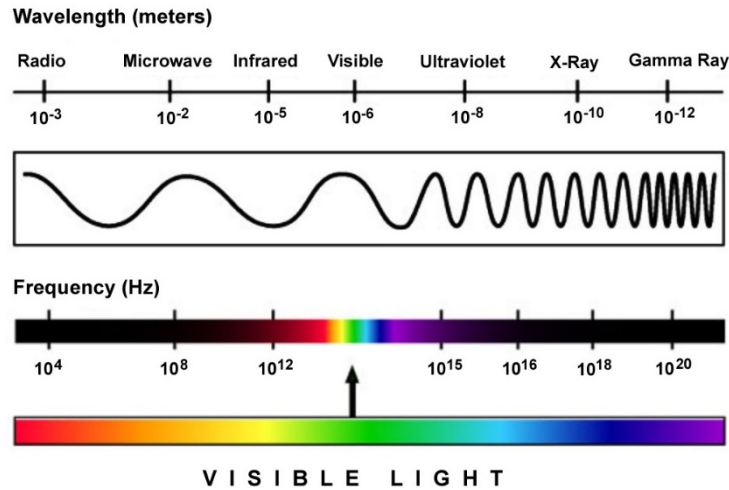


Figure 16 - Electromagnetic spectrum

- **Visible Light Spectrum (VLS) Electro-Optical Camera**

These cameras operate in the visible light spectrum (Figure 17) and are named electro-optical because they use electronic to pivot, zoom, focus and capture images. The imagery they yield can be in the form of full-motion video, still pictures, or even blended still and video images. The quality of the image and video is strictly related to the size of the sensor. Increasing the sensor size corresponds to an increase in weight and consequentially more energy to carry out the payload. The right choice of a sensor depends on the mission need and it is fundamental for the operation's final result. This sensor's type is generally used for video/image capturing or photogrammetric reconstruction.



Figure 17 - Photographic UAV sensor
Source: DJI

- **Thermal Infrared**

Thermal infrared sensors operate in the infrared range (IR) of the electromagnetic spectrum (700nm – 1mm) called IR or FLIR (Forward-looking InfraRed). Two types of camera are used on UAV as payload: cooled and non-cooled. Cooled cameras, (modern are cooled by cryo-cooler to a cryogenic temperature below 150°C) are often more expensive and heavier than non-cooled cameras but produce a higher quality image in the mid-wave infrared (MWIR) and longwave infrared (LWIR) band. In this band spectrum, the thermal contrast is high.

Non-cooled cameras use sensors that are at or just below ambient temperature and work through the change of resistance, voltage or current created when heated by infrared radiation it detects.

- **Spectral: Near-Infrared (NIR), Infrared sensors (IR), Multispectral and hyperspectral**

This class of payload is particularly useful in commission related to plant growth. Multispectral (Figure 18) and hyper-spectral imaging sensors can detect energy wavelength that exists outside of the typical visible light. This energy often sought for analysis is either Red Green Blue (RGB) band or infrared band. Scientists involved in the agricultural field often study the amount of energy reflected or absorbed by plant vegetation and this information is then analysed to determine the plant health or state (Albetis et al., 2018; Berni et al., 2009; Candiago et al., 2015).



Figure 18 - Multispectral camera and sensors
Source: Parrot sequoia

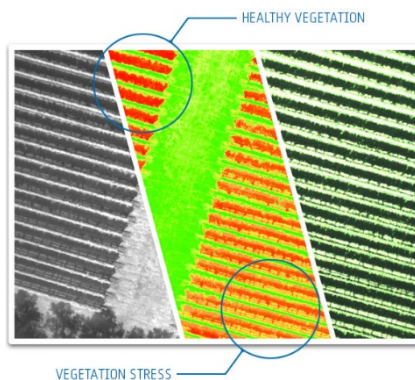


Figure 19 - Multispectral vegetation analysis

The Normalized Difference Vegetation Index (NDVI) is commonly used for this application (Stark, 2000, Pinter et al., 2003):

$$NDVI = (NIR - Red)/(NIR + Red) \quad (1)$$

The second most commonly used in plant health analysis is the Green Normalized Vegetation Index (GNVI) (Taylor, Vygodskaya, Gorshkova, & Fadeyeva, 1989):

$$NDVI = (NIR - Green)/(NIR + Green) \quad (2)$$

The biophysical interpretation of NDVI is the fraction of absorbed photosynthetically active radiation. These indexes can be used to inform prescription maps (Figure 19) for fertilising and seeding crops, as well as crop yield estimates so farmers can maximise the profit (Prasad et al., 2006).

2.2.2 Control methods

Missions and tasks could be conducted in different ways, according to aircraft control. The operation of the aircraft ranges from full manual control, stabilised or “remote control”, to automated flight profiles

without direct flight path control. The level of automation in the flight mission is dependent upon several factors, including, but not limited to, the number of repetitious aircraft movements required, aircraft proximity to other objects, and the dynamic nature of the mission. Control methods can be divided into Manual Control, Stabilized control, Planned control and autonomous control.

Manual control

In manual control, the operator has direct and unassisted control of aircraft configuration and flight path. This method of command, typically applied through a handheld console, allows the operator to make fine changes in aircraft pitch roll, yaw and throttle to perform all type of manoeuvres (Figure 20).

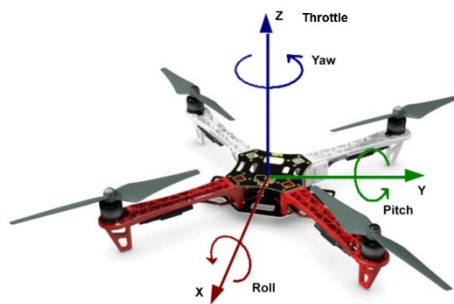


Figure 20 - Aircraft rotation angles

The console can be configured to provide exponential control depending on the degree of input applied, to reduce or amplify inputs and commands and the operator may also to provide direct control over aircraft subsystems such as flaps, landing gear and breaks. This method requires a skilled operator, with extensive training, experience and precise control over aircraft's flight path and predictable outcomes to control inputs and ensure safe operation; in this configuration, in fact, the UAV is sensible to the external input (like wind) that can reduce the stability during flight. Due to the difficulty of manually controlling an aircraft, many operators that are capable of full manual control have spent a lifetime flying remote control aircraft as a hobby.

Stabilized control

Under stabilised control, the operator has direct, assisted control of the aircraft's flight path. This type of aircraft control typically routes the operator's inputs from a handheld console through an autopilot onboard the aircraft that translates the direct inputs into desired outputs. Stabilized control ensures safe aircraft guidance, allowing the operator to maintain direct control of the aircraft's position and compensating the external forces, reducing the need for fine control. Stabilized control dramatically reduces the operator skill level required to effectively and safely control the aircraft while still providing dynamic control of the flight path. The majority of VTOL systems, used for applications that

require repetitive, precise positioning of the aircraft over an area of interest, such as large aerial mapping, are capable of stabilised control and this has resulted in significant growth of the VTOL market due to the ease of aircraft operation. The actual method for stabilised control includes:

Radio Control (RC) aircraft by an External Pilot (EP) using a third-person remote view of the UAV (very common for small UAVs)

Flight console (Figure 21), similar to a cockpit, using a forward fixed camera view to allow an external pilot to fly the UAV as in a simulator.

Virtual Reality (VR) methods employing the various form of FPV (First Person View) flying, including head-tracking techniques.



Figure 21 - Control station for Unmanned Vehicle
Source: Octopus ISR systems



Figure 22 - Mission Planner interface for mission flight design

Planned control

Under planned control, the operator has indirect, assisted control of the aircraft's flight path. This type of control is typically conducted through a graphical software interface that provides an overhead view of the aircraft's position overlaid on aerial or satellite imagery. The operator can usually plan the mission through the software's planning tools (Figure 22) and also upload commands to the aircraft during the flight to alter the flight path. The aircraft's autopilot determines the control surface and throttle inputs to position the aircraft on the desired flight path in a 3-D space, and the operator observes the behaviour of the aircraft to ensure that mission is conducted as desired. Planned control requires the least amount of direct operator skill for aircraft control, but a deep understand of the systems and expertise with mission software; however, the multitude of software interfaces for UASs vary significantly in complexity. The interfaces may vary to basic functionality that only needs high-level inputs from the operator to custom-tailored systems according to the mission's task, that requires the operator input for every possible variable in the mission. Planned missions are usually performed for repetitive and precise tasks. Autopilot control usually using a Global Network Satellite System

(GNSS) waypoint to define a flight plan and Automatic Take-off and landing (ATOL) capabilities are generally used in planned control.

Automated control

In the automated context, three major levels of autonomy have been identified:

- Reactive side: flight control system, actuator engine or propulsion control; aircraft flight mechanics and air data acquisition.
- Reflective side: flight path command and performance envelope protection, health manager and fault-tolerant control
- Decision-making side: fault detection and identification, mission goal manager.

This theoretical framework borrows from various discipline such as aeronautic, automatic control, robotics, computer science and engineering, artificial intelligence, operational research. In the automated control, the UAV is independent of the operator and can flight autonomously, take decision-based on the context, avoid obstacle and accomplish the mission according to the need.

2.3 UAS classification

UAS classification can vary according to different criteria. The U.S. Department of Defense categorises the UAS into five different groups according to their weight, from sUAS (small Unmanned Aircraft System) to larger UAS. In the future, the FAA (US Federal Aviation Authority) will also divide the UAS according to a risk-based classification depending on their potential impact on public safety. (Chen et al., 2016)

Category	Size	Maximum Gross Takeoff Weight	Average Operating Altitude (m)	Airspeed (km/h)
Group 1	Small	0-20	< 360 AGL	< 185
Group 2	Medium	21-55	< 1066 AGL	< 463
Group 3	Large	<1320	< 5486 AGL	< 463
Group 4	Larger	<1320	< 5486 AGL	Any airspeed
Group 5	Largest	<1320	< 5486 AGL	Any airspeed

Table 1 - UAS classification according to the US Department of Defense

UAV classification has generally followed an existing military description of the platform based on characteristics such as size, flight endurance and capabilities (Watts, Ambrosia, & Hinkley, 2012):

- **High Altitude Long Endurance (HALE)**: systems capable of flying over 1500 m of altitude and more than 24 hr of endurance. Designed performing long-range reconnaissance and surveillance missions



Figure 23 - Fixed wing UAV



Figure 24 - VTOL six-rotor UAV

- **Medium Altitude Long Endurance (MALE):** flying between 5000 – 15000 m of altitude, with a maximum of 24 h endurance.
- **Medium Range or Tactical UAV (TUAV):** for mission consisting of flights between 100 and 300 km. Smaller vehicles and operated within a more straightforward system than the HALE-MALE
- **Close-range UAV:** operation range of 100 km, probably the most prolific type of UAV, including roles as diverse as reconnaissance, target designation, airfield security, power-line inspection, crop-spraying and traffic monitoring
- **Mini UAV (MUAV):** UAV whose weight is under of 20 kg, operating ranges of up to about 30 km
- **Micro UAV (MAV):** UAVs having a wingspan no higher than 150 mm. Required for operations in urban environments, particularly within buildings. This type of UAV is very vulnerable to atmospheric turbulence
- **Nano-Air Vehicles (NAV):** the size of 10 mm, used in swarms for purposes such as radar confusion. They are also being proposed for ultra-short-range surveillance.
- **Remotely Piloted Helicopter (RPH):** aerial vehicle capable of performing Vertical Take-off and landing (VTOL). They are commonly used in missions that require hovering flight.
- **Fixed Wing:** fixed-wing UAV (Figure 23) in the civilian field is mostly used for long-distance, long-range and high-altitude missions, especially in environmental monitoring.
- **Flapping-Wings:** flapping wings try to reproduce the way birds or insects fly. Most of them are still under development.
- **Blimps:** blimps or “lighter-than-air” UAVs ensure lifting using their helium-filled ballonet, to allow long endurance. Since no energy is expended to lift the UAV, this savings can be used as a power source for displacement actuators.
- **Rotary wings:** the typical example of rotary wings UAVs are the helicopters: a two-rotors aircraft, with the main rotor giving the thrust and an anti-torque tail rotor. The most notable configuration are convertible VTOL, quadrotors, six-rotors (Figure 24), and eight rotors. The design using multiple rotors allows the simplification of forces generation and torque creation, as mentioned previously. The quad-rotor design eliminates the gyroscopic torques created by the spinning motors. This interesting configuration allows each rotor to have a smaller diameter than the equivalent ordinary helicopter rotor, allowing them to store less kinetic energy during flight. For small scale UAV, this makes the vehicle safer to interact within proximity.

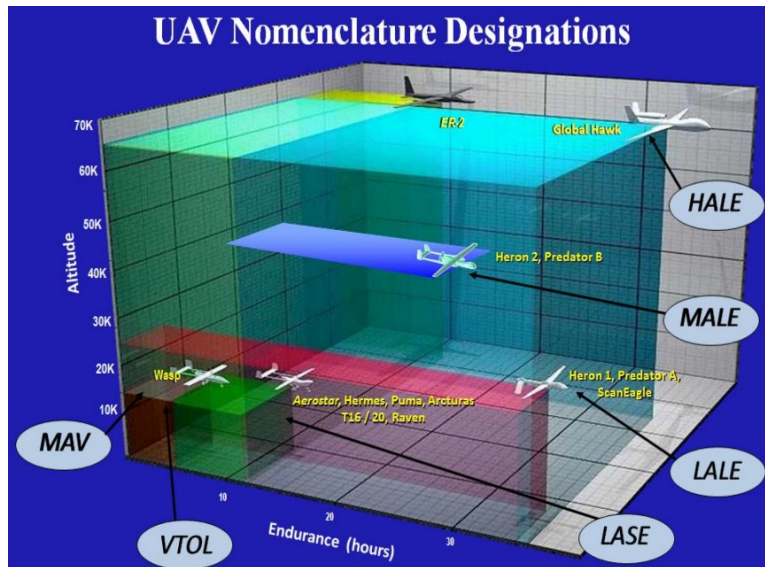


Figure 25 - UAV Classification according to dimension, Source: Watts 2012

2.4 UAV Regulation

The introduction of RPAS in the civil field and their commercial availability has understandably raised concern not only among the aviation community but in the public opinion, as to the probability of the aircraft becoming out of control and causing injury to person or property. Regulatory authorities have set up law and regulation, however in the last five years was difficult for the regulatory bodies to keep up the rapid technological evolution (Stöcker, et al. 2017). The regulation is divided into two activities, military and civilian.

The main regulatory bodies in the flight space administration, are synthesised in Table 2

Regulation Body	Area
ICAO (United Nation Agency)	Worldwide
FAA (Federal Aviation Administration)	USA
EASA (European Agency for Space and Aviation)	Europe
ENAC (Ente Nazionale Aviazione Civile)	Italy
CAA (Civil Aviation Authority)	UK
CAAC (Civil Aviation Administration of China)	Cina

Table 2 - Main regulatory bodies in the world for aviation

All unmanned aircraft, remotely piloted or fully autonomous, are subject to the provisions of Article 8 of the *Convention on International Civil Aviation* (1944) amended by the International Civil Aviation Organization (ICAO) assembly. UASs are different from manned aircraft, and this difference and the rapid commercial availability make

their introduction in the airspace channelling for regulatory bodies and the aviation community. With no person on board the aircraft, the airworthiness objective is primarily to target the protection of people and property on the ground. Airworthiness is defined as the suitability of an aircraft for safe flight, because each aircraft as an operating envelope, defined in terms of its attitude, inside of which is flyable, and outside of which it is unstable and probably unrecoverable.

The aviation community is committed to working together based on the following principle by EASA (European Aviation and Space Agency):

- UAV needs to be treated as new types of aircraft with proportionate rules based on the risk of each operation;
- Technologies and standards need to be developed for the full integration of UAV in the national airspace;
- Public acceptance is key to the growth of UAV services;
- The operator of a UAV is responsible for its use.

The ICAO has considered annexe regarding the use of UAS when directing the integration of UAS in non-segregated airspace: licensing, rules of the air, aircraft operation and airworthiness, aeronautical communication, security safeguarding international civil aviation against acts of unlawful interferences and the radio frequency spectrum (Gimenes et al., 2014).

On 2016, FAA and EASA have issued approval for flying small commercial UAVs, establishing the requirement of a certificate to allow the use for commercial work. This certificate applies to the individual who would be employed by a UAS operator certificate holder for a commercial work operation. The legislation of many countries emphasises the responsibility of the pilot and the need to be trained and licensed; in fact, actual regulation defines that all the responsibility for any damage to property or injuries belongs to the aircraft operator.

The regulation for commercial work and airspace delimitation is defined following common guideline. However, the critical part of the evolving regulation will be the extent to which UAV can be operated *Beyond Visual Line-Of-Sight* (BVLOS) in populated areas and/or without a dedicated pilot per each UAV (allowing a single pilot to operate or monitor more than one UAV at the same time).

2.3.1 Europe - EASA

In Europe, the first framework about UAV regulation was proposed in 2016 by the European Union as a common basis to harmonise regulation across different countries and enable more application; the final version is actually on developing (Figure 27) and will be effective in 2022. The EASA commission has proposed an operation centric, proportionate, risk-and performance-based framework for all types of Unmanned Aircraft, that will ensure the safe use of UAV in civil airspace and will create legal certainty for the entire industry and stakeholders.



Figure 26 - UAV Easa logo

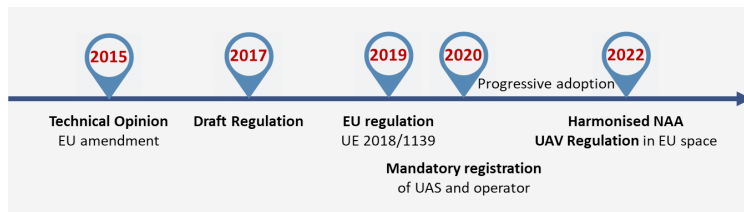


Figure 27 - Timeline of Drone Framework regulation approval, Source: EASA

The **main aspects** of the proposed regulation can be summarised as:

- Provides a framework to safely operate drones while allowing this industry to remain agile, to innovate and continue to grow. The risk posed to people on the ground and other aircraft, as well as privacy, security and data protection issues created, is also considered.
- Defines the technical and operational requirements for the drones. Technical requirements refer to the remote identification of drones. Operational requirements refer among others to geo-awareness, a system that informs the remote pilot when a drone is entering a prohibited zone. The proposal also addresses the pilots' qualifications. Furthermore, drone operators will have to register themselves, except when they operate drones lighter than 250g.
- Breaks new grounds by combining Product legislation and Aviation legislation. Indeed, design requirements for small drones will be implemented by using the legislation relative to making products available on the market (the well-known CE marking). The standard CE mark will be accompanied by the identification of the class of the drone (from C0 to C4) and by a do's and don'ts consumer information that will be found in all drone boxes. Based on the drone class, an operator will know in which area he can operate and what competence is required.
- Allows a high degree of flexibility for the EASA Member States; they will be able to define zones in their territory where either drones' operations are prohibited or restricted (for example to protect sensitive areas), or where specific requirements are alleviated.

Considering the board range of operation and types of UAV, three categories of operations and their associated safety requirements proportionate to the risk were proposed (Introduction of a regulatory framework for the operation of UAV, EASA, 2015) (Figure 28):

- **Open category** of UAV should not require authorisation by an aviation authority for the flight but stays within defined boundaries for the operation. In this category, UAV must fly under direct *Visual Line Of Sight* (VLOS): 500 m, at an altitude, not exceeding 150 m above the ground or water and outside of specified reserved areas (airport, environmental, security). UAV's weight should be less than 25 kg.

- **Specific category** will require a risk assessment that will lead to an operation's authorisation with specific limitations adopted to the operation. The specific category should cover operations that do not meet the characteristics of the open category where a specific risk needs to be mitigated by additional operational limitations or higher capacity of the associated equipment and personnel.
- **Certified category** is required for operations with a higher associated risk or might be requested voluntarily by organisations providing services such as remote piloting or equipment such as detect and avoid.



Figure 28 - EASA UAV categories

Based on the market's needs, priority has been given to the development of a regulation for operations in 'open' and 'specific' category. The subcategories of the "Open" are split according to the type of operation (A1 to A3) and the UAS class (C0 to C4) as summarized in Table 3 (Opinion n.1 Introduction of a Regulatory Framework for the operation of UAS in the "Open" and "Specific" category EASA, 2018). To support the management of a large number of RPAS operations, different traffic classes have been developed and insert in the European Regulation:

- Class I: reserved for RPAS EASA category A (VLOS only)
- Class II: Free route (VLOS and BVLOS)
- Class III: Organized commercial medium/long haul traffic (BVLOS only)
- Class IV: Special operations (VLOS and BVLOS)

RPAS class traffic is a set of flying rules operational procedures and systems capabilities applicable to the RPAS, the RPAS operator while performing a mission in the portion of airspace, and the services applicable in that airspace. Included in this registration is initial permission for *Beyond Visual Line-of-Sight (BVLOS)* that are critical for many of these operations to be economically viable opportunities.

Operation	Remote Pilot competency	UAS			UAS operator registration
Subcategory		Class	MTOM (j)	Electronic ID	
A1 Fly over people	Read consumer info	Privately built	< 250 g	No	No
		C0			
	Consumer info Online training Online test	C1	< 900 g		
A2 fly close to people	A1 + theoretical test in a centre recognised by NAA	C2	<4 kg	Yes + Unique SN identification	
A3 fly far from people	Consumer info Online training Online test	C3	< 25 kg	If required by the zone of operations	Yes
		C4			
		Privately Built			

Table 3 - "Open" sub-categories

This framework regulation has taken into consideration the developments in the international arena, e.g. work done in the ICAO, in the Joint Authorities for the Rulemaking of Unmanned Systems (JARUS) and of course in the USA (Federal Aviation Administration - FAA). The rules of the air will not be adopted for low-level RPAS operation maintaining the 1 km boundary as implemented around the world. Under this limit, the airspace will be revolutionised as shown in Figure 29.

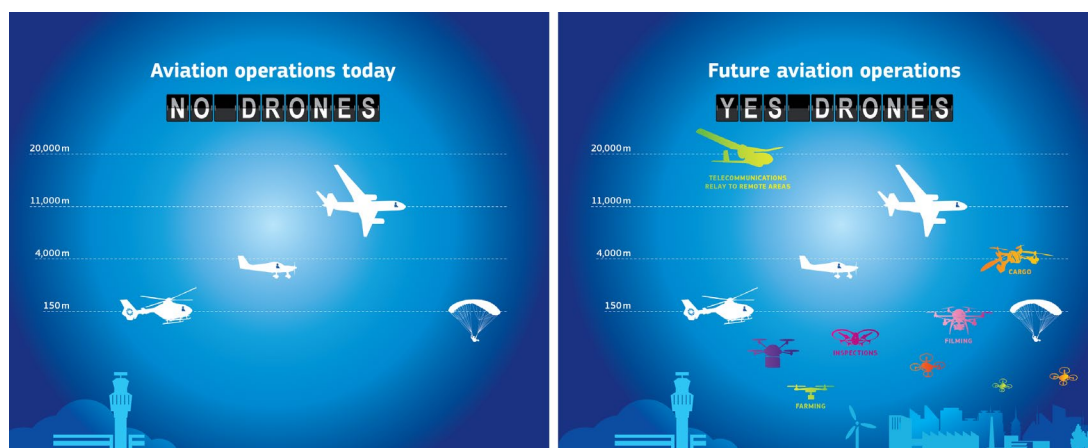


Figure 29 - Airspace with drones' regulation, Source: EASA UAV infographic

Another critical step in the regulation of the airspace is the Amsterdam Declaration in 2018 about the European Drone Services Market, which focuses on **U-space management (Unmanned Space)**. The Amsterdam declaration urges the European Institutions and industry to continue the good progress towards the delivery of the common European drone services market. The objective is to provide support to



Figure 30 - U-Space: <https://www.sesarju.eu/U-space>

the Member States in the implementation of the European drone regulations and to develop, in close cooperation with Member States and all stakeholders, an institutional framework for a competitive U-space services market to create a Single European Sky. Moreover, it provides support to the cities in their efforts to provide a fertile ground for innovative multimodal solutions, integrating the 3rd dimension into their urban planning processes;

In particular, the **U-space** covers altitudes up to 150 m, and the aim is the registration of UAV operators, their e-identification and geofencing. The basic concept is to develop a system that provides information on highly automated or autonomous UAV to fly safely and avoid obstacles or collision, similar to that of Air Traffic Management for manned aviation. Different level of services are defined in the U-space Blueprint (SESAR, 2017) as represented in Figure 31, and several private companies (such as D-flight, Altitude angel) are working on the implementation of U-space services for low altitude airspace monitoring and real-time tracking of UAV flying using e-identification.

U-Space level	Services	Date
U1 foundation services	e-registration e- identification geofencing	2019
U2 initial services	Drone operation management Procedural interfaces with air traffic control	2022
U3 advanced services	Complex operation Capacity management Detect and Avoid (DAA)	2027
U4 full services	Integrated interface with manned aviation Connectivity and digitalisation for drone and U-Space system	2035

Table 4 - U-space services

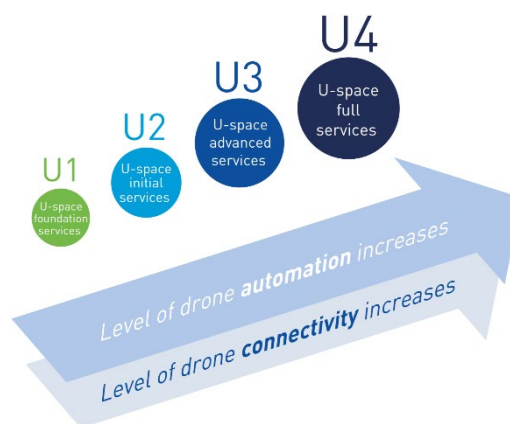


Figure 31 - U-space level of services

2.3.2 Italy

ENAC (Ente Nazionale Aviazione Civile) is the regulatory body in charge of manage airspace in Italy. This aviation authority, like every country in the European Union, will update the national regulation according to the European Framework from 2019 to 2022. Actual regulation “Regolamento Sistemi Aerei a Pilotaggio Remoto” published on 21-05-2018 is summarized in Table 5.

Italy	
Weight Limit	As per EASA Basic Regulation Annex I
Categories	Yes: 0.3 kg/ 2 kg / 25 kg
License	From 01.04.2016. Pilot Certificate for VLOS and < 25kg. [if < 0,3 kg, < 60km/h and rotors protection, no pilot certificate]. Otherwise Pilot License. Medical class LAPL for Pilot Certificate and medical class 3 for Pilot License
VLOS	Yes, EVLOS possible
BVLOS	Yes
Height Limit	VLOS: max 150 m
Operational limitations	Non-critical: > 150 m from congested area, 50 m from persons and property, in uncontrolled airspace, outside ATZ and > 5 km from airport. Sublasses exist
Remarks	ID plate on RPA and RPS. Simpler approval procedure for < 2 kg. No dangerous goods. Registration required > 25 kg. Requirements for privacy and data protection.

Table 5 - Italy UAV regulation, Source: European Drones Outlook Study 2016, EASA

The progressive implementation process of European Regulation is already started and will end by 2022 as in every National Aviation Authority in the EU.

2.3.3 USA - FAA

In the USA Federal Aviation Administration (FAA) is responsible for the regulation of the airspace. Different types of UAS operations are defined:

- **Governmental Operations:** for public aircraft operations, the FAA issues a *Certificate Of wavier or Authorization* (COA) that permits public agencies and organisation to operate aircraft, for a particular purpose, in a particular area. The certificate allows an operator to use a defined block of airspace and includes special safety provisions unique to the proposed operation. COAs usually are issued for a specific period.
- **Civil Operation:** any operation that does not meet the statutory criteria for a public aircraft operation is considered a civil aircraft operation and must be conducted following all FAA regulation applicable to the operation
- **Model Aircraft:** individuals flying for recreation must follow safety guidelines: fly below 150 m and remain clear of surrounding obstacles, keep the aircraft within visual line-of-sight (VLOS) at all times, do not interfere with manned aircraft operations, do not fly near people or stadium, do not fly under daytime visual flight rules and stay certain pre-defined distances away from airports or heliports.

Federal law requires that all aircraft (which includes UAS and radio/remote-controlled aircraft) flown outdoors must be registered with the FAA and marked with a registration number. Operators are responsible for flying with FAA regulation and guidelines and must observe the following rules:

Pilot requirements: must have a remote pilot, airman certificate, be 16 years old, pass the Security Administration (TSA) background security screening, have no physical or mental condition that would interfere with the safe small UAS operation.

Aircraft requirements: less than 25kg, over 25 kg must be registered online, and must undergo a pre-flight check to ensure UAS in condition for safe operation

Location requirements: class G airspace, typically the airspace very near the ground.

Operating rules: must keep the aircraft in visual line-of-sight fly under 400 feet, fly during the day, fly at or below 180km/h, yield right-of-way to manned aircraft, not fly over people, and not fly from a moving vehicle. Also, the FAA is working on U-Space implementation with several private companies (like Airmap, Altitude Angel) that are implementing the related services to track monitor in real-time every UAV moving in the low altitude airspace.

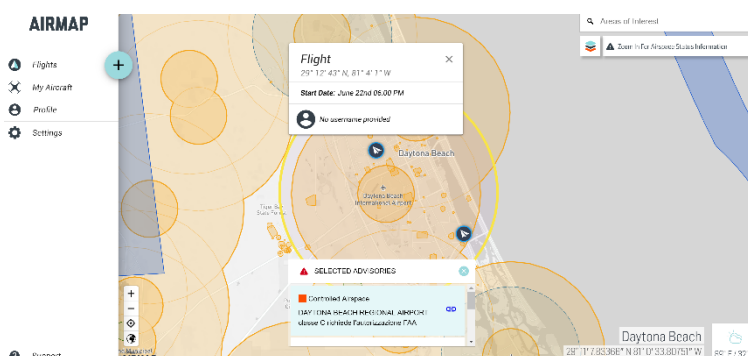


Figure 32 - Airmap interface for U-space management

2.3.4 China - CAAC

In China, the regulation on UAS is demanded to the *Civilian Aviation Administration of China* (CAAC), the Chinese equivalent of FAA or EASA. Last regulation was released in May 2017 and is written in Chinese only. The main difference from other international regulation consists on the mandatory registration of the UAV (>250 grams) on the CAAC “Unmanned machine real-name registration system”, using real name, valid ID number, mobile phones or email address, product model and serial number and purpose of use (Civilian Aviation Administration of China, 2017). From the 1st July 2017, this process is mandatory for pilots and drone’s operator that should also have insurance to cover liability for third parties on the ground. After the registration process, is permitted to fly under the following restriction:



Figure 33 - Civilian Aviation Administration of China (CAAC)

Maximum range: 120m is the maximum altitude that the UAV can reach; any aircraft above this level requires a commercial license. Most UAV had this limitation in the software itself. Like in the other country, China requires VLOS (Visual Line of Sight) flight. BVLOS (Beyond Visual Line of Sight) operation are not yet allowed.

Maximum weight: UAV that weighs more than 250 grams, as mentioned before, requires real-name registration on the CAAC online system and above 7 kg requires a licence from the CAAC.

No-fly-zones in China include airports, military installation and specific sites such as Beijing and sensitive areas like Xinjiang or Tibet.

2.5 Application in AEC (Architecture Engineering and Construction)

Unmanned technology and robotics in general, have different revolutionary application in every industry improving efficiency, reducing time and cost, safety and countless tasks.

UAS are used to obtain a desired set of information or to perform a specific mission, so the related application ranges from simple data capture to precise scientific measurement and complex operations. This range of application corresponding to a wide range of knowledge required by the UAS operator that can vary dramatically from little prerequisite knowledge to extensive and specialised training. The operations are conducted specifically to the purpose of the mission and the data collection required before the actual launch of the UAS.

Today UAV manufacturers, service providers and platform integrations are seriously considering the business potential in industry sectors (Rao, Gopi, & Maione, 2016). In this section, the main technical application of UAV in technical sectors and sector are summarised, as shown in

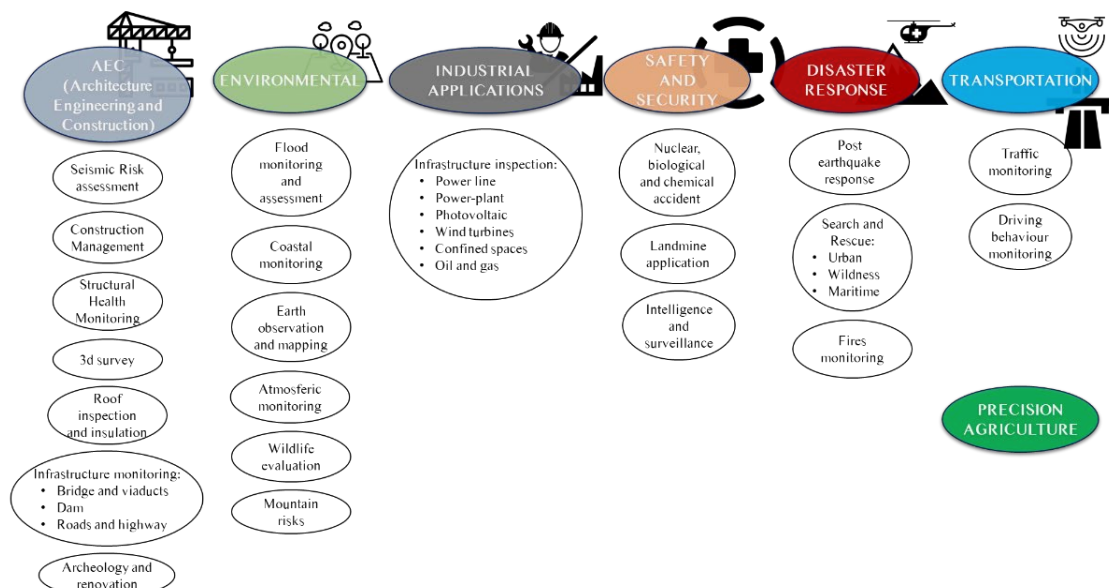


Figure 34 - UAV applications in technical sectors

Figure 34, with focus on AEC (Architecture Engineering and Construction).

Environmental

The possibility to mount different payloads and sensors makes the UAV a perfect platform for acquiring and collect environmental data and monitor the environment. The critical consideration for safe and cost-effective data collection is how to position the environmental sensor in order to acquire useful information from their location and/or path. *Dynamic Data-Driven Application Systems (DDDAS)* provide a means to position the UAVs in an efficient manner using the real-time data obtained from the sensors. The framework is driven by the goal of dynamically incorporating data obtained from the sensors. Moreover, UAV enables new possibilities in the survey, earth observation and acquisition of environmental spatial data providing a top view of the territory and 3d reconstruction without restoring to more expansive classical aerial photogrammetry. UAV can be used to survey areas of a limited extent such as open mines, little rivers, cultivated fields, not only to monitor the land evolution and local changes in the terrain morphology but also discover illegal uses of land resources. The use of this system in environmental sectors include, but are not limited to:

- Flood Monitoring and assessment
- Coastal monitoring
- Earth observation and mapping
- Atmospheric monitoring
- Wildlife evaluation
- Mountain risks

Industrial Inspection

Industrial sites often contain areas and facilities that are difficult to access or hazardous to humans. UAV can be very useful for inspecting the infrastructure where manned inspection is dangerous, decreasing the operational costs and execute the monitoring process, thanks to the possibility of remotely piloting the vehicle. Apart from the reduced cost and time, UAS does not pose a hazard to aircrews, can operate in diverse weather conditions and is less obtrusive to neighbouring communities or animals. The possibility to carry an electro-optic or thermal sensor as payload and stream in real-time videos is another main advantage. UAV industrial inspections can be segmented into: Local site inspections performed operating in VLOS at a lower altitude (typically below 150m) and Long-range utility inspections operating in BVLOS at higher altitude. The following infrastructure can be monitored and inspected to ensure structure reliability and safety:

- Power line
- Power-plant
- Photovoltaic modules (using thermal cameras)



Figure 35 - UAV for industrial inspection

- Wind turbines
- Confined Spaces
- Oil and gas

Safety and security

UAV can be used in hazardous public safety situations providing a cost-effective solution with a high return on investment for local public agencies. Three application of UAS technology for surveillance and security are: stationary surveying by rotorcraft that are operated on-site using tethered systems which guarantees unlimited autonomy (Figure 36);



Figure 36 - Tethered UAS for surveillance application

Long-range surveying in VLOS or BVLOS operated at altitudes of approximately 150 m to gather precise detail with dedicated zoom optics (Figure 37) or to screen larger areas as part of border security, maritime surveillance, and environmental protection.

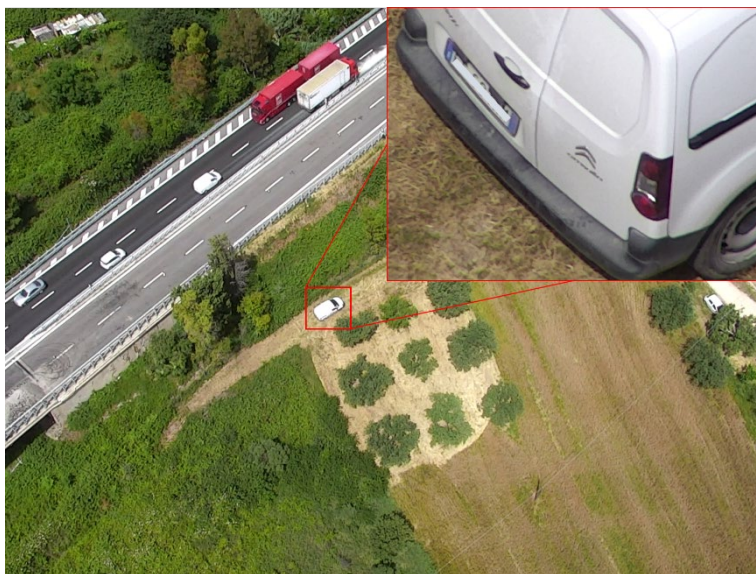


Figure 37 - Surveillance operation using UAS

Nuclear biological and chemical accident (NBC), landmine detection is another example of the teaming of manned and unmanned systems. In those two situations, it is often necessary to map areas which are difficult or impossible for people to reach. These tasks are a typical application of the robotic system, avoiding life-risk for technician and expert.

Disaster response and relief

Natural disasters represent an important factor that affects human life and development, and when it occurs the most crucial issue that needs be resolved is related to human life. In this context, time is a critical factor because Search and Rescue operation must be conducted quickly and efficiently in the first 72 critical hours after the disaster. UAV could be used for searching civilians in different scenarios, urban wildness or marine, and the possibility of using different payload (e.g. thermal) is a crucial factor for this operation. The objective in this initial stage, apart from S&R is also to quickly obtain data of the interested zones in the first moments after the disaster: the aircraft could be sent to a location where high impact is expected and perform the first assessment before any response and resources are deployed. This could be useful to know the condition before any intervention (Erdelj & Natalizio, 2016) and reconstruct the scene for post-event investigation and analysis. The initial assessment would include damage in the disaster zone, as well as the condition of the transportation network to assist in the planning of resource deployment. Destination and route could be set-up according to initial assessment. The possibility of gathering data in real-time and obtain valuable information is vital for organising a quick and successful post-disaster intervention.

A three-stage operational lifecycle can be proposed where UAVs participate in natural disaster management:

1. Pre-disaster preparedness concerning surveying-related events to set-up an *Early Warning System (EWS)*.
2. Disaster assessment providing situational awareness during a disaster in real-time and completing damage studies for logistical planning
3. Disaster response and recovery, including the Search and Rescue mission.
4. Post-disaster investigation analysis using photo and video data and photogrammetry or 3d scene reconstruction.

Each stage imposes a set of tasks demands on the UAVs with different time. High-resolution images and photogrammetric information gather can be used to produce hazard maps and post-disaster map to plan intervention quickly. In this direction, advancements in UAV instrumentation and computer science have enabled a valuable tool for rapid response: semi-automated and fully automated map creation.

The main challenges in the use of UAV in disaster-response are represented by the lack of infrastructure for communication in this scenario and the difficulty of real-time transmission. The identification and prioritisation of critical information should also be established for UAVs to collect data in the different phases of disaster response.

Transportation

The use of UAV can help in the collection of transportation-related information's (Kanistras et al., 2013, Salvo et al., 2014). Due to dynamic flow, uncertain environment and information widely spread in terms of geospatial area and time, traffic monitoring requires a flexible platform such as UAV. This vehicle can provide a global view of roads and freeways with relevant information such as real-time monitoring, travel time estimation, trajectories, lane occupancies and incidence response. Moreover, UAV can even act as an on-demand system for an unexpected situation such as an incident to acquiring data or transport First Aid Kit. The integration of the UAV to enhance the traffic monitoring system serving a backbone of *Intelligent Transportation System (ITS)* infrastructure.

Driving-behaviour monitoring can also be enhanced using this platform in research, to gather accurate and detailed vehicle trajectory. US National Highway Traffic Safety Administration (NHTSA) has identified six key metrics that must be quantified to determine and quantify potential misbehaviours: ID, speed, forward distance, lane change, lane change time, and acceleration. The calculation of these crucial metrics can be automated using computer vision algorithm (Zheng, Breton, Iqbal, & Sadiq, 2015).

Three of the main challenges of these uses are related to the capability of processing a large amount of data (Rathinam, Kim, & Sengupta, 2006), the affordability of the communications system and interface, and to the capability of keeping the camera in view of the road for a long period.

Precision agriculture: precision agriculture is an innovative trend in farm management, and it is considered to be the most significant market application of UAV, thanks to the main advantages related to the production increase. This technique involves the application of geospatial analysis and sensors to identify variation in the field and to deal with them using alternative strategies (C. Zhang & Kovacs, 2012, Raeva, et al., 2018). In agronomic research, new products and substances are tested on the field, with labour-intensive and typically weekly inspections of leaf properties by experienced staff. The assessment of the plant, in this qualitative method, it is based on size, condition and number of a plant leaf. The use of UAV is more flexible, precise and cost-effective to collect data necessary for the analysis and the consecutive action. Two different primary mission type can be identified in the use of UAV for precision agriculture: *Long-range*

surveying, used to gather data through remote sensing at an altitude of 150 m and *Long-range light payload* UAVs to precise spraying of chemicals (Sheba & Gladston Raj, 2018, Garre & Harish, 2018) at altitude below 50 m.

Non-technical sectors include, in a non-exhaustive way:

Aerial filming and photography: Filmmaking, Real estate, Marketing, News reporting.

Show, communication and entertainment (Santamarina-Campos & Segarra-Oña, 2018)

2.5.1 Application in Architecture Engineering and Construction



Figure 38 - UAV application in construction site

Architecture Engineering and Construction (AEC) is a complex sector where innovation is usually slow due to consolidated methods and techniques, to the complex supply chain and environment that influence the entire process (Pries & Janszen, 2006, Winch, 2010, McKinsey Company, 2015). Management will play an increasingly crucial role in the construction industry, and main UAV application in this sector is strictly linked with construction site management (Dupont et al., 2017, Wen & Kang, 2014). UAV will have different applications in civil engineering works (Liu et al., 2014, Douglas M. et al., 2016, Sebbane, 2018) and can contribute to the digitalisation of this industry coupled with other technology (Vacanas et al., 2015), to reduce time and cost. The main idea is to use the UAV as an item to collect and achieve useful and reliable information using a dynamic, mobile and soon autonomous vehicle to perform repetitive and low-value tasks. The elaboration and extraction of useful information from the acquired data is the key in the rapid and valuable integration of these systems. The possibility to

automatic collect, detect, extract relevant information and in the future to act, will be the turning point in the use of this technology.

Below summarised some of the main application and sub-discipline in civil engineering in which UAV applications can yield great benefits:

Seismic Risk Assessment

The use of UAV plays a key role in risk mitigation and analysis for Seismic Risk assessment of buildings and infrastructures. Parameters for risk analysis are project-specific and generally gathered using satellite images, GPS technology or visual inspection by a technician. The possibility to collect building inventory data (that usually are not accessible, or belong to the government) in a cheap, fast and less labour intensive way is fundamental for Seismic Risk Assessment. Blueprints and geographic information are not usually publicly available, but the geometric features of building and infrastructure can be obtained from a mid/large-scale survey performed with UAV. The analysis of the data and the automatic feature extraction (such as dimensions and number of stories) from images and video using computer vision, to automate and speed up the process, is an open-point (Crommelinck et al., 2016). Moreover, reliable spatial information can be used to calculate the fragility curve, create reliable Seismic Fragility Databases to perform spatial analysis for the post-earthquake scenario. The use of deterministic data improves the reliability of the assessment results. Also, post-earthquake investigation and observation of structural damage, traditionally performed by technicians could be improved thanks to the use of UAV (Fernandez Galarreta F. et al., 2015).

Construction Management

Larger construction project such as civil infrastructure, bridges, viaduct, dams and plant usually require the coordination of hundreds of workers and pieces of construction machinery on the same site. With the use of UAV, construction managers can monitor the entire site with enhanced visibility, remotely, without accessibility constraint (Irizarry, Ph, Asce, Costa, & Ph, 2015) achieving data for tracking the construction progress (Rakha & Gorodetsky, 2018). The global view of the site is also useful to gain a clear perspective of the whole project, perform risk analysis and for Health and Safety reason to prevent an accident, constantly monitoring workers and construction site (Siebert & Teizer, 2014).

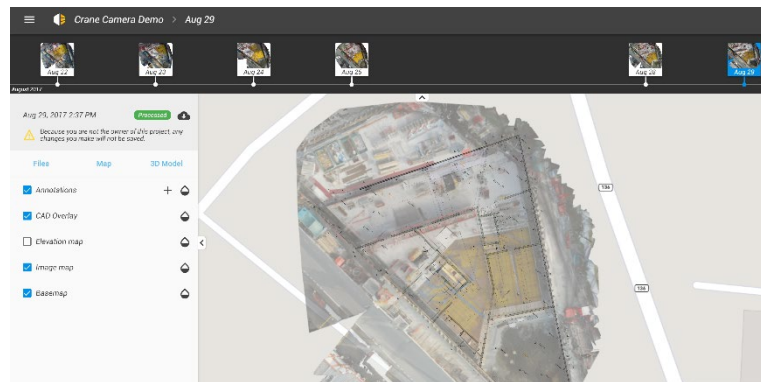


Figure 39 - Construction works progress, Source: Pix4d

A typical representation of construction site includes as-built documentation and project blueprint, often photography from the technician on-site to monitor construction progress on a fixed basis and computer-generated imagery. The use of UAV allows the use of aerial photography, orthophotos 3d model with built-in measuring tools, cad drawing and map overlay, timeline progress analysis (Figure 39), and remotely virtual inspection (outdoor and indoor) during works. Moreover, UAS reduces the risks of injuries by workers, improve management efforts and quality enhancing on-site productivity. The main challenges in use for construction management consist on the flight reliability in construction sites that present restriction such as obstacles and unstable airflow, and the possibility to dynamically optimise route and path planning. Transmission of real-time images and videos is another challenge that will be overcome by the use of new telecommunication infrastructure.

Structural Health and Monitoring (SHM)

Structural Health Monitoring is a component of civil engineering for safety and integrity verification of civil structure. Structure's conditions are generally monitored using sensors and sensing system. However large quantitative of images, videos and information on 3d spaces can be captured very quickly using UAVs with different sensors ensuring the correct characterisation of the existing condition (Sankarasrinivasan, et al., 2015). Also, important structural detail of building and bridges can be acquired with zoom sensors from far distances especially in bridges and viaduct that difficult to reach (Figure 40).



Figure 40 - Joint detail from UAV survey with 30x zoom

Performing continuous and regular acquisition can contribute to monitoring the SH condition of a specific structure during the time. Autonomous UAV can unlock the potential of continuous monitoring, performing the same pre-programmed pattern on a time-dependent basis. Moreover, object recognition of acquired data can facilitate integration and monitoring in a BIM environment (States & States, 2017). The goals of an UAV-driven visual performance monitoring procedure is to:

1. Collect images or videos from the most informative views on a project site
2. Analyse them with or without a priori building information models to reason about performance deviations during construction
3. Monitor ongoing operations for productivity and safety
4. Characterise the currently existing condition of civil infrastructure items
5. Visualise and communicate the most updated state of work-in-progress with on-site and off-site project participants.

3d Survey and mapping (data acquisition)

The growing availability of cameras sensor, photogrammetry techniques and software give the possibility to obtain high-quality 3d reconstruction and orthophoto of the building, areas of intervention and whole construction sites. This accurate 3d reconstruction has become essential for the non-traditional mapping application. The use of UAS (with GPS, mission planning and pre-programmed path), and emerging mobile mapping platform, in general, provide additional economical and practical advantages. The use of rotorcraft to capture pictures and videos combined with photogrammetry allows the creation of 3d point

cloud of the scene, Digital Elevation Model (DEM) (Uysal et al., 2015) and digital surface model (DSM), textured 3d model, orthophoto, contour lines and vector data in a semi-automated or fully automated way (Remondino, et al., 2012). Also, the use of UAV enhanced the possibility to obtain precise as-built documentation and speed-up the process acquisition and building monitoring (Eschmann et al., 2012). In this acquisition process, climate and external condition have a direct impact on the required time and possibility to perform the operations, moreover, the quality of the results is directly influenced by the sensor characteristics, UAV flight stability and electronics efficiency. Inspection and accurate specific survey are also possible in a tall building or vertical structure (Russo et al., 2018) such as skyscraper (Roca et al., 2013).

Roof inspection and insulation

In building maintenance, roof's inspection represents a challenge due to risks related to working at height and sometimes inaccessibility of place. UAVs equipped with a high-resolution camera can be used to collect data such as images and videos to perform a visual inspection, and thermal cameras to graphically depict energy inefficiency in the roof (Figure 41). The identification of temperature variation within the building is useful to quickly find areas of wet insulation and potential leaks. The thermal sensitivity or Noise-Equivalent Temperature Difference (NETD) is the measurement of the smallest temperature difference that thermal imagery can detect in the presence of electronic noise. High sensitivity (and low NETD) thermal imagery shows more temperature differences and thus more patterns.

The lower the thermal sensitivity, the more detailed and less noise present on the thermogram. High-resolution images are needed when observing the roof from a greater distance, such as in flyover.



Figure 41 - Thermal image acquired with UAS

Infrastructure monitoring

Civil infrastructures such as bridges and viaducts, dams, roads and highway are complex systems with very high risks associated with their collapse. For this reason, despite the high project lifetime, they request continuous monitoring, inspection and maintenance operation, to ensure safety and continuous usage. Visual inspection requires a long time, the interruption of the operations to perform analysis, specialised equipment and qualified technicians that follow standardised guidelines. The need for a better solution, discussed in deep in chapter 4, leads to the use of UAV as a perfect instrument for survey and inspection. The data can be obtained easily, without any interruption of operation and works, and can be post-processed using specialised software and technology such as Virtual Reality (VR) and Mixed Reality (MR) (Karaaslan, Bagci, & Catbas, 2018).

The main challenges that have to be faced, analysed in the present work, deal with acquisition plan, navigation through complex environment and structure, a methodology to acquire valuable data and a methodology for 3d reconstruction and post-process analysis. Moreover, the inherent nature of a structural inspection mission using UAV implies the interaction of different domains including, UAV stabilisation and control, navigation obstacle avoidance, wireless communication, GPS and computer vision aided navigation.



Figure 42 - Virtual asset inspection
Source: Pix4d

References

- Albetis, J., Jacquin, A., Goulard, M., Poilvé, H., Rousseau, J., Clenet, H., ... Duthoit, S. (2018). On the Potentiality of UAV Multispectral Imagery to Detect Flavescence dorée and Grapevine Trunk Diseases. *Remote Sensing*, 11(1), 23.
- Berni, J., Zarco-Tejada, P., Suárez, L., González-Dugo, V., & Fereres, E. (2009). Remote sensing of vegetation from UAV platforms using lightweight multispectral and thermal imaging sensors. *International Archives of the Photogrammetry, Remote Sensing and Spatial Information Sciences*, 38(September), 1–6.
- Candiago, S., Remondino, F., De Giglio, M., Dubbini, M., & Gattelli, M. (2015). Evaluating multispectral images and vegetation indices for precision farming applications from UAV images. *Remote Sensing*, 7(4), 4026–4047.
- Chen, H., Wang, X., & Li, Y. (2009). A survey of autonomous control for UAV. In *Artificial Intelligence and Computational Intelligence, 2009. AICI'09. International Conference on* (Vol. 2, pp. 267–271).
- Chen, S., Laefer, D. F., & Mangina, E. (2016). State of Technology Review of Civilian UAVs. *Recent Patents on Engineering*, 10(3), 160–174.
- Civilian Aviation Administration of China, C. (2017). Management Program Aircraft Airworthiness - AP-45-AA-2017-03.
- Colomina, I., & Molina, P. (2014). Unmanned aerial systems for photogrammetry and remote sensing: A review. *ISPRS Journal of Photogrammetry and Remote Sensing*, 92, 79–97.
- Crommelinck, S., Bennett, R., Gerke, M., Nex, F., Yang, M. Y., & Vosselman, G. (2016). Review of automatic feature extraction from high-resolution optical sensor data for UAV-based cadastral mapping. *Remote Sensing*, 8(8).
- Douglas M. Marshall Richard Kurt Barnhart, E. S. M. M. (2016). *Introduction to unmanned aircraft systems* (Second edi). CRC Press.
- Dupont, Q. F. M., Chua, D. K. H., Tashrif, A., & Abbott, E. L. S. (2017). Potential Applications of UAV along the Construction 's Value Chain. *Procedia Engineering*, 182(3), 165–173.
- EASA (European Aviation Safety Agency). (2017). NPA 2017-05 (B) Introduction of a regulatory framework for the operation of drones Unmanned aircraft system operations in the open and specific category, 05(01), 128. Retrieved from https://www.easa.europa.eu/system/files/dfu/NPA_2017-05_%28B%29.pdf
- Erdelj, M., & Natalizio, E. (2016). UAV-assisted disaster management: Applications and open issues. *2016 International Conference on Computing, Networking and Communications, ICNC 2016*.
- Eschmann, C., Kuo, C.-M., & Boller, C. (2012). Unmanned Aircraft Systems for Remote Building Inspection and Monitoring. *Proceedings of the 6th European Workshop on Structural Health Monitoring, July 3-6, 2012, Dresden, Germany*, 2, 1–8.
- European Aviation Safety Agency (EASA). (2015). European Aviation Safety Agency Introduction of a regulatory framework for the operation of unmanned aircraft, 1–50.
- Fahlstrom, P. G., & Gleason, T. J. (2012). *Introduction To UAV System*.
- Federal Aviation Administration Aerospace forecast. (2016). FAA Aerospace forecast. *FAA Aerospace*, 91.
- Fernandez Galarreta, J., Kerle, N., & Gerke, M. (2015). UAV-based urban structural damage assessment using object-based image analysis and semantic reasoning. *Natural Hazards and Earth System Sciences*, 15(6), 1087–1101.
- Garre, P., & Harish, A. (2018). Autonomous Agricultural Pesticide Spraying UAV. *IOP Conference Series: Materials Science and Engineering*, 455, 012030.
- Gimenes, R. A. V., Vismari, L. F., Avelino, V. F., Camargo, J. B., De Almeida, J. R., & Cugnasca, P. S. (2014). Guidelines for the integration of autonomous UAS into the global ATM. *Journal of Intelligent and Robotic Systems: Theory and Applications*.
- Gonzalez, L. F., Montes, G. A., Puig, E., Johnson, S., Mengersen, K., & Gaston, K. J. (2016). Unmanned aerial vehicles (UAVs) and artificial intelligence revolutionizing wildlife monitoring and conservation. *Sensors (Switzerland)*, 16(1).
- Irizarry, J., Ph, D., Asce, M., Costa, D. B., & Ph, D. (2015). Exploratory Study of Potential

- Applications of Unmanned Aerial Systems for Construction Management Tasks, 2, 1–10.
- Kanistras, K., Martins, G., & Rutherford, M. J. (2013). A Survey of Unmanned Aerial Vehicles (UAVs) for Traffic Monitoring, 221–234.
- Karaaslan, E., Bagci, U., & Catbas, F. N. (2018). Artificial Intelligence Assisted Infrastructure Assessment Using Mixed Reality Systems. *ArXiv Preprint*, arXiv:1812.05659.
- Liu, P., Chen, A. Y., Huang, Y. N., Han, J. Y., Lai, J. S., Kang, S. C., ... Tsai, M. H. (2014). A review of rotorcraft unmanned aerial vehicle (UAV) developments and applications in civil engineering. *Smart Structures and Systems*, 13(6), 1065–1094.
- Lu, H., Li, Y., Mu, S., Wang, D., Kim, H., & Serikawa, S. (2018). Motor anomaly detection for unmanned aerial vehicles using reinforcement learning. *IEEE Internet of Things Journal*, 5(4), 2315–2322.
- Luis Rodolfo Garcia Carrillo, Alejandro Enrique Dzul Lopez, R. L. and C. P. (2012). Quod Rotorcraft Control: Vision-based Hovering and Navigation, (Springer).
- Ma'sum, M. A., Arrofi, M. K., Jati, G., Arifin, F., Kurniawan, M. N., Mursanto, P., & Jatmiko, W. (2013). Simulation of intelligent unmanned aerial vehicle (uav) for military surveillance. In *Advanced Computer Science and Information Systems (ICACSIS), 2013 International Conference on* (pp. 161–166).
- McKinsey Company, . (2015). The construction productivity imperative, (June).
- Pinter, P. J., Hatfield, J. L., Schepers, J. S., Barnes, E. M., Moran, M. S., Daughtry, C. S. T., & Upchurch, D. R. (2003). Remote Sensing for Crop Management, 69(6), 647–664.
- Prasad, A. K., Chai, L., Singh, R. P., & Kafatos, M. (2006). Crop yield estimation model for Iowa using remote sensing and surface parameters, 8, 26–33.
- Pries, F., & Janszen, F. (2006). Construction Management and Economics Innovation in the construction industry : the dominant role of the environment Innovation in the construction industry : the dominant role of the environment, (March 2013), 37–41.
- Raeva, E. P., Šedina, E. J., & Dlesk, E. A. (2018). UAV photogrammetry techniques for precision agriculture. *Proceedings, 7th International Conference on Cartography and GIS 2018*, (June).
- Rakha, T., & Gorodetsky, A. (2018). Review of Unmanned Aerial System (UAS) applications in the built environment: Towards automated building inspection procedures using drones. *Automation in Construction*, 93(May), 252–264.
- Rao, B., Gopi, A. G., & Maione, R. (2016). The societal impact of commercial drones. *Technology in Society Journal*.
- Rathinam, S., Kim, Z., & Sengupta, R. (2006). Vision Based Following of Structures using an UAV, (March).
- Reg Austin. (2010). *Unmanned Aircraft Systems. Human Factors in Aviation*.
- Remondino, F., Barazzetti, L., Nex, F., Scaioni, M., & Sarazzi, D. (2012). Uav Photogrammetry for Mapping and 3D Modeling – Current Status and Future Perspectives. *ISPRS - International Archives of the Photogrammetry, Remote Sensing and Spatial Information Sciences*, XXXVIII-1/, 25–31.
- Roca, D., Lagüela, S., Díaz-Vilarinho, L., Armesto, J., & Arias, P. (2013). Low-cost aerial unit for outdoor inspection of building façades. *Automation in Construction*, 36, 128–135.
- Russo, M., Carnevali, L., Russo, V., Savastano, D., & Taddia, Y. (2018). Modeling and deterioration mapping of façades in historical urban context by close-range ultra-lightweight UAVs photogrammetry. *International Journal of Architectural Heritage*, 00(00), 1–20.
- Salvo, G., Caruso, L., & Scordo, A. (2014). Urban traffic analysis through an UAV. *Procedia - Social and Behavioral Sciences*, 111, 1083–1091.
- Sankarasrinivasan, S., Balasubramanian, E., Karthik, K., Chandrasekar, U., & Gupta, R. (2015). Health Monitoring of Civil Structures with Integrated UAV and Image Processing System. *Procedia Computer Science*, 54, 508–515.
- Santamarina-Campos, V., & Segarra-Oña, M. (2018). Drones and the Creative Industry. Springer International Publishing.
- Sebbane, Y. B. (2016). *Smart Autonomous Aircraft*. CRC Press.
- Sebbane, Y. B. (2018). *Intelligent autonomy of UAVS*. Chapman & Hall/CRC.

- SESAR. (2017). U-space blueprint - SESAR Joint Undertaking.
- Sheba, K. U., & Gladston Raj, S. (2018). Efficient Data Cleaning Algorithm and Innovative Unique user Identification Algorithm using Hashing and Binary..., (January).
- Siebert, S., & Teizer, J. (2014). Mobile 3D mapping for surveying earthwork projects using an Unmanned Aerial Vehicle (UAV) system. *Automation in Construction*, 41, 1–14.
- Stark, R. (2000). New technique for remote estimation of vegetation.pdf.
- States, U., & States, U. (2017). Evaluation of computer vision- and 4D BIM-based construction progress tracking on a UAV platform, 1–10.
- Stöcker, C., Bennett, R., Nex, F., Gerke, M., & Zevenbergen, J. (2017). Review of the current state of UAV regulations. *Remote Sensing*, 9(5), 33–35. <https://doi.org/10.3390/rs9050459>
- Taylor, P., Vygodskaya, N. N., Gorshkova, I. I., & Fadeyeva, Y. V. (1989). Theoretical estimates of sensitivity in some vegetation indices to variation in the canopy condition, (2007).
- Uysal, M., Toprak, A. S., & Polat, N. (2015). DEM generation with UAV Photogrammetry and accuracy analysis in Sahitler hill. *Measurement: Journal of the International Measurement Confederation*, 73, 539–543.
- Vacanas, Y., Themistocleous, K., Agapiou, A., & Hadjimitsis, D. (2015). Building Information Modelling (BIM) and Unmanned Aerial Vehicle (UAV) technologies in infrastructure construction project management and delay and disruption analysis, 9535, 1–11.
- Watts, A. C., Ambrosia, V. G., & Hinkley, E. A. (2012). Unmanned aircraft systems in remote sensing and scientific research: Classification and considerations of use. *Remote Sensing*, 4(6), 1671–1692.
- Wen, M.-C., & Kang, S.-C. (2014). Augmented Reality and Unmanned Aerial Vehicle Assist in Construction Management, 1570–1577.
- Winch, G. M. (2010). How innovative is construction ? Comparing aggregated data on construction innovation and other sectors – a case of apples and pears How innovative is construction ? Comparing aggregated data on construction innovation and other sectors – a case of apples, (March 2013), 37–41.
- Zhang, C., & Kovacs, J. M. (2012). The application of small unmanned aerial systems for precision agriculture : a review, 693–712.
- Zhang, W., Qi, J., Wan, P., Wang, H., Xie, D., Wang, X., & Yan, G. (2016). An easy-to-use airborne LiDAR data filtering method based on cloth simulation. *Remote Sensing*, 8(6), 1–22.
- Zheng, C., Breton, A., Iqbal, W., & Sadiq, I. (2015). Driving-Behavior Monitoring Using an Unmanned Aircraft System (UAS) Driving-Behavior Monitoring Using an Unmanned Aircraft System (UAS), (August).
- Zhou, G., Yang, J., Li, X., & Yang, X. (2012). Advances of Flash Lidar Development Onboard Uav. *ISPRS - International Archives of the Photogrammetry, Remote Sensing and Spatial Information Sciences*, XXXIX-B3(September), 193–198.

3. Three-dimensional reconstruction and segmentation using photogrammetry

Digital photogrammetry combined with the use of UAV allows simple and effective 3d reconstruction of large areas and objects.

In this chapter, an overview of digital photogrammetry techniques is presented as well as the state of the art of 3d reconstruction from images. Photogrammetry principles and Structure from Motion (SFM) and Multi-View Stereo (MVS) algorithm for the creation of point cloud are described, with focus on point cloud segmentation for the extraction of useful information from these objects. Moreover, starting from the consolidated workflow, a procedure for point cloud segmentation, that will be used for Bridge and viaduct surveying, using image analysis is described.

3.1 Photogrammetry: Description, principles and 3d reconstruction

Photogrammetry is a survey technique, in the science of Geomatics, belonging to the field of Remote Sensing (RS), that allows extracting *quantitative* information and data from photographs, recovering the exact **position, shape and dimension** of surface points (Schenk, 2005). For this reason, photogrammetry (derived from the three Greek words *Phos* = light, *gramma* = something drawn, *metrein* = measurement) can be defined as “the science of measuring photos”.

The geometric data can be extracted starting from the coordinate of any points in the photo. Obviously, from a single photo (two-dimensional plane) it is possible to extract only two-dimensional information, therefore, to extract three-dimensional information is necessary to use the so-called *stereoscopic view*, the same properties used by human vision to see objects spatially. The principle of triangulation, represented in Figure 43, allows the calculation of three-dimensional coordinates of any points, starting from two or more photos taken from different positions.

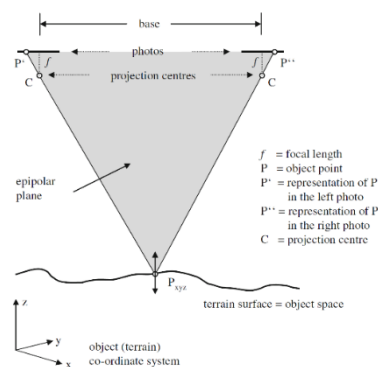


Figure 43 - Geometry in an oriented stereo model.

Reaching this objective, it is possible to digitise points, lines and areas for map production or calculate distances, areas volumes slope.

The significant advantages of photogrammetric techniques consist on the possibility to acquire information when it is not possible to reach the object or for large areas (e.g. image areas far away), or when the measure is needed without physical contact (e.g. archaeological finds). Aerial imaging is based on photogrammetry application: development of photogrammetry is in fact closely connected with that of aviation and photography thanks to their characteristics that perfectly fits on surveys need's. The first aerial cameras use a large film format sensor (230 by 230 mm) compared with full size of 24 by 36 mm (the original full-frame format of both analogue and digital camera sensor); the sensor was necessary to receive proper resolution on the photos. Furthermore, no lens change or zoom was used to provide high stability and proper lens correction. Nowadays consumer cameras, that can be used in photogrammetry with medium accuracy claim, have reached a high technical standard of good resolution and are available for low prices. Furthermore, digital photogrammetry and digital workflow for image elaboration has many advantages compared with traditional photogrammetry and has decreased time and cost for elaboration. For this reason the application in different field, from geoscience (Westoby et al., 2012) to engineering and industry is very convenient.

Also laser scanner equipment represents today a valid alternative, and sometimes a supplement, to photogrammetry to get three-dimensional point cloud with high accuracy (Baltsavias, 1999); however, this process is time-consuming and expansive compared with photogrammetric methods.

The result's quality of a photogrammetric survey is strictly affected by the sensors used to acquire data (Micheletti, Chandler, & Lane, 2015), and capture photo, but also influenced by different factors such as:

- **Sensor size:** defines the area that will be impressed by light. The big area corresponds to more light in the sensor and more detail and quality. The full format (that refers to the analogue film used in the analogue digital camera) is represented by the so-called "full-frame" format of 26 by 36 mm. In Figure 44, a comparison between different formats is represented.
- **Resolution:** number of pixels in the photo; this parameter should be compared with the sensor size; pixel size should not be less than $4\mu\text{m}$;
- **Photo acquisition parameters:** distance setting (focus), focal length, aperture: the maximum f-number (lens-opening) should not be less than 1:2.8; exposure time should have a range of at least 1..1/1000s and ISO lower as possible;

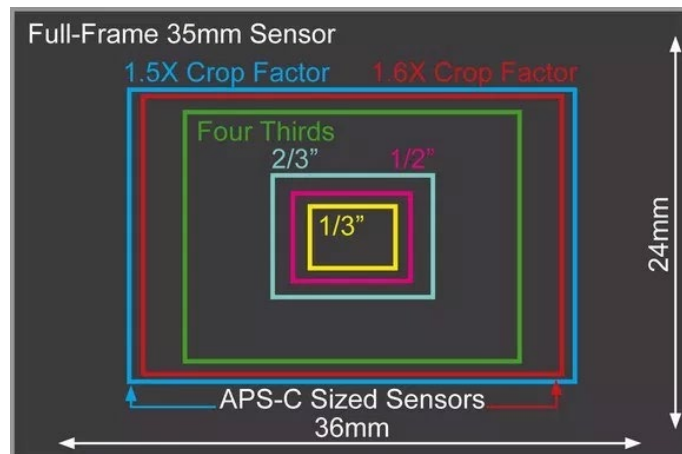


Figure 44 - Camera sensor sizes

- **Image format acquisition:** the digital format used to store the photos influence the number of information acquired. Different compression format (e.g. JPG) compress the photo cutting the information nonvisible to the human eye. Store the photo in non-compressed format (e.g. RAW) avoid and minimise the loss of quality.
- **Stabilisation:** stabilisation is a fundamental factor to stable guaranty image and photo analysis, avoiding blur effect.

3.1.1 Photogrammetry classification

Classification can be made according to different criteria such as output data, or according to the distance between the object and the camera. Traditional photogrammetry is based on paper support, while digital photogrammetry output is a digital representation of the surveyed object/area. According to the distance between the object and camera, the classification includes:

Micro-photogrammetry (60 cm)

The camera is located near the object and is used to acquire detailed information with mm level.

Close-range or terrestrial photogrammetry (1 m - 30 m)

In Terrestrial and Close-range Photogrammetry, the camera is located on the ground, and handheld, tripod or pole mounted. Usually, the output consists of drawings, 3D models, measurements, or point clouds. Everyday cameras are used to model and measure buildings, engineering structures, forensic and accident scenes, mines, earthworks, stockpiles, archaeological artefacts, film sets. In the computer vision community, this type of photogrammetry is sometimes called Image-Based Modelling.

UAV photogrammetry (30 m – 300 m)

UAV photogrammetry stays in between close range and aerial and it is performed thanks to the use of UAV to produce accurate map,

orthophotos 3d model of the target scene. The main advantages are related to the full flexibility, complete object coverage and cm-level accuracy. Specific information's are discussed in paragraph 3.2.

Aerial photogrammetry (from 300 m to 20.000 m)

In Aerial Photogrammetry, the camera is mounted on an aircraft and is usually pointed vertically towards the ground. Multiple overlapping photos of the ground are taken as the aircraft flies along a flight path. The aircraft traditionally have been fixed-wing manned craft, but many projects now are done with UAVs. Traditionally these photos were processed in a stereo-plotter (an instrument that lets an operator see two photos at once in a stereoview) but today are processed by automated desktop systems.

Satellite

The space photogrammetry embraces all aspects of the extra-terrestrial photograph, and subsequent measurement wherein the camera may be fixed on earth, contained in an artificial satellite, or positioned on the moon or a planet. The term photo interpretation is applied to that branch of photogrammetry wherein aerial or terrestrial photographs are used to evaluate, analyse, classify, and interpret images of objects which can be seen on the photographs. Consequently, photogrammetry must be considered as a combination of measurement and interpretation.

Features	Close-range	UAV	Conventional airborne
Capture geometry	Terrestrial horizontal and oblique views;	Full flexibility: nadir, oblique, horizontal, upwards;	Nadir (vertical), oblique
object visibility	facades/vertical faces	Complete object coverage	Land cover, terrain, roofs
Area coverage	Single objects	Single objects to approx. 0.15 km ² (multi-rotor) Single objects to approx. 0.45 km ² (fixed wing)	1- n km ²
Typical ground resolution per pixel (RGB camera)	in mm-range	in cm-range or less	> = 5 cm
Multitemporal acquisition	As often as needed	As often as needed, depending on weather Regulatory restrictions	Depending on weather and budget
Optical sensors	RGB, NIR, Thermal	RGB, Multispectral, Thermal, Hyperspectral	RGB, Multispectral, Thermal, Hyperspectral

Table 6 - Close range to Aerial photogrammetry comparison

3.1.2 Geometric photogrammetry principles

The relation between the camera position and the focal length influence the displacement and distortion of the captured photo. If the camera is far away from the object and if the angle would be as small as possible (super-telephoto) the projection rays would be nearly parallel, and the displacements near to zero. Image satellite belongs to this case. The opposite extreme case is photos taken with a fisheye lens which have an opening angle up to 180° , called whole-sky-system. The best case is to have a photo as distance as possible to minimise distortion; therefore aerial and terrestrial photos have a wide-angle camera that enhances the radial-symmetric displacement as pre-requisite to view and pairs image stereoscopically. The two fundamental steps in the photogrammetric process involve image orientation and camera position:

1. Image orientation

The first step in the reconstruction workflow is the reconstruction of the photo's orientation, to define the exact position of photos which are being used within the object (or terrain) coordinate system. The photo position is unequivocally defined from the information stored from the digital camera, such as coordinates of the projection centre and three rotation angles, as well as the camera's focal length. The first goal is to obtain six parameters of the exterior orientation (Figure 45).

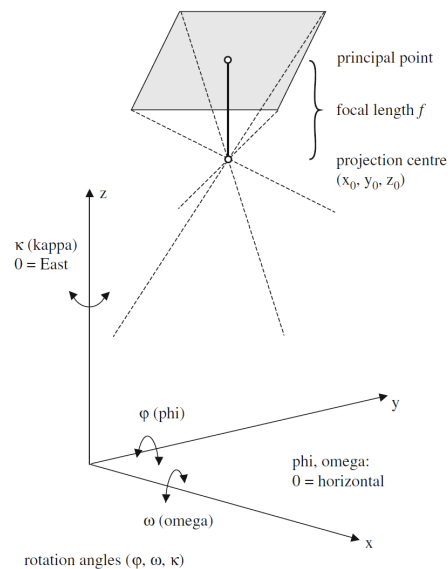


Figure 45 - Focal length, projection centre and rotation angle

In case of aerial nadir photos, the rotation angle related to x and y-axis will normally be near to zero. Subsequently the different coordinates systems (CS) must be defined: camera CS and three-dimensional object CS (usually a rectangle system, connected with an ellipsoid to define elevation). The relation between focal length f and height above ground h_g , is defined as “Mean photo scale M_b ”:

$$M_b = f/h_g$$

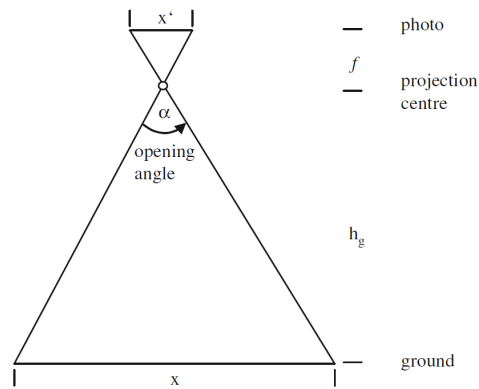


Figure 46 - Relation between focal length and height

2. Relative camera position

To get three-dimensional coordinates of an object, different photos taken from at least two different positions are needed. The point $P(x,y,z)$ is calculated as an intersection of two rays $[P' \rightarrow P]$ and $[P'' \rightarrow P]$ and the accuracy of the result depend among others from the angle between both rays. The smaller is this angle the less is the accuracy. The scheme for stereo camera position is represented in Figure 47: A is the distance between the point P and the camera, and B is the distance between both cameras. The angle between both projection rays depends on the ratio A/B (in the aerial case called the *height-based ratio*); the accuracy of the acquisition increases increasing distance B. For surface reconstruction the parallel case Figure 47 (a) is suitable for surface reconstruction while the convergent case Figure 47 (b) often leads to higher precision, especially in the z-direction.

For aerial photogrammetric acquisition, the strip scheme is used as represented in Figure 48:

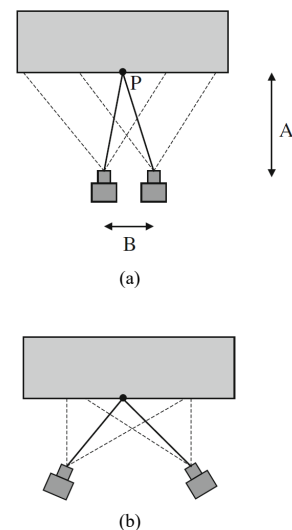


Figure 47 – Parallel (a) and convergent (b) camera position

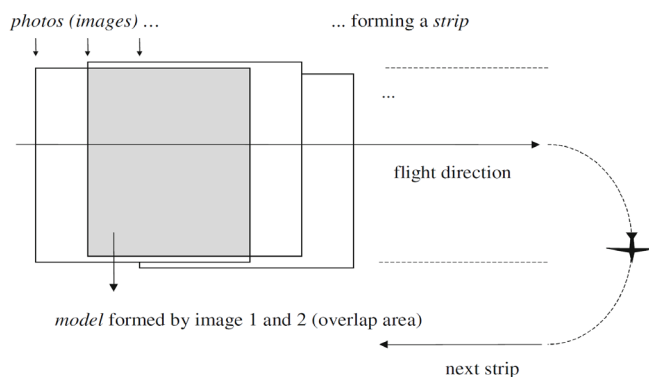


Figure 48 – Aerial photogrammetric strip reconstruction

The strip represents all overlapping images taken subsequently within one flight line. Block all the images of a strip, the base distance

between the projection centres of neighbouring images are translated to acquire the subsequent strip.

3.2 UAV in Aerial photogrammetry

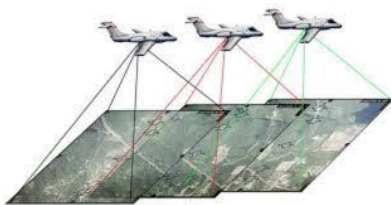


Figure 49 – Aerial photogrammetry survey

The aerial photogrammetry can be considered as the principal means through the photogrammetry has developed. It was the fundamental data source for making maps by photogrammetric means. In last years the use of UAS from military to geomatics field became common thanks to the application in the close-range aerial domain, representing a cheap alternative to manned aerial photogrammetry. As discussed in chapter 1 this rapid development can be explained by the spreading of a low-cost platform combined with digital cameras and GNSS system, and the rising of digital photogrammetry (Linder, 2016). Today the use of UAS compared with traditional airborne platform (Figure 49) decrease the operational costs, reduce the risk of access in harsh environment and still maintain high accuracy potential (Remondino et al., 2012). Moreover, the use of VTOL UAV, without the need of runway to take-off, allows to quickly derive high temporal and spatial resolution images in rapid response to the emergency when critical information is needed.

Using aerial photogrammetry with UAV it is also possible to obtain a map, digital model of surface and 3d data of the surveyed area (Colomina & Molina, 2014, Nex & Remondino, 2014).

3.3 Photogrammetric Algorithms for 3d reconstruction: SFM-MVS

Photogrammetric principles and algorithms allow, as discussed, the reconstruction of 3d scene starting from different images acquired respecting stereographic criteria. The use of computer vision for the implementation of photogrammetric algorithms allows a reliable generation of valuable 3d point cloud from 2d imagery. *Structure from Motion* is the most reliable algorithm used both from open-source and commercial computer vision software.

Structure from motion (SFM) is a topographic survey technique that has emerged from advances in computer vision and traditional photogrammetry since the 1980s with the development of software GUI (Graphical User Interface). It can produce high-quality, dense, three-dimensional point clouds of a scene/area with a minimal financial cost.

In contrast to traditional photogrammetry, *SFM* uses an algorithm to identify matching features in a collection of overlapping digital images and calculates the camera location and orientation from the differential position of multiple matched features (Figure 50).

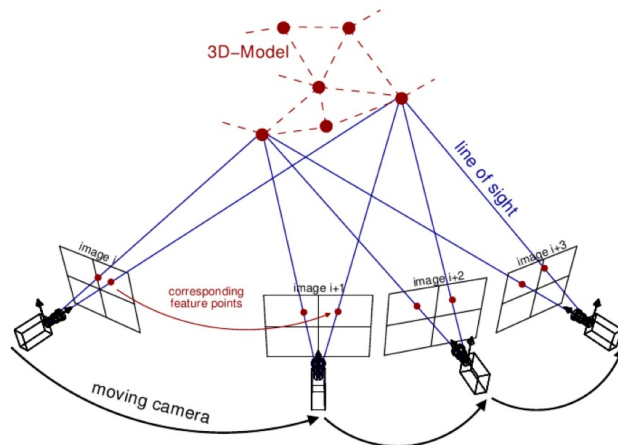


Figure 50 - 3d reconstruction detecting camera position

Based on these calculations overlapping imagery can be used to reconstruct a “sparse” 3d point cloud model of the acquired scene. Later the model from SFM is refined to a much more excellent resolution using **Multi-Stereo-View** methods, with cheap hardware and software and fast times compared with other digital surveying techniques.

The application of SFM in geoscience field, geomatics and survey recently spread thanks to the significant advantages and applicability combined with new technologies. Today the use of SFM in geoscience became relevant thanks to the emergence of affordable commercial user-friendly software and rapid developments of UAVs. The impact of SFM is arguably going to be higher than that associated with airborne Light Detection and Ranging (Lidar) because this technique and developed technology democratise data collection and development of fine-resolution 3d models at all scales. With photogrammetry, to produce advanced data products, very little input data are required: as little as a photo set from an uncalibrated, compact and often cheap, camera.

3.3.1 SFM-MVS workflow for 3d reconstruction

SFM, as applied in geoscience and survey is more than a single technique, is a workflow employing multiple algorithms developed from traditional photogrammetry, survey techniques and three-dimensional (3d) computer vision. The full workflow is known as Structure from Motion Multi-View Stereo (SFM – MVS) to account for the Multi-View stereo algorithms used in final stages. Different open-source softwares are available for free (e.g. MicMac (Rupnik et al.,

2017)) and also many commercial SfM-MVS software packages that do not detail specific procedure applied to solve the problem. This paragraph aims to understand the basic concept for 3d reconstruction starting from uncalibrated imagery; for a deep understanding of mathematical formulas the interested reader can find relevant information on (D.G. Lowe, 1999, David G Lowe, 2004). The basic process to reconstruct the 3d scene geometry from a set of images where the extrinsic and intrinsic calibration parameters are unknown, could be divided into three main steps:

- 1) Image analysis for and matches for estimation of unknown camera parameters;
- 2) Application of Structure from Motion (SfM) algorithm and
- 3) Multi-View Stereo for 3d dense cloud generation.

The detailed workflow for 3d reconstruction (Snavely et al., 2008) is summarised as follows (Figure 51)

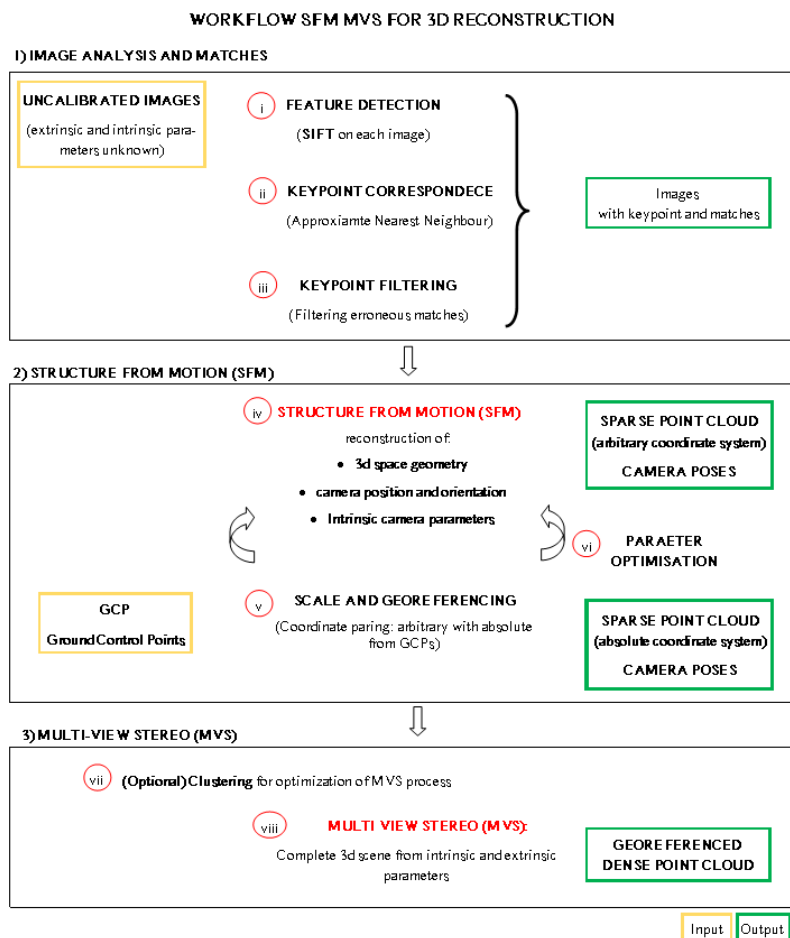


Figure 51 - SfM MVS workflow for 3d reconstruction

1) Image analysis and matches

- (i) Detection of image features on the key point
- (ii) Keypoint correspondence between different images
- (iii) Identification of geometrically consistent matches

2) SFM

- (iv) “SFM” of simultaneously estimating 3d scene geometry: **camera pose** and **internal camera parameters** through bundle adjustment,
- (v) Scaling and georeferencing of the resultant scene geometry
- (vi) Optimisation of the identified parameters in the bundle adjustment using known Ground Control Points (GCP)

3) MVS

- (vii) Clustering image sets for efficient processing
- (viii) Application of MVS algorithms

(i) Feature detection (SIFT algorithm)

The fundamental question driving the development of feature detection was how to best extract descriptors of local points from images, in a way that those points were invariant to changes in orientation, scale, illumination or 3d position. This first step involves the identification of common point (**key point**) on several different photographs, allowing different images to be matched and the scene geometry reconstructed. Many different techniques to identify key points have been developed based on matching image statistics (Lucas & Kanade, 1981), identify corner like features, or later by using eigenvalues of smoothed outer products of the gradient (Mikolajczyk & Schmid, 2005). In order to match points from different viewing angle for wide baseline matching, it is necessary to detect **feature points** (e.g. a set of pixels) that are invariant to changes in orientation, scale and light condition. For this purpose, different detectors and feature type are available (Mikolajczyk & Schmid, 2005) but the **Scale Invariant Feature Transform (SIFT)** (D.G. Lowe, 1999) is used most widely, thanks to its robustness against changes in 3d viewpoint for non-planar surface (David G Lowe, 2004). This algorithm follows four major stages:

1. **Detection of spatial extrema.** The first step involves the efficient identification of location and scales that can be assigned to the same object from different viewpoints. The approach used, a space-scale, detects locations that are invariant to scale changes by searching stable features across a continuous function of scale; after a monochrome intensity image is convolved with a Gaussian function incrementally at different scales, the difference between consecutive Gaussian

images are subtracted. The preferred sampling frequency in both scale and space is analysed, detecting most of the stable and useful features.

2. **Keypoint localisation.** SIFT perform a precise fit of a 3d quadratic function for each candidate keypoint to nearby data for location, scale, and the ratio of principal curvatures. A large number of key points are identified, removing the points that may have low contrast, or poorly localised along an edge (with high ratio of principal curvatures) (Figure 52). The density of keypoint identified on the image depends on the resolution of image, texture and sharpness.

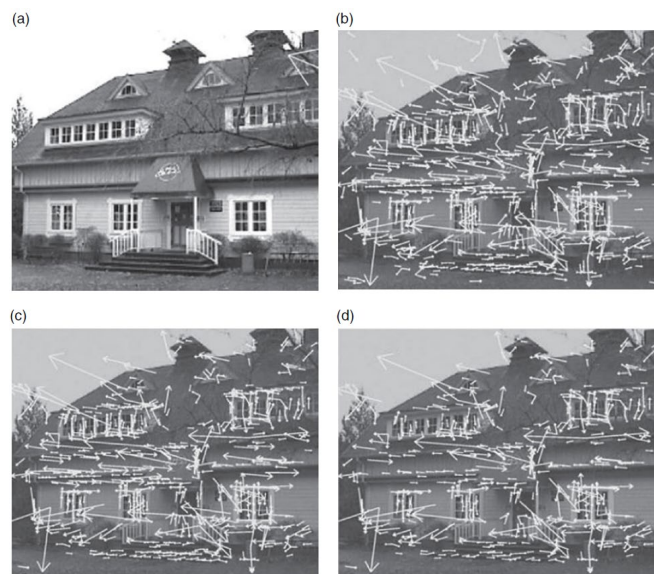


Figure 52 - Stages of keypoint localization (b) and reduction (c) for final result (d)

3. **Orientation assignment.** A consistent orientation for each key point is assigned through analysis of dominant directions of local intensity gradients using the Gaussian-smoothed image closest to the scale of the key point. A second peak in the orientation histogram is identified (within 80% of the highest peak) a second key point is created at that location and scale but with a different orientation.
4. **Keypoint descriptor.** Finally, a descriptor for each key point is required that is sufficiently distinctive yet is as invariant as possible to changes in 3d viewpoint or illumination. Gradient magnitudes and orientation are sampled around each keypoint, rotated relative to the key point orientation. A Gaussian weighting function is applied to these gradients to avoid large gradients far from the centre of the descriptor determining the specific descriptor. The resulting descriptor has been shown to discriminate individual key points from large databases.

(ii) Keypoint correspondence

One point has been detected and located in each image, correspondence between key points in different images need to be determined, considering that there is no guarantee that any given keypoint will have a partner in another image. Moreover, it is necessary to discard points with no good match. Working on 128-dimension keypoint data of the SIFT, the algorithm used the ratio of the Euclidean distance of the *nearest neighbour* with that of the second nearest, specifying a minimum value of 0.8. The “distance ratio” criterion was observed to eliminate 90% of false matches while discarding only less than 5% of correct matches. The complexity of keypoint descriptors and the typically large number of key points mean that performing an exhaustive brute-force Euclidean nearest neighbour search in such high-dimensional space is both challenging and computationally expensive. An efficient solution to this problem has been k-dimensional trees (or k-d trees), that at each level, points into the bin using a different dimension, often splitting the data using the median value as a splitting point. The resulting nearest neighbour search works recursively, and the advantage of the data is that it quickly eliminates a vast region of the search space. However, owing to the “curse of dimensionality”, problems arise with high dimensional spaces of complex keypoint descriptors. For this reason, Lowe notes that cutting off the Approximate Nearest Neighbour (ANN) search after only checking the first 200 nearest-neighbour candidates provides a considerable time saving while only losing less than 5% of correct matches.

(iii) Identify geometrically consistent marches

Another step is applied to filter out any remaining erroneous matches, to maintain only the correct correspondence. With multiple key points identified in a pair of images of the same scene, the **fundamental matrix (F-matrix)** for the image pair is calculated. The F-matrix, specifying the relationship between the two images, constrains the location of correctly identified key points in both images and can be calculated using the eight-point algorithm. This algorithm using eight-point matches on two uncalibrated views, and a set of a linear equation to reconstruct a scene up to a projective transformation where all points lying on a single line will remain aligned in this way. Using the Random Sample Consensus Methods (RANSAC) candidate f-matrix are calculated over several iterations; this method that is fast, accurate and robust, assumes that all key points can be divided into two sets: outliers and inliers. A perfect model will ignore all outliers and would be computed exclusively from inliers. The threshold of the maximum image dimension should be 0.6%. Other approaches are available and used in different software, indeed, RANSAC has been shown to perform poorly when outliers are many grates in number than inliers as they can distort a fitting process.

With the key points limited to those with geometrically compatible matches, the links between every image pair can be identified and organised into tracks: connected sets of matching key points through the library of images used in the reconstruction; a minimum of two keypoint located in three images are required for a track. Maps of consistent tracks can then be made, identifying the connectivity of each image.

(iv) Structure from Motion (SFM)

While the entire workflow is commonly called Structure from Motion, SFM is the single process of simultaneously estimating the 3d scene structure, camera position and orientation, and often intrinsic camera calibration parameters. The intrinsic camera parameters (required to model internal aberrations), can be described by different camera models; instead, the *extrinsic camera parameters* (camera position and orientation) represent the rigid body transformation between the 3d scene coordinates and the camera coordinate system.

Bundle adjustment produces a jointly optimal 3d structure and viewing parameter estimate. The parameters estimate that applies to both structures and camera variations are made by minimising the value of a cost function that quantifies the model fitting error.

The SFM process produces a sparse point cloud and reconstructed camera poses, and through further processing, it is possible to obtain more detailed higher-quality surface reconstruction (applying MVS techniques to produce a detailed dense point cloud).

(v) Scale and georeferencing

The generated point cloud through SFM process (that provides relative camera location and scene geometry), is generated in an arbitrary coordinate system. Absolute distances between cameras or between reconstructed points can never be recovered from images alone, regardless of how many camera points are used (Szeliski, 2011). Georeferencing and scaling the obtained point cloud requires a minimum of three ground control points (GCPs) with XYZ coordinates for a seven-parameter linear similarity transformation, which includes three global translation parameters, three rotation parameters and one scale parameter. Alternatively, georeferencing and scaling can be performed in a “direct” method from known camera position derived from Real-Time Kinematic (RTK) differential GPS measurement and the Internal Measurement Unit (IMU) of the vehicle. A conventional hybrid approach (used with UAV) of the two existing methods, uses direct georeferencing to provide approximate camera location to initialise bundle adjustment and then uses external GCPs to better constrain the solution (Ryan et al., 2015, Rippin et al., 2015). Moreover, many SFM MVS software allows the user to locate the target from the imagery directly. The arbitrary coordinates of the targets from the SFM-

MVS model are paired with the absolute coordinates of the GCP's and used to derive a similarity transformation.

(vi) Refinement of parameter values (optimisations for image alignment)

This process consists on the recalculation of the intrinsic and extrinsic parameters using the information derived from the GCPs. The input of the previous step, in fact, provides additional information on the 3d geometry that can be used to further reconstructed geometry and refine camera parameters. Errors in the estimate of the intrinsic and extrinsic camera parameters arising from the previous process (SFM) can lead to non-linear deformation of the final model. Moreover, the known coordinates provide an additional source of error in the minimisation of the non-linear cost function during the bundle adjustment step. With this external information included in the model, the bundle adjustment can be re-executed to optimise the image alignment with this new information. The spatial distribution of the GCPs influences the optimisation process, where no GCPs do not adequately cover the area of interest and optimisation may be detrimental to the overall survey accuracy.

(vii) Clustering for MVS

The workload and computational resource consumptions are highly related with the amount of data (images) that the system has to process; when the number of images increases, the computational burden of such approach and memory increases rapidly, place a practical limit on the number of images that can be matched simultaneously. The solution of this problem is *Image clustering*, splitting a large project into different chunks, and at the end of the MVS process merging all together with the results in a single 3d point cloud. Commercial Software packages like Agisoft Photoscan (Agisoft LLC, St. Petersburg, Russia), Reality Capture (Capturing Reality s.r.o., Bratislava, Slovakia) allows the user to manually identify chunks of images to speed-up the MVS process and reduce memory requirements. Moreover, some MVS algorithms solve a depth map for each image in turn and then merge the separate reconstruction. This solution permits process parallelisation but at the expense of highly redundant depth maps that require further post-processing to clean and merge. In contrast, the best-performing MVS algorithms reconstruct the overall scene geometry using images simultaneously.

(viii) MSV image marching algorithms

The Multi-View Stereo process produces a much denser cloud then the sparse point cloud generated by SFM (at least two orders of magnitude denser). The goal of this process is to provide a complete 3d scene reconstruction starting from a collection of images with intrinsic and

extrinsic parameters (already calculated in the previous process, with SIFT and SFM).

There is a wide variety of MVS algorithms (SIETZ et al.2006), from Computer Vision research, that can be basically divided into four classes:

1. *Voxel-based methods* represent the 3d scene volume directly using voxel occupancy grids (S.M. Seitz e C.R. Dyer, 1997). Limited in accuracy by the resolution of the grid, these methods require the knowledge of the bounding box that contains the scene.

2. *Surface evolution-based methods* use deformable polygonal meshes that are iteratively evolved to minimise a cost function (Furukawa & Ponce, 2009) but require an initialisation that limits their applicability.

3. *Depth-map merging methods* compute individual depth maps for each image which are then combined into a single 3d model (Li et al., 2010). The use of a depth map (an image representing the distance from the viewpoint to the 3d scene object) made these algorithms very accurate for crowded scenes.

4. *Patch-based methods* represent scenes by a collection of small patches (Lhuillier et al., 2005), which are both simple and effective and do not require initialisation.

A *patch-based MVS* (PMVS) algorithm, divided into three steps (Matching features, expanding patches and Filtering incorrect matches) has been developed by (Furukawa & Ponce, 2009). This algorithm performs well compared with MVS.

A non-exhaustive list of SFM software available is shown in Table 7.

Software	Application	Type	Developed by	OS
3DF Zephyr	Aerial, Close-Range	Proprietary	3d flow Srl Italy	Windows
Agisoft Metashape (Photoscan)	Aerial, Close-Range	Proprietary	Agisoft LLC, Russia	Windows, macOS, Linux
Autodesk ReCap	Aerial, Close-Range	Proprietary	Autodesk Inc, USA	Windows
Bentley ContextCapture	Aerial, Close-Range	Proprietary	Bentley Inc, USA	Windows
Bundler	Research / demonstrative	Open-source	University of Washington	Windows
COLMAP	Aerial, Close-Range	Open-source	GPL licensed	Windows, macOS, Linux
DroneDeploy	Aerial	Proprietary	DroneDeploy, USA	Windows, macOS, Android, iOS
IMAGINE Photogrammetry	Aerial	Proprietary	Hexagon AB, Sweden	Windows
iWitnessPRO	Aerial, Close-Range	Proprietary	DCS Inc, WA	Windows
Microsoft PhotoModeler	Aerial, Close-Range	Proprietary	Microsoft, USA	Windows
Meshroom	Aerial, Close-Range	Open-source	IMAGE research team, EU	Windows, Linux
MicMac	Aerial, Close-Range	Open source	Institut national de l'information géographique et forestière, France	Windows, macOS, Linux
Open Drone Map	Aerial, Close-Range	Open-source	Community	Windows, macOS, Linux
OpenSFM	Research / demonstrative	Open source	OpenCV, Simplified BSD license	Windows, macOS, Linux

OpenMVG	Research / demonstrative	Open source	Community	Windows, macOS, Linux
Photomodeler	Aerial, Close-Range	Proprietary	Photomodeler Technologies, Canada	Windows
Python Photogrammetry Toolbox GUI	Research / demonstrative	Open-source	Pierre Moulon and Arc-Team	Windows, macOS, Linux
Pix4D	Aerial	Proprietary	Pix4d S.A., Switzerland	Windows, macOS, Android, iOS
SFM tool for Matlab	Research / demonstrative	Open-source	Vincent Rabaud	Windows, macOS
Multiple View Geometry function for Matlab	Research / demonstrative	Open-source	Andrew Zissermann	Windows, macOS
RealityCapture	Aerial, Close-Range	Proprietary	Capturing Reality sro, Slovakia	Windows
VisualSFM	Aerial, Close-Range	Open-source	Changchang Wu	Windows, macOS, Linux

Table 7 - Software and library for SFM-MVS

It should be considered that while open source software generally offers greater transparency, source code and use different algorithms, commercial software does not release information of algorithms used (that can be sometimes proprietary). However, the general workflow and basic algorithms commonly used are well synthesised by the described workflow summarised in Figure 51.

Also, the continuous evolution of computer vision techniques, development and refinement of algorithms in the different process steps suggest that further improvements will be implemented very quickly, reducing memory consumption, increasing elaboration speed and point cloud density and accuracy (Brook, 2017).

3.4 Point cloud classification

Currently, analytical tools, such as the algorithm for acquisition and software for the generation and manipulation of the photogrammetric data, are well developed by scientists. However, these methods are highly empirical and both quantitative and qualitative data rely on analysts. Consequentially replication of the current results can be difficult. For this reason, to ensure data quality and result's accuracy, researchers are focusing on standardisation and protocol for information extractions and the integration in the complete process workflow.

The output of the photogrammetric reconstruction process (and also from Lidar acquisition) consists of a 3d point cloud of the captured environment with million or billion points. Despite the board availability of point cloud, there is still a relevant need for an automatic method and integrated workflow to extract valid information and provide 3d data with meaningful attributes. Features like geometry and material properties provide significance to the objects represented in 3d,

adding value to the entire reconstruction process. Automated or semi-automated procedures decrease operator time and speed-up the entire workflow. *Point cloud analysis* is at its infancy, and today different techniques and algorithms exist to treat this type of data; in particular, point cloud segmentation and classification are very active research topics. *Segmentation* is the process of grouping point clouds into multiple homogeneous regions with similar properties (such as geometric, radiometric), while *classification* is the definition and assignments of point to specific classes, called “labels”, according to different criteria. These two processes allow relevant information’s extraction from the acquired data. Moreover, outlier elimination, spatial analysis and object simplification are other active research fields.

It is essential to consider that while the output of Lidar and photogrammetric acquisition is the same, the generated point cloud can be very different in terms of accuracy, resolution and information, due to the different nature of the acquisition technique. In chapt.4 different survey methods and instruments will be detailed and compared. For Lidar point cloud the American Society For Photogrammetry and Remote Sensing (ASPRS) proposed in “Las Specification” (Sensing, ASPRS 2013) different standardised classes in which the objects in point cloud can divide (Table 8). These classes are also valid for the photogrammetric point cloud.

Classification value	Meaning
0	Never classified
1	Unassigned
2	Ground
3	Low Vegetation
4	Medium Vegetation
5	High Vegetation
6	Building
7	Low Point
8	Reserved
9	Water
10	Rail
11	Road Surface
12	Reserved
13	Wire - Guard (Shield)
14	Wire - Conductor (Phase)
15	Transmission Tower
16	Wire-Structure Connector
17	Bridge Deck
18	High Noise
19-63	Reserved
64-255	User Definable

Table 8 - ASPRS point cloud class

To extract relevant information from point cloud it is necessary to segment and classify the interesting object inside the acquired scene. There are multiple research studies related to these two topics, provided by the different field of application (cultural heritage, building modelling, heritage documentation, robotics). A non-exhaustive review of segmentation and classification methods is presented in (Ozdemir & Remondino, 2018).

Segmentation methods can be subdivided into five main classes (Nguyen & Le, 2013), according to the segmentation criteria (Figure 53).

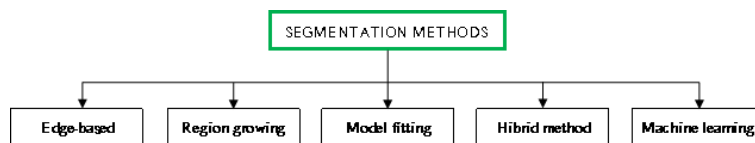


Figure 53 - Point cloud segmentation methods

Edge-based segmentation (Rabbani et al., 2006) use algorithms for edge detection to outlines the borders of different region and to group points inside the boundaries to deliver final segments. *Region growing* methods start from one or more points featuring specific characteristics and then grow around the neighbouring point with similar characteristics such as curvature, surface orientation etc.. (Rabbani et al., 2006). *Segmentation by model fitting* is based on the observation that many human-made objects can be decomposed into geometric primitives like planes, sphere and cylinders. Primitive shapes are then fitted onto point cloud data and the points that conform to the mathematical representation of the primitive shaper are labelled as one segment. *Hybrid segmentation technique* uses a combination of more methods combined; the accuracy depends on the target scene and objects. Finally, *Machine learning methods* are based on classification performed by machine learning algorithms (including deep learning on neural network (Zeiler & Fergus, 2014)). Machine learning is a specific discipline of computer vision that using Artificial Intelligence algorithms allows the computer to make decisions based on empirical and trained data. Learning that allows the computer to take decision can be unsupervised or supervised (and reinforcement learning): unsupervised learning is a class of problems in which one seeks to determine how the data are organized. In supervised learning, data are provided “labelled” to make the machine learn how to perform a task correctly. Dataset and features play a reasonably significant role in the use of machine learning because these methods are based on the quantity and quality of the input data. Review of machine learning techniques applied to semantic segmentation of images and on 3d data is presented in (Garcia-Garcia et al., 2017). One of the more accurate

and large dataset for 3d segmentation using Neural Network is 3d PointNet (Qi et al., 2017), developed by Stanford University.

Subsequently, **Classification** of each segmented points can be achieved using three different approaches:

- *supervised approach*, where semantic categories are learned from a dataset of annotated data and the trained model is used to provide a semantic classification of the entire dataset.
- *Unsupervised approach* where data is automatically partitioned into segments based on a user-provided parametrisation of the algorithms
- *Interactive approach* where the user is actively involved in the segmentation/classification loop by guiding the extraction of segments through feedback.

Most of these segmentation algorithms are tailored to work with the 2,5D surface model assumption, provided by Lidar-based survey, or analysis on 3d space.

In this work, to perform 3d point cloud segmentation of specific object and scene, for aerial survey of infrastructure (such as bridges and viaducts), an approach based on 2d-image analysis using machine learning is presented. The procedure is based on segmentation of the image in the dataset using image analysis transferring and projecting this information on the 3d point cloud. Image classification and segmentation techniques are well developed and consolidated, algorithms are mature, and with proper training dataset, the high precision accuracy level is reachable (Lokanath et al., 2017). The technique used to highlight an object and create an alpha mask around it on the image is *instance segmentation*. The object recognition can be split into four different methodologies (Figure 54):

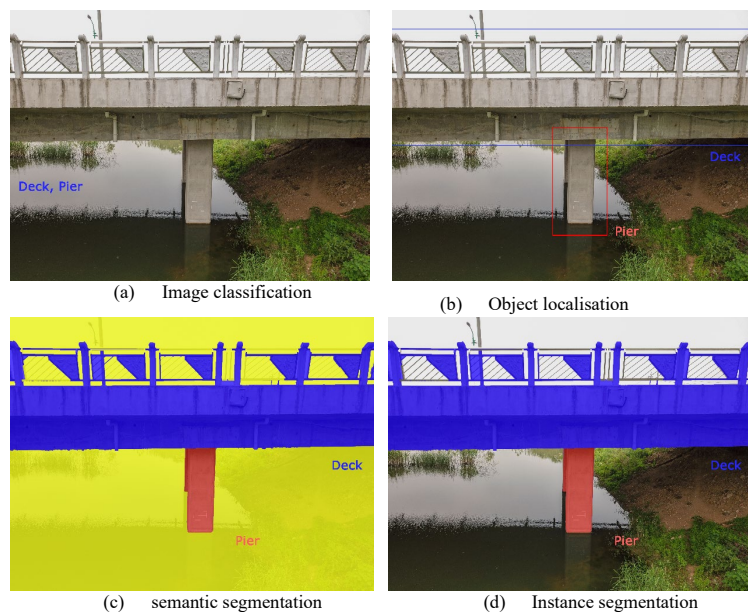


Figure 54 - Object recognition and scene understanding

- a) **Image classification** is used to predict a set of labels to characterise the contents of an input image;
- b) **Object detection** builds on image classification but allows to localise each object in an image. The image is now characterised by 1. Bounding box (x,y coordinates) for each box 2. An associated class label for each bounding box
- c) **Semantic segmentation** algorithms require to associate every pixel in an input image with a class label (including a class label for the background). While semantic segmentation algorithms are capable of labelling every object in an image, they cannot differentiate between two objects of the same class. This behaviour is especially problematic if two objects of the same class are partially occluding each other, we have no idea where the boundaries of one object end and the next one begins.
- d) **Instance segmentation** algorithms compute a pixel-wise mask for every object in the image, even if the objects are of the same class label. The algorithm not only localised each object but predicted their boundaries as well.

Instance segmentation is well performed using Mask-RCNN (Convolutional Neural Network) (He et al., 2017) architecture that enable to segment complex objects and shaper from images and was built on previous object detection work of *R-CNN* (Girshick et al., 2014) *Fast R-CNN* (Girshick, 2015) and *Faster R-CNN* (Ren et al., 2017). With adequate labelled data, Mask-RCNN allows the automatic segmentation and construction of pixel-wise masks for every object in a given image: in infrastructure survey, the model is trained to perform structure recognition and split the different structural part, such as deck and piers as shown in Figure 55.

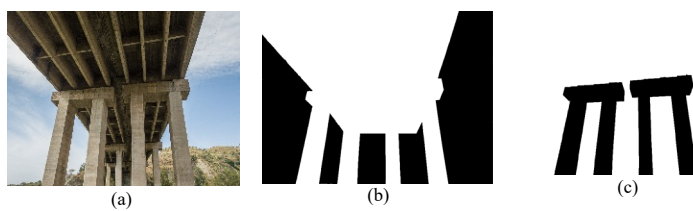


Figure 55 - Mask R-CNN for bridge (b) and piers (c) segmentation

The main objective is to start with an acquired aerial picture (Figure 55 a), isolate the structure from the background as shown in (Figure 55 b) and identify and split viaduct simple structural part such as piers (or deck) from the rest of the structure (Figure 55 c). The deck is univocally obtained from the subtraction of the pier mask (Figure 55 c) from overall structure mask (Figure 55 b) or vice-versa.

Image segmentation and labelling can be obtained using a trained neural network able to recognise the object. The workflow to perform the train starting from few datasets is presented in Figure 56. Starting from the

image dataset, selecting significant images, a training dataset is created.

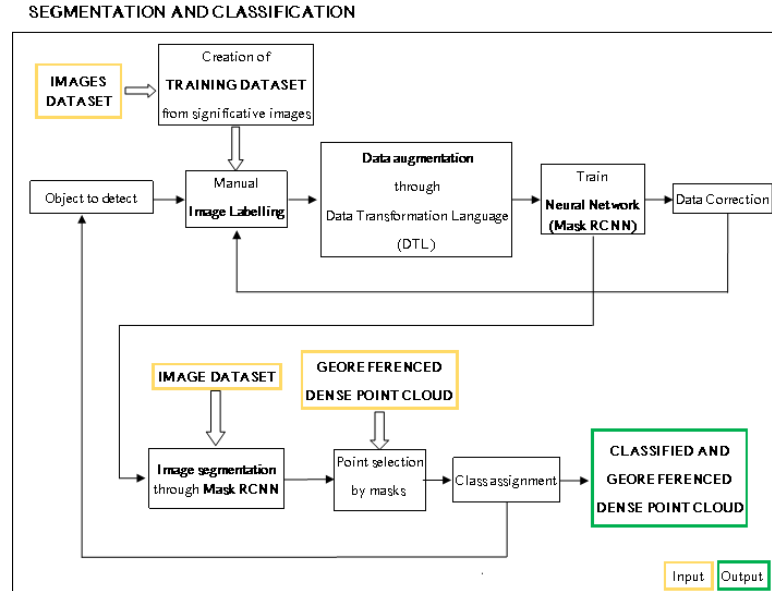


Figure 56 - Segmentation and classification process

The training dataset, after the adequate manual annotation of the object through the labelling process, is used to train the model to recognise the object in the images. Labelling operations are easily performed on a sample training dataset of significant images, which is then augmented using Data Transformation Language (DTL). Simple operation of scaling, rotating and mirroring the images the augmentation of the labelled image in the dataset. This dataset is then used to train Mask RCNN neural network. The results are then corrected and reported on the training dataset performing the iterative process until the accuracy needed in the results is acceptable.

The segmentation is then applied to the entire dataset creating one mask for each image (Figure 57), according to structural parts identified. 2d masks are then applied to identify the point on the 3d point cloud, using the “Selection of point by masks”.

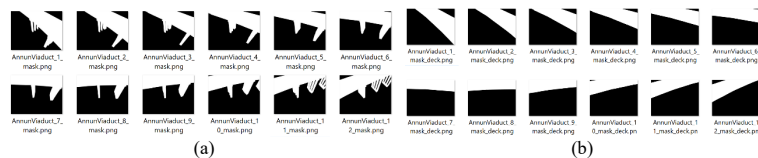


Figure 57 - Classified dataset with an alpha mask on overall structure (a) and deck (b)

Point cloud semantic classification is subsequently made assigning the selected point to the different class according to the 2d classification. The results of classification method applied to a sample dataset are shown in Figure 58 with coloured point cloud (a), and

classified point (b) cloud with deck highlighted in purple and pier highlighted in red.



Figure 58 - Colorized 3d point cloud (a) and classified 3d point cloud (b)

The quality and precision of the segmentation and classification strictly rely on the accuracy of the trained model in order to fit at the pixel-wise level the masks around the structure needed.

The overall workflow for 3d reconstruction from images, including the image classification and segmentation, is synthesised in Figure 59.

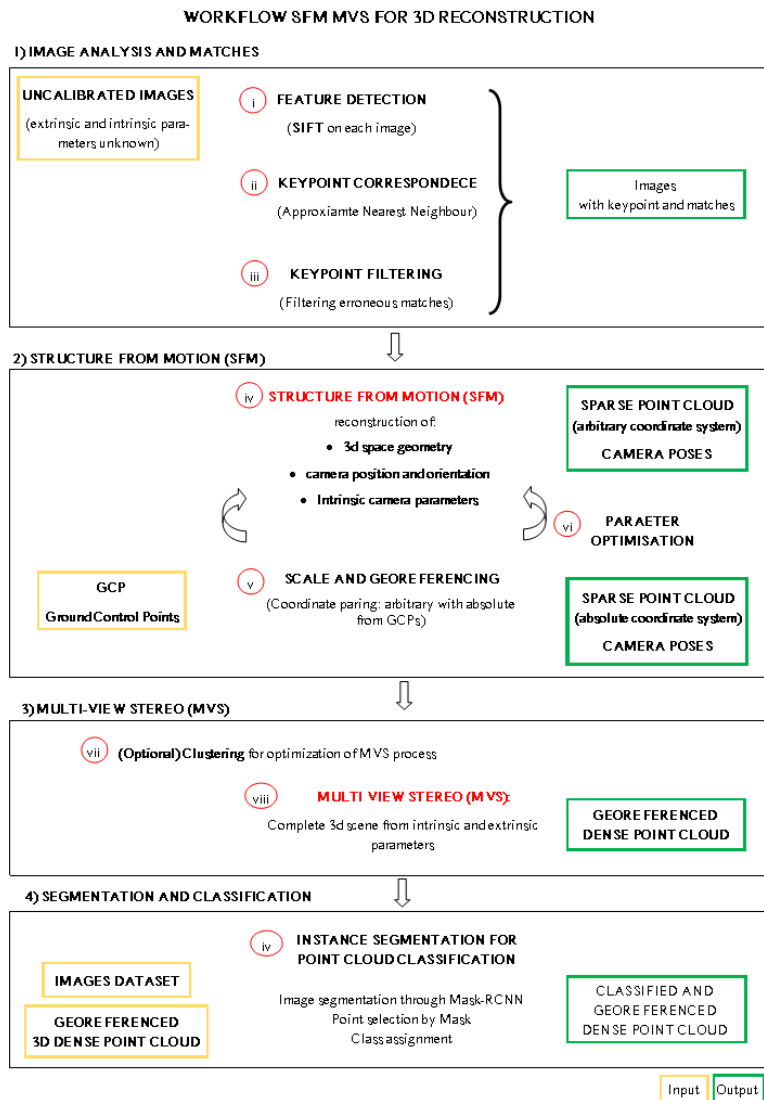


Figure 59 - Complete workflow for Point cloud reconstruction and classification

References

- Baltsavias, E. P. (1999). A comparison between photogrammetry and laser scanning. *ISPRS Journal of Photogrammetry and Remote Sensing*, 54(2–3), 83–94.
- Brook, M. (2017). *Structure from motion in the geosciences*. New Zealand Geographer (Vol. 73). Wiley Blackwell.
- Colomina, I., & Molina, P. (2014). Unmanned aerial systems for photogrammetry and remote sensing: A review. *ISPRS Journal of Photogrammetry and Remote Sensing*, 92, 79–97.
- Furukawa, Y., & Ponce, J. (2009). Carved visual hulls for image-based modeling. *International Journal of Computer Vision*, 81(1), 53–67.
- Garcia-Garcia, A., Orts-Escolano, S., Oprea, S., Villena-Martinez, V., & Garcia-Rodriguez, J. (2017). A Review on Deep Learning Techniques Applied to Semantic Segmentation, 1–23.
- Girshick, R. (2015). Fast R-CNN. *Proceedings of the IEEE International Conference on Computer Vision, 2015 Inter*, 1440–1448.
- Girshick, R., Donahue, J., Darrell, T., & Malik, J. (2014). Rich feature hierarchies for accurate object detection and semantic segmentation. *Proceedings of the IEEE Computer Society Conference on Computer Vision and Pattern Recognition*, 580–587.
- He, K., Gkioxari, G., Dollar, P., & Girshick, R. (2017). Mask R-CNN. *Proceedings of the IEEE International Conference on Computer Vision, 2017-October*, 2980–2988.
- Lhuillier, M., Quan, L., & Member, S. (2005). A Quasi-Dense Approach to Surface Reconstruction from Uncalibrated. *IEEE Transactions on Pattern Analysis and Machine Intelligence*, 27(3), 418–433.
- Li, J., Li, E., Chen, Y., Xu, L., & Zhang, Y. (2010). Bundled depth-map merging for multi-view stereo. *Proceedings of the IEEE Computer Society Conference on Computer Vision and Pattern Recognition*, (March 2014), 2769–2776.
- Linder, W. (2016). *Digital Photogrammetry* (Fourth Edi). Springer.
- Lokanath, M., Kumar, K. S., & Keerthi, E. S. (2017). Accurate object classification and detection by faster-RCNN. *IOP Conference Series: Materials Science and Engineering*, 263(5).
- Lowe, D.G. (1999). Object recognition from local scale-invariant features. *Proceedings of the Seventh IEEE International Conference on Computer Vision*, 1150–1157 vol.2.
- Lowe, David G. (2004). Distinctive Image Features from. *International Journal of Computer Vision*, 60(2), 91–110.
- Lucas, B., & Kanade, T. (1981). An iterative Image registration technique with an application to stereo vision. In *DARPA Image Understanding Workshop* (p. 10).
- Micheletti, N., Chandler, J. H., & Lane, S. N. (2015). Investigating the geomorphological potential of freely available and accessible structure-from-motion photogrammetry using a smartphone. *Earth Surface Processes and Landforms*, 40(4), 473–486.
- Mikolajczyk, K., & Schmid, C. (2005). A performance evaluation of local descriptors. *IEEE Transactions on Parttern Analysis and Machine Intelligence*, 23.1-23.6.
- Nex, F., & Remondino, F. (2014). UAV for 3D mapping applications: A review. *Applied Geomatics*.
- Nguyen, A., & Le, B. (2013). 3D point cloud segmentation: A survey. *IEEE Conference on Robotics, Automation and Mechatronics, RAM - Proceedings*, (November), 225–230.
- Ozdemir, E., & Remondino, F. (2018). Segmentation of 3D photogrammetric point cloud for 3D building modeling. *International Archives of the Photogrammetry, Remote Sensing and Spatial Information Sciences - ISPRS Archives*, 42(4/W10), 135–142.
- Qi, C. R., Su, H., Mo, K., & Guibas, L. J. (2017). PointNet: Deep learning on point sets for 3D classification and segmentation. *Proceedings - 30th IEEE Conference on Computer Vision and Pattern Recognition, CVPR 2017, 2017-Janua*, 77–85.
- Rabbani, T., van den Heuvel, F. a, & Vosselman, G. (2006). Segmentation of point clouds using smoothness constraint. *International Archives of Photogrammetry, Remote Sensing and Spatial Information Sciences - Commission V Symposium "Image Engineering and Vision Metrology"*, 36(5), 248–253.
- Remondino, F., Barazzetti, L., Nex, F., Scaioni, M., & Sarazzi, D. (2012). Uav Photogrammetry for Mapping and 3D Modeling – Current Status and Future Perspectives. *ISPRS - International*

- Archives of the Photogrammetry, Remote Sensing and Spatial Information Sciences*, XXXVIII-1/, 25–31.
- Ren, S., He, K., Girshick, R., & Sun, J. (2017). Faster R-CNN: Towards Real-Time Object Detection with Region Proposal Networks. *IEEE Transactions on Pattern Analysis and Machine Intelligence*, 39(6), 1137–1149.
- Rippin, D. M., Pomfret, A., & King, N. (2015). High resolution mapping of supra-glacial drainage pathways reveals link between micro-channel drainage density, surface roughness and surface reflectance. *Earth Surface Processes and Landforms*, 40(10), 1279–1290.
- Rupnik, E., Daakir, M., & Pierrot Deseilligny, M. (2017). MicMac – a free, open-source solution for photogrammetry. *Open Geospatial Data, Software and Standards*, 2(1).
- Ryan, J. C., Hubbard, A. L., Box, J. E., Todd, J., Christoffersen, P., Carr, J. R., ... Snooke, N. (2015). UAV photogrammetry and structure from motion to assess calving dynamics at Store Glacier, a large outlet draining the Greenland ice sheet. *Cryosphere*, 9(1), 1–11.
- S.M.-Seitz, & C.R.-Dyer. (1997). Photorealistic Scene Reconstruction by Voxel Coloring. *IEEE International Conference on Computer Vision*, 35, 151–173.
- Schenk, T. (2005). Introduction to Photogrammetry. *Department of Civil and Environmental Engineering and Geodetic Science*, 95.
- Sensing, R. (2013). LIDAR format- American Society for Photogrammetry & Remote Sensing, (November 2011), 1–28.
- Snavely, N., Seitz, S. M., & Szeliski, R. (2008). Modeling the world from Internet photo collections. *International Journal of Computer Vision*, 80(2), 189–210.
- Szeliski, R. (2011). *Computer Vision: algorithms and applications*. (D. Griers & F. Schneider, Eds.), *Texts in computer sciences* (Vol. 42). Springer.
- Westoby, M. J., Brasington, J., Glasser, N. F., Hambrey, M. J., & Reynolds, J. M. (2012). “Structure-from-Motion” photogrammetry: A low-cost, effective tool for geoscience applications. *Geomorphology*.
- Zeiler, M. D., & Fergus, R. (2014). Visualizing and understanding convolutional networks. *Lecture Notes in Computer Science (Including Subseries Lecture Notes in Artificial Intelligence and Lecture Notes in Bioinformatics)*, 8689 LNCS(PART 1), 818–833.

4. Bridge system and traditional survey

In this chapter, an overview of bridge and viaduct system, in the infrastructure context is presented. A description of the structural components, basic structural static scheme and classification criteria are discussed according to actual literature.

Monitor and inspection of infrastructure are fundamental to ensure adequate level of service and avoid any risk and losses related to structural failure. Focusing on this important aspect, the state of the art in monitoring and survey methodologies is discussed with attention on traditional methodologies and on the application of 3d reconstruction using the presented computer vision algorithm SFM-MVS. All these methodologies are used to gather data, especially geometrical information, the first step for an adequate maintenance operation and the structural analysis. The different advantages and disadvantages of each methods are compared both in quantitative and in qualitative terms. Inserire qua parte sui Principi strutturali?



Figure 60 - Viaduc de Millau, France

4.1 Bridges systems: description and components

The bridge is defined by AASHTO (Association of American State Highway and Transportation Officials) as “a structure, including supports, erected over a depression or an obstruction (such as water, highway and railway) having a track or passageway for carrying traffic or other moving loads” (Imhof, 2004). Bridge engineering is a field of civil and structural engineering dealing with various disciplines such as surveying, plan, design, analysis, construction, management and maintenance. These structures as a part of a more complex transportation systems generally serving as mean of development for territory and as “lifelines” for social infrastructure systems. Managing company and technician, have a great responsibility not only for structural safety (i.e. bridge must guarantee project design characteristics, and not deform or collapse under loads) and serviceability (closure of this structure may cause several damages to the transportation system) of these strategic structures, but also for the social impact of this strategic system. In particular, considering the life cycle approach, the value of maintenance is fundamental (Rioja, 2013) in the entire structures’ file. Nowadays, western countries such as Europe and America have to face the deterioration of bridges and viaducts that had exceed their project lifetime (on average 50 years). The life-cycle approach to structure and new technology offers new methodologies and instruments to face this deterioration. To schedule adequate maintenance intervention, both ordinary and extraordinary, an adequate level of knowledge and detailed mapping is necessary.

Bridge system description and classification, and different methodologies for the survey are presented to identify critical issue on the key component of different system and analyse the survey instrument used to gather adequate data for the initial assessment.

Bridge systems and subcomponents

Structural components of bridges are based on parametric definitions involving deck types and various bridge properties. Bridge structures are composed by the superstructure, bearing, substructure and accessories (Figure 61) (WeiWei & Teruhiko, 2013).

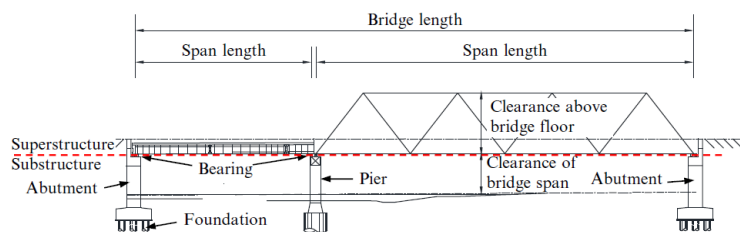


Figure 61 - Bridge components

- *Superstructure* represents the portion of the bridge above the bearings and supported by them, including deck, girder, truss. Traffic loads are carried by the deck and the other portions of the superstructure take the loads passing over it and transmit them to the substructures. The superstructure may only include a few components, such as reinforced concrete slab in a slab bridge, or several components such as the floor beams, stringers, trusses, and bracings in a truss bridge. In suspension cable-stayed bridges, components such as suspension cables, hangers, stays, towers, bridge deck, and the supporting structure are part of the superstructure.
- *Bearings* is a component of the bridge transmitting the loads received from the deck on to the substructure allowing also controlled movement of the structure due to temperature variation or seismic activity. A bearing represents a boundary between superstructure and substructure.
- *Substructure* is the portion of the bridge below the bearing that transmits all those loads to the ground. It includes abutments, piers, wing walls, retaining walls and foundation structures like piers and drilled shafts that can be made of wood, masonry, stone, concrete and steel. While the abutments refer to the supports located at the beginning and end of the bridge, and piers refer to the intermediate supports, both are vertical structures used to support the loads and to transmits them to the foundation; loads can come from the bridge's bearings, or directly from the superstructures.
- *Accessory structures* are structure members subordinate to the main bridge structure, such as parapets, service ducts, and track slabs.

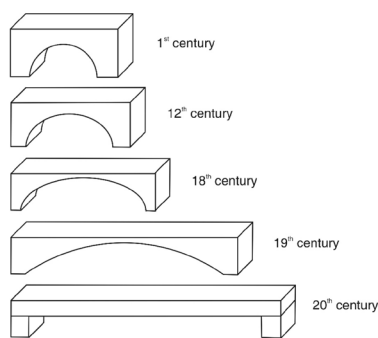


Figure 62 - Development of massive bridge shape over time, Source: (Proske, 2009)

Accessory's structure dead-weight shall be considered in the design, but their load carrying capacities are generally ignored.

The distance between centres of two bearings at supports is defined as the *span length* or clear span; the distance between the end of wing walls at either abutments, or the deck lane length (for bridges without abutments) is defined as total bridge length. Instead deck width is the sum of the carriageway width, sidewalk width, shoulder width, and the individual elements required to make up the desired bridge cross section.

4.2 Bridge classification

The evolution of bridges is strictly linked with the evolution of construction materials and consequentially construction principles: starting from stone bridges and arch principles, the development of materials such as steel and composite material (i.e. reinforced concrete) enable the possibility to increase and exceed the traditional limit. This is not true only by shear dimensions or span length, but also a shift from structures mainly exposed to moments to structures exposed to normal forces such as arch bridges and suspension bridges. This shift is also related to the impact of construction costs and overall costs.

Depending on the classification criteria, bridges can be classified in several ways (in general terms of bridge's superstructure) according to the following characteristics:

- i. Materials of construction
- ii. Usage
- iii. Span length
- iv. Position-movable bridges
- v. Span types
- vi. Geometric shape
- vii. Structural form

4.2.1 Material of construction

Construction materials must fulfil some further requirements such as materials properties independent from temperature conditions, limited deterioration time, limited deformations under loads, limited costs and technology for bridge construction. Bridges can be identified by materials from which the superstructure is built:

- stone and masonry;
- timber/wood;
- steel composite materials;
- concrete and reinforced concrete, pre-stressed concrete;
- carbon fibre and advanced materials.

While concrete is by far the most popular construction material used worldwide, frequently a combination of different materials is used in bridges building. Highway bridges superstructures, for example, may have reinforced concrete deck and steel main girders.

4.2.2 Usage

Categorization can be according to the utility (or function) that the bridge is designed to carry, such as road traffic, rail traffic, pedestrian, pipeline or waterway for barge traffic:

- Highway bridges
- Railway bridges
- Pedestrian bridges
- Pipeline bridges
- Airport runway bridges
- Aqueduct bridges
- Combined bridges, designed for two or more function



Figure 63 - Pedestrian bridge: Millennium bridge, England

Moreover, another classification could be made according to the temporary or permanent nature of the structure: temporary bridges that can be easily assembled and then take apart, or permanent bridge; temporary bridges are generally used in natural disaster or for military purpose.

4.2.3 Span length

Span capacity of a bridge depends on many factors, such as their structural form, construction materials, design methods, and construction techniques; structural design scheme are linked with certain span length range: e.g. beam bridge are suitable for short-span meanwhile cable-stayed bridge is generally used for long spans. According to (Taly, 1998) bridges can be classified as follows:

Culverts	$L \leq 6 \text{ m}$
Short-span bridges	$6 \text{ m} \leq L \leq 38 \text{ m}$
Medium-span-bridges	$38 \text{ m} \leq L \leq 125 \text{ m}$
Long-span bridges	$L \geq 125 \text{ m}$

Table 9 - Long span bridge classification

The concept of “super long-span bridge”, defining a bridge with a span much longer than any existing bridges (length $>125 \text{ m}$), has been recently proposed by (Tang, 2017).

4.2.4 Position-movable bridges

A movable bridge is a bridge that can move to allow boats' or barges' passage, with the advantages of lower construction cost due to the absence of high piers and long approaches. Three types of movable bridge can be categorized as:

- *Bascule Bridges*, whose main girders can be lifted together with a deck about the hinge located at the end of the span (Figure 65);



Figure 64 - Bascule Bridge: Tower Bridge, England

- *Swing Bridges* where the girders together with the deck can be swung about the vertical support ring at the pier in the middle;



Figure 65 - Reedham Swing Bridge, England

- *Lift bridges* where gantries are provided at the piers and at either end of the span. In lift bridges the system, both girder and floor, is lifted up by a hydraulic arrangement.



Figure 66 - Lift Bridge, USA

4.2.5 Interspan relation

According to the interspan relation, generally the bridge structure can be classified as simply supported, continuous, or cantilever bridges, as shown in Figure 67 (WeiWei & Teruhiko, 2013):

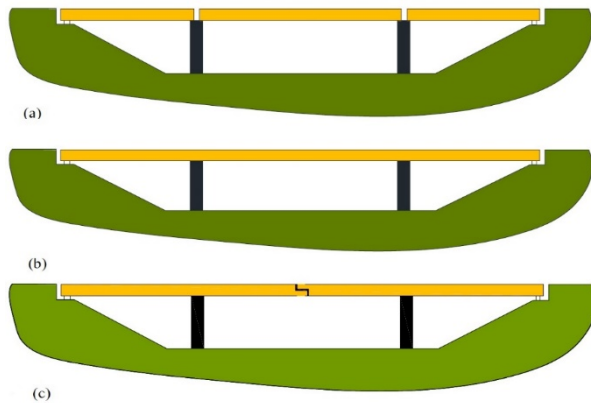


Figure 67 - (a) simply supported bridge, (b) continuous bridge, (c) cantilever bridge

(a) Simply supported bridge

In a simply supported bridge the structure is divided into several individual spans with relatively short-span length; the load carrying member is simply supported at both ends. They are statically determinate structures generally designed with constant girder height to simplify design and construction, due to the maximum bending moment at the mid-span and maximum shear force at girder ends.

(b) Continuous bridge

Continuous bridges are statically indeterminate structures, whose spans are continuous over three or more supports. The continuous bridges have been used extensively in bridge structures due to the benefit of higher span-to-depth ratio, higher stiffness ratios, reduced deflections, less expansive joints and less vibration. In these structures the positive bending moment is much smaller than that in simply supported span due to the absence of negative bending at the intermediate piers; thus, they generally need smaller sections and have considerable saving compared to simply supported bridge construction. Moreover, due to the larger negative bending moment and shear forces at intermediate supporting sections, larger girder depth is generally used. In addition, in continuous bridge, bearings can be placed at the centre of piers so the loads at piers are transmitted centrally. From the other side, the design is more complex for different reasons: they are statically indeterminate, the concrete deck is easy to crack in the negative bending moment zone and bottom steel girder is vulnerable to buckling. Also, due to temperature variation large internal forces may occur on the structure.

(c) *Cantilever bridges*

The cantilever bridge is a bridge whose main structure is cantilevered, which are used to build girder bridges and truss bridges. Compared with simply supported and continuous bridges, they have different advantages: are suitable for foundation with the uneven settlement and have a larger span capacity. For cantilever bridges with balanced construction, hinges are usually provided at contra flexure points of a continuous span, and an intermediate simply supported span can be suspended between two hinges.

4.2.6 Geometric shape

According to the geometrical shape of the superstructure, bridges can be classified as:

- *Straight bridges* if the bridges axis follows a straight line, to avoid extra forces such as torsions and to simplify bridge design, analysis and construction;
- *Skew bridges* often used in highway design when the geometry cannot accommodate straight bridges; AASHTO LRFD Bridge Design Specifications (2004) suggest that the skew angle under 15° can be ignored, while for angles larger than 30° the effects of skew are usually considered significant and need to be considered in the analysis. Moreover, the torsional effects (due to the skew support arrangements) and tendency to rotate under seismic load must be taken into account in the design.
- *Curved bridges* are more complex than straight or skew in both design and construction. While highway or railway follows a straight alignment or little curvature, curved bridges are commonly used for pedestrian bridges to provide the users a unique spatial experience or for the aesthetic purpose only. Like the skew, the bearing arrangements in curved bridges need to be carefully designed.

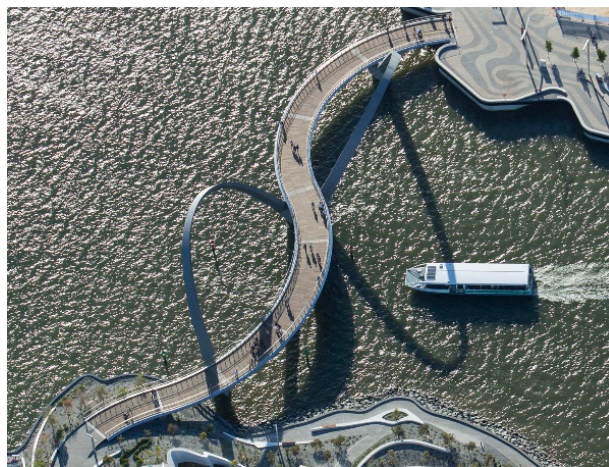


Figure 68 – Example of pedestrian curved bridge: Elizabeth Quay Bridge, Australia
Source: Arup

4.2.7 Structural form

Structural form affects the whole service life of the bridge, including design, construction, repair and maintenance; for this reason, classification by structural form is still the common way. Bridges with different structural forms have their load transfer path and a suitable range of application. Bridges are classified into:

- *Beam bridges* are the most common, inexpensive and simplest structural forms supported between abutments or piers. The weight of the beam and other external load need to be resisted by the beam itself, and the internal forces include the bending moment and shear force. For these reasons, only materials that can work well both for compression and tension can be used to build beam bridges (e.g. reinforced concrete or pre-stressed concrete, combined reinforced concrete and steel). Sometimes beam bridges are also classified into slab, beam and girder, however, this category can be classified as the same type because of their similar load transfer mechanism.



Figure 69 - Beam bridge: Lake pontchartrain causeway, USA

- *Rigid-frame bridges* consist of superstructure supported on vertical or slanted monolithic legs (columns), in which the superstructure and substructure are rigidly connected to act as a unit (can be considered as a beam); this typology is used for medium-span length for economic advantages. The integral structure includes braced rigid-frame bridges and V-leg rigid-frame bridges. The rigid connections between superstructure and substructure transfer bending moment, axial forces and shear forces providing significant structural benefits (e.g. moments at the centre of the deck are smaller than the corresponding moments in a simply supported bridge, so a shallower cross section can be used). From the other side, as statically undetermined structure they are complex to design and construct compared with simply supported or continuous bridges.



Figure 70 - Rigid-frame bridge: Shibanyo bridge, China

- *Truss bridges* are bridge whose load-bearing superstructure is composed of a truss, a structure of connected elements forming triangular units. In order to simplify the calculation and for security concerns, trusses are generally assumed as the pinned connection between adjacent truss members; therefore, the truss members like chords, verticals and diagonals act only either in tension or compression. Gusset plate connections are generally used, then the bending moments and shear forces of members should be considered for evaluating the real performance of truss bridges. According to these assumptions, the truss members can be in tension, compression, or sometimes both in response to dynamic loads. Thanks to its simple design methods and efficient use of materials, this type of bridge is economical to design and construct. Moreover, the good seismic performance makes this type of bridges perfect for seismically active area. Short-span truss bridges are built as simply supported while the large span truss bridges are generally built as continuous truss bridges or cantilever truss bridges. The maximum single span of the continuous truss bridge is 440 m in Tokyo Gate Bridge in Japan (Figure 72).



Figure 71 - Tokyo Gate Bridge, Japan

- *Arch bridge* is a bridge shaped as an upward convex curved arch to sustain the vertical loads. A simple arch bridge works by transferring its weight and other loads partially into a horizontal thrust restrained by the strong abutments at either side. The arch rib

needs to carry bending moment, shear force, and axial force in real service conditions. The current world's largest arch bridge was built in Chongqing, China (Figure 73) and has a span length of 552 m.



Figure 72 - Arch bridge: Chaotianmen Bridge, China

- *Cable-stayed bridges* is a structure made of main tower(s), cable stays, and main girders. Several points in each span between the towers are supported upward in a slanting direction with inclined cables.

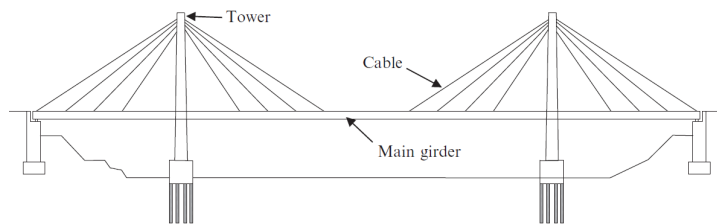


Figure 73 - Cable stayed bridge components

The internal forces due to both dead load and live load are much smaller in cable-stayed bridges; from a mechanical point of view, this typology is statically indeterminate continuous girder with spring constraints. Cable-stayed bridges are also highly efficient in the use of materials due to their structural members mainly works in either tension or compression. Cable-stayed bridges have the second-longest spanning capacity and they are practically suitable for spans up to around 1 km. The longest cable-stayed bridge is Russky Bridge in Russia (Figure 75) with a span of 1104 m.



Figure 74 - Cable stayed bridge: Russky Bridge, Russia

- *Suspension bridges* are a continuous girder suspended by suspension cables, which pass through the main towers with the aid of a special structure known as a saddle, and end on big anchorages that hold them. The essential parts of a suspended stayed bridges are the tower, hanger, main girder, and anchorage.

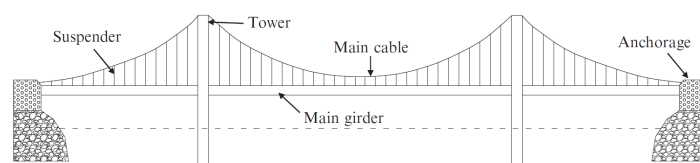


Figure 75 - Suspended bridge components

The main forces in a suspension bridge are tension in the cables and compression in the towers. The deck, which is usually a truss or a box girder, is connected to the suspension cables by vertical suspender cables or rods, called hangers, which are also in tension. The weight is transferred by the cables to the towers that in turns transmit to the anchorages on both ends of the bridge and finally to the ground. The suspension cable can only sustain the tensile forces, which is different from the compressive forces in the arch.

The use of suspended bridges allows to reach longer span achievable than any other type of bridges and they are practical for spans up to around 2 km. The Akashi Kaikyo bridge (Figure 77) in Japan is the bridge with the longest central suspended span of 1,9 km realized. The project of the Strait of Messina suspended bridge (Figure 78) in Italy to connect Calabria and Sicily regions consist in a 3 300 m single span length suspended bridge. The design phase is completed but the realization was cancelled by the Italian government.



Figure 76 - Suspended bridge: Akashi Kaikyo Bridge, Japan



Figure 77 - Strait of Messina suspended bridge

4.3 Bridge's maintenance

Infrastructure maintenance and monitoring, in particular critical structures as bridges and viaduct, is an actual problem that western country has to face, especially in area exposed to high seismic risk. The first document and regulation about the maintenance activity to be performed on infrastructure and bridge's "Retrofitting guidelines for Highway Bridges" was emitted in the US Federal Highway Administration (FHWA) in 1983; the first research program, financed by FHWA, to investigate and evaluate the seismic risk assessment of bridges started in 1992. The output of that research was released on 1995, "Seismic Retrofit Manual for Highway Bridges" and updated until today in the "Seismic Retrofitting Manual for Highway Structures: Part 1 Bridges" (Buckle et al., 2006) Seismic Retrofitting Manual for

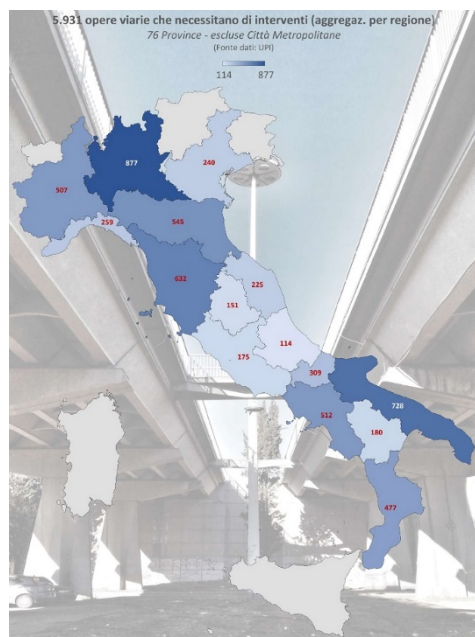


Figure 78 - Distribution of bridges and viaduct in Italy per region, Source UPI

Highway Structures: Part 2 Retaining structures, slopes, tunnels, culverts and roadways” (Power et al., 2004).

In Europe the Eurocode 8 part 2 contains a document for “Design of structure for earthquake resistance: Bridges” (Holst et al., 2011a) and the evaluation of seismic risks, but the code for assessment and retrofitting of structures limits their analysis only on existing buildings (Eurocode 8 part 3 “Assessment and retrofitting of buildings” (Holst et al., 2011b). In Italy, actual regulation on design is contained in “Norme tecniche per le Costruzioni” NTC2018 (Ministero delle Infrastrutture e dei Trasporti, 2018). Moreover, “Civil protection Department” (DPC) has activated research in collaboration with Italian University about “Evaluation and reduction of seismic risk of existing bridges”. The main objective is to develop a procedure to evaluate the structural condition of the existing bridge for risk mitigation.

In Italy “Union of Italian Province” (UPI) has developed a recent report (Unione Province Italiane, 2018) about the actual condition of Italian infrastructure focusing on Bridges and Viaducts that have exceeded their life cycle (almost 50 years). The report was the result of the investigation requested by the Italian Minister for Transportation (MIT) after the collapse of Morandi Bridge in Genova (2018). Italian provinces have to manage almost 100.000 km of roads with 30.000 bridges, viaducts and tunnels. The status of these bridges is reassessed in (Figure 80):

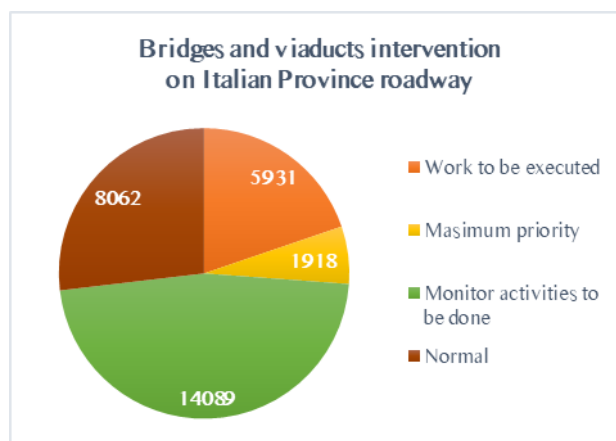


Figure 79 - Status and distribution of Italian Province bridges and viaduct

The estimated cost for the monitoring of 14.000 bridges is about 566 million and estimated costs of intervention for actual bridges is 2.7 billion. This count excludes the intervention on the regional and national highway, managed by public or joint venture (public-private) company like Autostrade per l'Italia (ASPI) (4200 bridges and viaducts) and Anas (13.000 bridges and viaduct) (Figure 81). Each of this company has its own monitoring system and standard manual to ensure maintenance and control operation.

The analysis of major damages concentration can guide the inspection process to the critical parts of the structure. The major damages on bridges and viaducts induced from external forces such as seismic loads, can be divided according to super and substructure: major damages and cause of collapse are in fact concentrated on deck and piers (Pinto et al., 2009): deck doesn't have anti-seismic resistance function and major cause of collapse are essentially due to hammering between adjacent span and losses of support. Piers, that must support the deck and transfer loads to the foundation, can collapse for inadequate flexural ductility or defects, shear resistance and inadequate design of beam/pier joint.

An adequate level of knowledge is the first step to set-up the maintenance plan and schedule inspection on a regular basis. For this reason, survey techniques are necessary to understand the health of the construction and prevent heavy damages and collapse. In Figure 81 different sensors on a cable stayed bridge are presented from (Ni & Wong, 2012). In the next paragraph actual methodology for the survey of bridges are presented in the next paragraph.

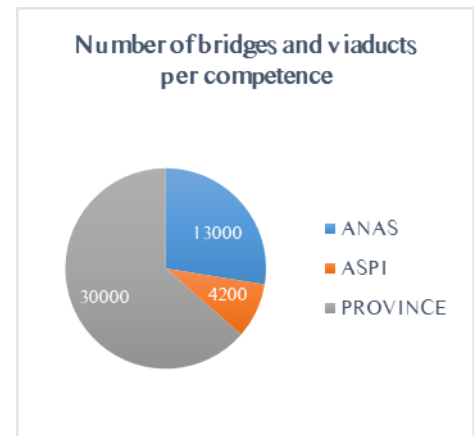


Figure 80 – Distribution of bridges in Italy managed per managing company (excluding city and region)

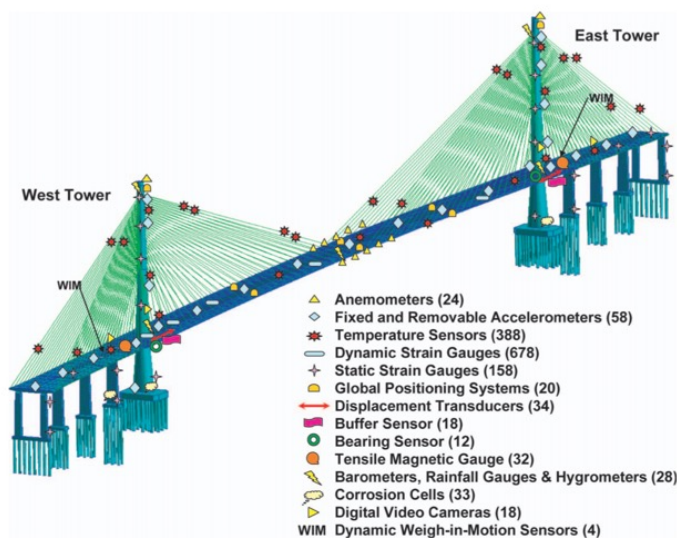


Figure 81 - Sensors for real time monitoring of cable stayed bridge,
Source: (Ni, 2012)

4.4 Survey techniques for monitoring and inspection

Structure from motion represents the latest and significant advance in digital surveying, thanks to their non-invasive characteristics, the possibility to acquire information rapidly and with low economical expenditure, without any contact with the object/area to be surveyed. The use of photogrammetry in surveying and monitoring spread in recent years thanks to a combination of several factors: significative advancements in computer vision algorithms, increased computational

power and major availability of instruments to acquire information and powerful software to elaborate data. Another key factor is represented by numerous advantages compared with traditional surveying techniques, such as the possibility to acquire information and move the analysis phase after the survey, in the office. The potential of the technology is at the beginning, and the improvements in techniques and algorithm will contribute to the technology growth in the next years.

Approaches to acquiring digital topographic data can be categorized in two main typologies: direct approaches that require contact by the surveyor with the object/area of interest, and indirect methods, that permit measurement of an object/area whilst remains remote. Obviously the choice of the survey techniques that the surveyor should face, depend on different factors, related to the expected results such as: (i) data accuracy and precision, (ii) the intended usage of the captured data, (iii) the constraints such as time and money for the operation and (iv) the expertise in the usage of both hardware and software for acquiring and processing data.

The existing techniques actually used for survey and data acquisition include: Total Stations (TS), differential Global Positioning System (dGPS), photogrammetry, laser scanner, airborne laser scanning (ALS) and terrestrial laser scanning (TLS) or Light Detection And Ranging (LIDAR) (Brook, 2017). Compared with these traditional techniques SFM is very cheap and fast, can offer truly 3d information, and with adequate use of ground control points (GCP) can rival other digital survey methods for spatial accuracy. Moreover, with the use of more precise onboard GNSS navigation (e.g. RTK-GNSS) the spatial accuracy can be improved (Gerke & Przybilla, 2016, Cryderman et al., 2014).

4.4.1 Direct surveying approach

Visual Inspection

Visual inspection is the commonly used direct method to acquire information and survey bridges and viaducts, performed by an expert technician on site. It's a non-disruptive test that consists on visual



Figure 82 - Visual inspection performed using crane

individuation of defects and definition of the ordinary and extraordinary maintenance operation.

This inspection is based on Numerical Evaluation Method to assign degradation numerical index. In case of serious and complex damage to the structure, it's necessary to perform deeper inspection with destructive methods. The main disadvantages of this method consist in the use of a crane to inspect the substructure, with an expert on it (Figure 82). During the survey, traffic and regular functionality of the infrastructure must be interrupted.

Total Station (TS)

Total station (Figure 83) or electronic distances measurement devices are the classical and most common instruments for topographic surveying when high accuracy on a few points (less than 100) is required. The main advantages consist on the possibility to accomplish survey operation with an accurate chose of the point that better represent the topography of the area, in every condition, even when sky view is limited and in zones without GPS signal. The expert judgment in the choice of survey points, make TS the most efficient of the surveying approaches (Wheaton et al., 2010, James Brasington et al., 2003), while from the other side is strictly dependent on the expertise of the surveyor. The subjectivity of the surveyor in the choice of the point, the need of physically visit those targets and have appropriate access, and the need of at least two operators (one at the station and one at the other target point of interests) represent the main disadvantages in using TS. Moreover, the obtained measurements are restricted to being in a local coordinate system, unless the point is "back-sighted" to a point with "known" real world characteristics and measurements.

In bridge surveying, the need to access to the target point represents a great obstacle due to the difficult position and condition of bridges, that usually are at height, or upon a river or a street.

Differential GNSS

The unique way to get real-world coordinates consists in the use of Global Navigation Satellite Systems (GNSS), usually America-based Global Positioning System (GPS), Russia GLObal Navigation Satellite System (GLONASS), recently Europe-based Galileo system and China-based Beidou. GNSS systems, and at the beginning GPS, has been used for surveying and mapping since the 1990s and initially was employed to provide control points for traditional triangulation-based surveying techniques. From the 1990s this has been used as a surveying method in its own right.

Similar to TS the data acquisition requires a surveyor to visit each point of interest with a *rover* receiver, that sends all the acquired information to a *base* station. The accuracy depends on the balance between point accuracy and speed of survey chosen. Rover's position is calculated in

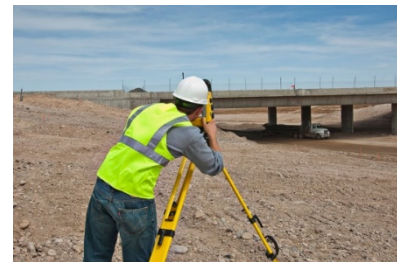


Figure 83 – Bridge survey using Total Station (TS)



Figure 84 - GPS base,
Source: Leica Geosystem



Figure 85 - DJI UAV with RTK system for accurate survey

real-time relative to the base which is set-up on a tripod over a known point and this real-time function is facilitated via radio link; hence modem and radio antenna are required at both base and rover. Alternatively, rover data can be post-processed relative to the temporary base station or to a permanent base station such as those part of the national and international geodetic system.

Two different GPS mode can be used for surveying: “Static” or “continuous”. In *static* mode multiple observations are logged and averaged per point and GNSS can be used to acquire up to several tens of point per hour. This survey mode is useful if the GNSS-derived 3d point data are being used either as input to other survey methods such as photogrammetry reconstruction, using Ground Control Point, or to validate and compare the accuracy of the results with other survey methods. In *Continuous* mode several thousand of points per hours can be acquired. *Real-Time Kinematic* (RTK) (Figure 85) mode is one type of continuous survey that requires a direct radio or mobile telephone modem link between base and rover receiver but has the benefit of providing the final accuracy to the surveyor in the field at the point of interest.

The output of the differential GPS (dGPS) survey data are commonly imported to the geographic information system (GIS) where the point can be converted into Digital Elevation Model (DEM) for land representation. dGPS data accuracy is dependent on the number and the geometry of satellites used to compute a point and on the equipment set-up and survey mode used. The surveyor judgmental chose for the point of interest introduces a subjectivity factor that should rely on the expertise of the technician, like in TS survey. However, with this technique, it's possible to obtain sub-centimetre accuracy, similar to Terrestrial Laser Scanning (J. Brasington et al., 2000, Casas et al., 2006, Hugenholtz et al., 2013) and more accurate than Airborne Laser Scanning. Additionally, GPS accuracy is strictly dependent on environmental factors that can influence satellite signal and radio link between base and rover. Specifically, for bridge surveying, the big issue consists on the lack of GNSS signal under the bridge, making the acquisition complicated or incomplete.

4.4.2 Indirect surveying approach

Indirect approaches are enabled by remote digital surveying that removes the need for a surveyor to physically visit the target point of interest and so offers an opportunity for surveying inaccessible landforms. Moreover, automation of digital surveying has increased point acquisition rate, spatial coverage (enabling the possibility of reproducing 3d data), decreased time for surveying, removed the judgment of sample point selection, and most important moved the analysis from the field to the digital environment, in the post-processing phase. It must be emphasized that each of these remote methods

requires precise GCPs for georeferencing the survey into real-world coordinates. Last UAV includes GPS with RTK systems built-in and linked *base* station in order to minimize the necessity of acquiring GCP. Remote digital surveying, all of which produce raw 3d point clouds of the target scene, can be summarized in two main categories according to the used technology: Lidar (LIght Detection and Ranging) commonly known with the name of the used instrument, laser scanner, and digital photogrammetry and SFM-MVS. The analysis of photogrammetry SFM_MVS specific survey for bridges will be deeply discussed in chapter 5

Lidar (terrestrial and aerial laser scanning)

The process used by a laser scanner to acquire spatial information and generate a 3d point cloud of the environment it's called Light Detection and Ranging (LIDAR). Laser scanners emit a laser pulse and record the time that it takes for that pulse to return to the scanner, thousands or ten thousands of times per seconds. Laser travel at a constant speed and knowing the direction in which the laser was, the distance from the scanner of any reflecting surface and the remote coordinates of the point reflection are known. The item can be used for aerial survey, mounted on an aircraft, or for a terrestrial survey on a tripod according to the area to be acquired. Airborne Laser Scanner (ALS) comprise systems design to be mounted on aircraft integrate with Inertial Measurement Unit (IMU) for positioning and correction of aircraft pitch, yaw and roll. The accuracy of ALS data depends on the dGPS and inertial measurement unit (Hodgson & Bresnahan, 2004) and in a complex natural environment can result in large vertical offset surface (Heritage & Milan, 2009). Obtained data from ALS are also frequently confronted with systematic errors in the digital terrain model (DTM) / digital surface model (DSM). Airborne Laser Scanner is commonly used to scan large areas at territorial scale, but due to vertical accuracy, between 0,1 m and 0,5 m (Gallay, 2013), are not suitable for bridge survey.

Terrestrial Laser Scanning (TLS) (Figure 86), mounted *in situ* on conventional survey tripods, comprise a unit for laser acquisition, GNSS unit and IMU to geo-localize data, and photographic sensor to record RGB (Reed-Green-Blu) value. TLS is optimised for precision at a given range because the laser beam spreads with increasing distance from the instrument. Acquisition range can vary from indoor or close-range surveys (tens meter of distance) to landform (kilometres), and consequently, laser required to achieve this range, speed and point accuracy can vary markedly. A review of TLS methods and data processing has been produced by (Smith, 2015) and applications in civil engineering are presented in (Berenyi et al., 2010).

LIDAR acquisition presents several benefits compared with other survey methods besides the obvious merits of spatial extent/coverage and speed (Alho et al., 2009); the main advantages are:



Figure 86 - Laser scanner on a bridge survey

- Independence from time of the day and land cover
- The laser pulse can penetrate through sparse vegetation (enabling both vegetation height and “bare-earth” elevation to be determined simultaneously, thanks to an algorithm for man-made artefacts removal (Sithole & Vosselman, 2006) and through cracks and slit (Law et al., 2015).
- High accuracy and high level of detail acquired.

From the other side, a large amount of data and high detail requires high computational power and post-processing time and can be regarded as a constraint if fast and low detail tasks are needed. Another major disadvantage is represented by the needs of multiple scan position not only to avoid blind spots behind obstacles but also to gain spatial coverage required. Moreover, high hardware costs (from 30.000€ to 120.000€) and weight (minimum 30 kg) and labour-intensive acquisition can limit the extent and frequency of surveys. For bridge surveys, the use of TLS can be a very complex operation due to bridges nature (bridges are designed to connect separate spaces, and for this reason often are at high altitude or upon a river) and inaccessibility of places (e.g. acquiring data of deck's bridge upon a river present different problems and practical disadvantages). For these reasons the use for bridge inspection guaranty high precision but it can't be considered as the best method (Truong-Hong & Laefer, 2014).

4.4.3 Aero photogrammetry and SFM-MVS for survey

As described in the previous chapter, aerial mapping through piloted aircraft was the first application and development of photogrammetry. Aircraft enable, in function of flying height, the best combination of spatial coverage and ground resolution. The widespread usage of photogrammetry has been enhanced by reliable automation of photogrammetric process (e.g. the use of uncalibrated images that simplify the acquisition process) and technology advancements in computer science, coupled with the availability of electronics and consequentially low costs UAV. As discussed, the SFM-MVS process, in contrast with traditional photogrammetry, allows the reconstruction of the 3d scene utilizing multiple (overlapping) uncalibrated images from multiple viewpoints. While traditional photogrammetry requires high labour on relatively manual post-processing, using SFM-MVS scene geometry, camera position and orientation are retrieved simultaneously. Moreover, this process represents the cheapest acquisition method (Mader et al., 2015) in terms of labour cost and capital expenditure. Using adequate instruments and techniques the delivered results in terms of accuracy can be compared to the best achieved with any other topographic surveying method, both direct or indirect (Marcus & Fonstad, 2008). Reconstructing 3d space in the office allows post survey analysis and extraction of relevant information according to the task needed.

The only limitations are represented by the dependency on external ambient light condition (Marcus & Fonstad, 2008, Gienko et al., 2014), the high computational power needed to elaborate data, actual impossibility to elaborate live data on field to understand attributes that the point cloud will have; moreover the software used for point cloud analysis and elaboration is very much in its infancy, and will rapidly improve in the next years.

As discussed, instrument's choice is related to multiple factors such as external condition, environment and desired output: in the next two table a quantitative comparison between different instruments (Table 10), and different advantages and disadvantages (Table 11) are summarized.

Survey method	Advantages	Disadvantages
Visual inspection	Technical workers on site	Time and cost consuming Personnel dependent (subjective) traffic interruption
Total Station (TS)	Low cost Accurate	High cost Resolution may be insufficient to measure small changes Systematic errors on some landforms
dGPS	High accuracy Range of methods have been developed to suite different surveying requirements Line of sight not required	High cost Some methods have low productivity Lock on 6+ satellites required
Lidar (ALS)	High productivity can be used during night Survey area difficult to access Not affected by vegetation cover	High cost Resolution may be insufficient to measure small changes Systematic errors on some landforms
Lidar (TLS)	High accuracy	Unable to capture all aspects of complex topographies Need of equipment positioning
Photogrammetry	High productivity One setup, no operators required Capture continuous information	Low resolution Equipment must be left in position for long periods of times (depending on survey) Doesn't work with fog, mist and rain
SFM_MVS	Cheap Fast Method independent of spatial scale	Reproducibility

Table 10 – Advantages and disadvantages of Survey methods

Survey method	Type	Spatial extent	Spatial Resoution	Data acquisition rate	3d point accuracy
		(km)	(pt m2)	(point/hour)	(m)
Visual inspection	Direct	0,1	-	-	-
Total Station (TS)	Direct	0,1 - 1	0,1 – 5	Hundreds	<0,01
dGPS	Direct	2,4 – 1	0,1 – 5	Thousands	0,005
Lidar (ALS)	Indirect	5 – 100	0,2 – 10	Milions	0,2
Lidar (TLS)	Indirect	0,01 – 5	100 - 10.000	Milions	0,05
Photogrammetry	Indirect	5,0 – 50	0,5 – 10	Ten of thousands	0,5
SFM_MVS	Indirect	0,01 – 1	1 - 10.000	Milions	0,01 - 0,2

Table 11 – Quantitative comparison of survey methods

References

- Alho, P., Kukko, A., Hyypä, H., Kaartinen, H., Hyypä, J., & Jaakkola, A. (2009). Application of boat-based laser scanning for river survey. *Earth Surface Processes and Landforms*. <https://doi.org/10.1002/esp.1879>
- Berenyi, A., Lovas, T., & Barsi, A. (2010). Terrestrial Laser Scanning - Civil Engineering Applications. *Proceedings of the Isprs Commission V Mid-Term Symposium Close Range Image Measurement Techniques*, 38(5), 80–85.
- Brasington, J., Rumsby, B. T., & McVey, R. A. (2000). Monitoring and modelling morphological change in a braided gravel-bed river using high resolution GPS-based survey. *Earth Surface Processes and Landforms*, 25(9), 973–990. [https://doi.org/10.1002/1096-9837\(200008\)25:9<973::AID-ESP111>3.0.CO;2-Y](https://doi.org/10.1002/1096-9837(200008)25:9<973::AID-ESP111>3.0.CO;2-Y)
- Brasington, James, Langham, J., & Rumsby, B. (2003). Methodological sensitivity of morphometric estimates of coarse fluvial sediment transport. *Geomorphology*, 53(3–4), 299–316. [https://doi.org/10.1016/S0169-555X\(02\)00320-3](https://doi.org/10.1016/S0169-555X(02)00320-3)
- Brook, M. (2017). *Structure from motion in the geosciences*. New Zealand Geographer (Vol. 73). Wiley Blackwell. <https://doi.org/10.1111/nzg.12161>
- Buckle, I., Friedland, I., Mander, J., Geoffrey, M., Nutt, R., & Power, M. (2006). Seismic Retrofitting Manual for Highway Structures: Part 1 – Bridges. *Fhwa*, (January). [https://doi.org/10.1016/S0140-6736\(05\)73946-5](https://doi.org/10.1016/S0140-6736(05)73946-5)
- Casas, A., Benito, G., Thorndycraft, V. R., & Rico, M. (2006). The topographic data source of digital terrain models as a key element in the accuracy of hydraulic flood modelling. *Earth Surface Processes and Landforms*. <https://doi.org/10.1002/esp.1278>
- Cryderman, C., Mah, S. B., & Shufletoski, A. (2014). Evaluation of UAV photogrammetric accuracy for mapping and earthworks computations. *68*(4), 309–317.
- Gallay, M. (2013). Direct acquisition of elevation data : Aribone Laser Scanning. *Geomorphological Techniques*, 1(January 2013), 1–14. Retrieved from http://www.geomorphology.org.uk/geomorph_techniques
- Gerke, M., & Przybilla, H.-J. (2016). Accuracy Analysis of Photogrammetric UAV Image Blocks: Influence of Onboard RTK-GNSS and Cross Flight Patterns. *Photogrammetrie - Fernerkundung - Geoinformation*, 2016(1), 17–30. <https://doi.org/10.1127/pfg/2016/0284>
- Gienko, G. A., & Terry, J. P. (2014). Three-dimensional modeling of coastal boulders using multi-view image measurements. *Earth Surface Processes and Landforms*. <https://doi.org/10.1002/esp.3485>
- Heritage, G. L., & Milan, D. J. (2009). Terrestrial Laser Scanning of grain roughness in a gravel-bed river. *Geomorphology*. <https://doi.org/10.1016/j.geomorph.2009.03.021>
- Hodgson, M. E., & Bresnahan, P. (2004). Accuracy of Airborne Lidar-Derived Elevation: Empirical Assessment and Error Budget. *Photogrammetric Engineering & Remote Sensing*, 70(3), 331–339. <https://doi.org/10.14358/pers.70.3.331>
- Holst, J. M. F. G., Rotter, J. M., Calladine, C. R., Eoin Dunphy, NORM, E. S. N. E. Euro., DNV, ... Starnes, J. H. (2011a). Eurocode 8 Part 2: Design of structure for earthquake resistance: Bridges. *Journal of Constructional Steel Research*, 54(2), 18–20. <https://doi.org/10.2514/2.2772>
- Holst, J. M. F. G., Rotter, J. M., Calladine, C. R., Eoin Dunphy, NORM, E. S. N. E. Euro., DNV, ... Starnes, J. H. (2011b). Eurocode 8 Part 3: Assessment and retrofitting of buildings. *Journal of Constructional Steel Research*, 54(2), 18–20. <https://doi.org/10.2514/2.2772>
- Hugenholtz, C. H., Whitehead, K., Brown, O. W., Barchyn, T. E., Moorman, B. J., LeClair, A., ... Hamilton, T. (2013). Geomorphological mapping with a small unmanned aircraft system (sUAS): Feature detection and accuracy assessment of a photogrammetrically-derived digital terrain model. *Geomorphology*. <https://doi.org/10.1016/j.geomorph.2013.03.023>
- Imhof, D. (2004). *Risk assessment of existing bridge structures*. University of Cambridge.
- Law, D. W., Holden, L., & Silcock, D. (2015). The assessment of crack development in concrete using a terrestrial laser scanner (TLS). *Australian Journal of Civil Engineering*, 13(1), 22–31. <https://doi.org/10.1080/14488353.2015.1092635>

- Mader, D., Blaskow, R., Westfeld, P., & Maas, H. G. (2015). UAV-Based acquisition of 3D point cloud - A comparison of a low-cost laser scanner and SFM-tools. *International Archives of the Photogrammetry, Remote Sensing and Spatial Information Sciences - ISPRS Archives*, 40(3W3), 335–341. <https://doi.org/10.5194/isprsarchives-XL-3-W3-335-2015>
- Marcus, W., & Fonstad, M. (2008). Optical remote mapping of rivers at sub-meter resolutions and watershed extents. *Earth Surf. Process. Landforms*, 33(December 2007), 1491–1501. <https://doi.org/10.1002/esp>
- Ministero delle Infrastrutture e dei Trasporti. (2018). Aggiornamento delle “Norme Tecniche per le Costruzioni” - NTC 2018, 1–198.
- Ni, Y. Q., & Wong, K. Y. (2012). Integrating Bridge Structural Health Monitoring and Condition-Based Maintenance Management. *4th International Workshop on Civil Structural Health Monitoring*, 6–8.
- Pinto, P. E., Franchin, P., & Lupoi, A. (2009). Valutazione e consolidamento dei ponti esistenti in zona sismica, 7.
- Power, M., Fishman, K. L., Makdisi, F., Musser, S., Richards, R., Youd, T. L., ... Youd, T. L. (2004). Seismic Retrofitting Manual for Highway Structures: Part 2 - Retaining Structures, Slopes, Tunnels, Culverts and Roadways. *Mceer*, (August), 370p.
- Proske, D. (2009). *Safety of historical stone arch bridges*. Springer.
- Rioja, F. (2013). What Is the Value of Infrastructure Maintenance? A Survey. *Infrastructure and Land Policies*, 347–365. Retrieved from [https://www.lincolinst.edu/pubs/dl/2304_1644_LPConf_2012_ch13_What Is the Value of Infrastructure Maintenance.pdf](https://www.lincolinst.edu/pubs/dl/2304_1644_LPConf_2012_ch13_What%20Is%20the%20Value%20of%20Infrastructure%20Maintenance.pdf)
- Sithole, G., & Vosselman, G. (2006). Bridge detection in airborne laser scanner data. *ISPRS Journal of Photogrammetry and Remote Sensing*, 61(1), 33–46. <https://doi.org/10.1016/j.isprsjprs.2006.07.004>
- Smith, M. W. (2015). Direct acquisition of elevation data: Terrestrial Laser Scanning. *Geomorphological Techniques*, 1, 1–14. Retrieved from http://www.geomorphology.org.uk/geomorph_techniques
- Taly, N. (1998). *Design of Modern Highway Bridges*. McGraw-Hill. Retrieved from <https://books.google.it/books?id=VABFAQAIAAJ>
- Tang, M. C. (2017). Super-long span bridges. *Structure and Infrastructure Engineering*, 13(6), 722–730. <https://doi.org/10.1080/15732479.2016.1187635>
- Truong-Hong, L., & Laefer, D. F. (2014). Application of Terrestrial Laser Scanner in Bridge Inspection: Review and an Opportunity. *IABSE Symposium Report*, 102(9), 2713–2720. <https://doi.org/10.2749/222137814814070190>
- Unione Province Italiane. (2018). Nota stampa Ponti : i risultati del monitoraggio delle Province, 0–3.
- WeiWei, L., & Teruhiko, Y. (2013). *Bridge Engineering* (Vol. 53). Elsevier. <https://doi.org/10.1126/science.45.1151.66>
- Wheaton, J. M., Brasington, J., Darby, S. E., & Sear, D. A. (2010). Accounting for uncertainty in DEMs from repeat topographic surveys: Improved sediment budgets. *Earth Surface Processes and Landforms*, 35(2), 136–156. <https://doi.org/10.1002/esp.1886>

5. UAV geometrical survey of bridges

The different kind of bridges structural components introduced in the previous chapter and the complexity of the bridge environment makes the UAV the best acquisition instrument for survey tasks and data acquisition. The methodology for aerial survey of bridge using aerial survey with UAV and photogrammetry is presented in this chapter. Also the automatic extraction of the geometrical feature was performed using the developed methodology and the results are presented on an online platform for the visualization and extraction of data.

5.1 Methodology for aerial survey of bridges using UAV and photogrammetry

The combination of Unmanned Aerial Vehicle (UAV) and computer vision algorithms for 3d model reconstruction and analysis, makes this solution the perfect *inspection platform* for infrastructure surveying, bridge and viaducts inspection and monitoring. The main advantages related to the use of these combined technologies are summarized below:

- Remote piloting (BVLOS operation)
- Possibility to reach inaccessible zones
- Details of joint and structural parts
- Inspection can be performed without interrupt regular traffic or services
- Automatic flight plan for data acquisition
- Repeatability of operations and inspection process during time
- Digital database updated on regular basis
- Extraction of geometrical features
- 3d model remote collaborative inspection
- Photo and video analysis for defects and deterioration
- Reduction of time and costs compared with compared with traditional inspection
- Non-invasive techniques for deformation monitoring

From the other side different challenges and open point in the acquisition phase must be faced:

- Flight in complex environment (presence of obstacles, vegetation near the structure)
- Normative limitation for remote piloting in BVLOS
- Complex objects, thin parts and occlusion requires manual flight or dedicated UAV (i.e. confined inspection)
- Weak or not reliable GPS signal under the bridge

After the acquisition phase, main challenges in data analysis are represented by:

- Segmentation of 3d point cloud
- Extraction of key information
- Visualization and sharing of output models
- No possibility to verify the quality of the data during acquisition process

As presented in the previous chapter the use of UAV technology in infrastructure surveying recently spread from 2013. Different applications and case studies have been presented in last 5 years (Ham et al., 2016, Khaloo et al., 2018, Hackl et al., 2018, Chen et al., 2018, Morgenthal & Hallermann, 2014, Escobar-Wolf et al., 2018, Lovelace, 2015). Instead the integration of UAV survey with BIM workflow and the use for displacement measures are recent (Hallermann et al., 2018, Yoon et al., 2018). However, due to the different disciplines involved in this application and to the recent and new technology used, actually a standard methodology and workflow for data acquisition and analysis is not elaborated (Hallermann & Morgenthal, 2014). The use of this technology it's not yet available as a standard inspection platform and it's highly task and human dependent. Moreover, the competence needed for acquisition and data analysis involves the different field of science and requires different knowledge in aeronautics, civil engineering, electronics, computer vision and 3d graphics. For this reason, different professional figures are involved in the inspection process with different competence sectors. Actually, the technician it's also a pilot, but in the future process standardisation allows pilot to go on site and capture data, and engineers to analyse data and take decisions

Moreover, acquisition techniques depend on different factors such as Level of Detail required, payload and sensors, and data analysis and extraction of crucial characteristics from a large dataset (e.g. 3d point clouds or TB of images) are not yet standardized. In this paragraph a methodology for the standardization of the bridge's inspection process through aerial inspections with UAV and photogrammetry is presented in Figure 88:

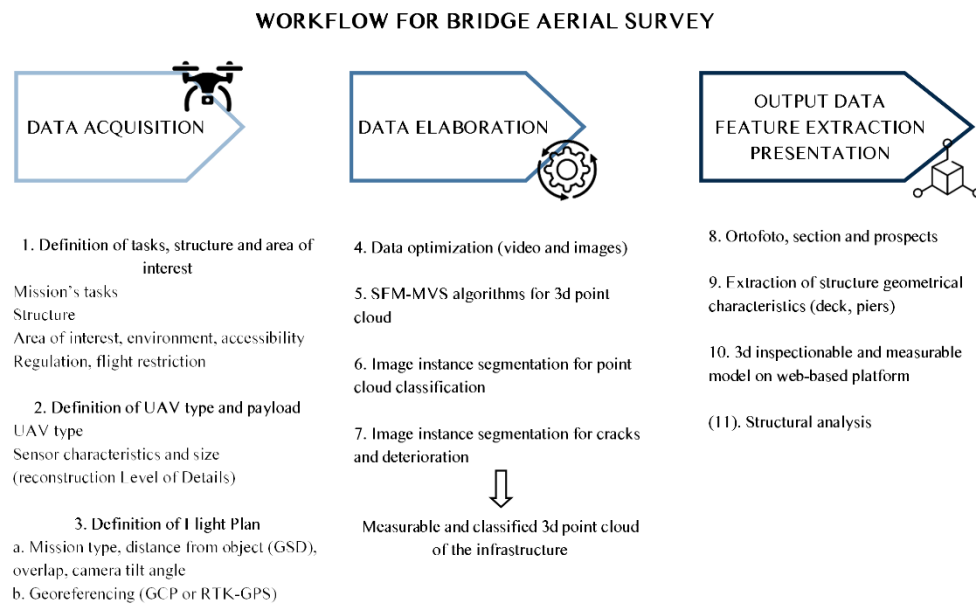


Figure 87 - Workflow for UAV photogrammetry bridge survey

Three main phases for the bridge survey and 3d reconstruction using UAV can be identified: the first is the planning and acquisition phase according to task objective, structure and area. The main issue is represented by the correct setting of the flight acquisition plan and environment. In the second phase, the acquired data (e.g. photo or video) are elaborated to extract a measurable and classified 3d point cloud of the infrastructure. In the third phase, the extraction of the relevant characteristics is performed with the use of a web-based platform to visualize and analyse the results, allowing to perform a virtual inspection of the scene and extract information's for future analysis.

5.1.1 Data acquisition

1. The definition of tasks, structure and Area of Interest is the first step in the 3d reconstruction workflow. The objective of the mission will define the accuracy and kind of output needed; according to the structure level of detail in the acquisition and key structural part could be defined. The area of interest should be considered to analyse the complexity of the environment, considering the accessibility of the area, ensuring that every part of the structure is accessible and to locate the take-off and landing point (often take-off and landing point can be the same). Moreover, it's necessary to consider, according to local regulation if the area of the survey has flight restriction (e.g. distance from the airport, no-fly zone) to require flight authorization and to define a flight virtual fence.

2. Definition of UAV and payload it's necessary to optimize time and costs of the tasks, according to the mission needs.

UAV can vary according to the dimension of the area to be acquired and dimension of the structure. Large UAV with interchangeable payloads can be used for long span bridge, while commercial UAV with fixed RGB camera payload can be suitable for short span bridge.

Payload and sensor are the fundamental choices to ensure the required Level Of Detail and quality of the results. With RGB camera payload the sensor size has direct effects on the resolution of the obtained model. Information can be acquired via video with the subsequent extraction of the frame, or via photo, both in compressed and raw format (to capture more light information). The second method is preferred due to the high resolution achievable. Moreover, camera should be set-up with following settings:

- Lower ISO possible
- Fixed diaphragm aperture (because of aperture influence in the reconstruction process)
- fixed exposure time.

3. Flight plan setup is the last phase in mission planning. To obtain an accurate 3d model it's necessary to setup: flight plans according to photogrammetric principles and georeferencing through Ground Control Points (GCP) or using a UAV with high precision GPS on board (Real Time Kinematic RTK-GPS).

3 a. Flight plans:

- Flight height or perpendicular distance from the object (GSD)
- Mission type (free, waypoint, strip or circular path)
- overlap between images
- camera tilt angle

Flight height or perpendicular distance from the object, and camera sensors are used to determine the **Ground Sampling Distance (GSD)** (Equation) parameter defined as correspondence of cm in the real world with pixel on the photo, expressed in cm/pixel. In Figure 89 the scheme for the GSD calculation is presented:

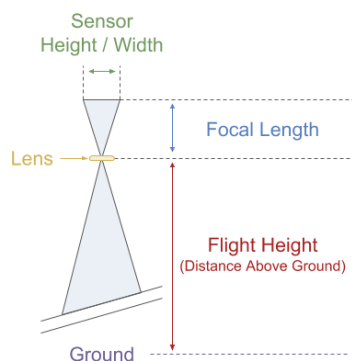


Figure 88 - GSD calculation scheme

$$GSD_w = \frac{Flight\ Height * Sensor\ Width}{Focal\ Length * Image\ Width}$$

Equation 3 – GSD calculation

The spatial area captured on each image is calculated from the GSD using Equation :

$$\begin{aligned} im_w\ ground &= GSD \cdot im_w \\ im_h\ ground &= GSD \cdot im_h \end{aligned}$$

Equation 4 - Captured area on image; w = image width, h= image height

From this data it's possible to calculate the position of the UAV to cover an assigned area with defined Overlap; to ensure a good level of reconstruction almost 80% of overlap coverage is required. GSD and overlap vary from different mission type.

According to relative camera position and photogrammetric principles discussed in chapter 3, two main flight mode can be used to acquire dataset: free mission and waypoint navigation follow a predefined path. Path planning and influence on reconstruction is presented in (Yang et al., 2018). In **free mission**, the pilot has the complete control of the UAV, while the camera shutter interval can be set for acquiring data at a fixed interval. This mission type is used for complex environment if the UAV doesn't have proximity sensor installed or if installed sensors are not sufficient to perform automatic flight; however, as far as the registration of the flight can be useful to repeat the operation, this mission type is highly dependent on the pilot and manual control.

Waypoint navigation are generally executed following two main path type: strip path (for terrain acquisition and large areas) or circular path more suitable to acquire 3d information. In mission using **Strip path** the UAV cover the entire area performing strip in both direction longitudinal and transversal (Figure 90).

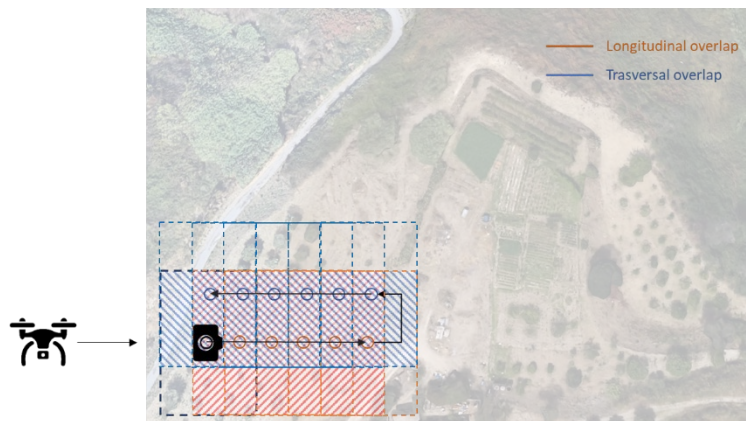


Figure 89 - UAV route and terrain acquisition

Assuming the camera parallel to UAV route, longitudinal overlap is function of im_h while transversal overlap is function of im_w (Figure 90).

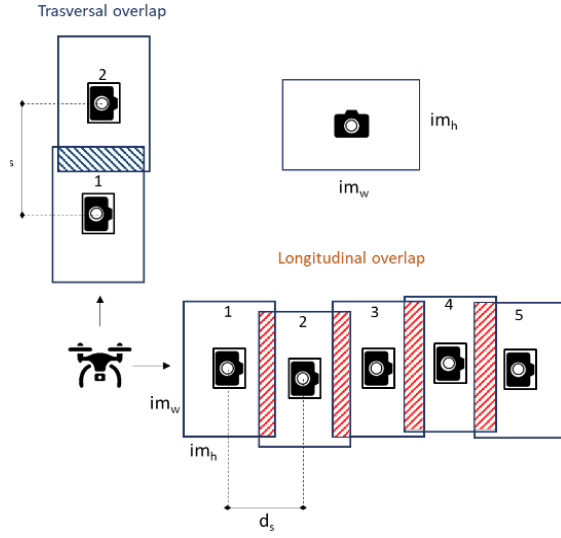


Figure 90 - Longitudinal and transversal overlap

The distance d_s between two consecutive shoots, for a defined overlap, can be calculated from the im_w and im_h parameters that are function of GSD and height of flight (Equation 4).

$$d_{s\ long} = im_{h\ ground} \cdot (1 - Overlap_{long})$$

$$d_{s\ trasv} = im_{w\ ground} \cdot (1 - Overlap_{trasv})$$

Equation 5 – Distance between two consecutive shoots

Time interval between two consecutive shoots can be calculated at fixed UAV speed with velocity calculation.

$$T_{shoot} = d_s / v_{UAV}$$

Equation 6 – Time interval between two consecutive shoots

Number of horizontal strips for an assigned area with UAV camera parallel to UAV route (Figure 92) can be calculated as (Equation):

$$N_{strip} = a / d_{s\ trasv}$$

Equation 7 – Number of horizontal strips for camera parallel to UAV route

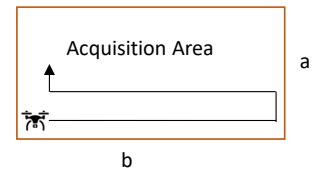


Figure 91 - Acquisition area and UAV route

Also, the inclination of the camera (tilt) (Figure 93) influences the accuracy of 3d reconstruction.

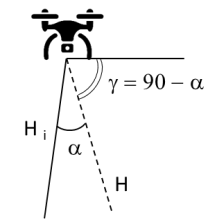


Figure 92 - Camera tilt (γ)

Nadir photos (vertical camera perpendicular to terrain) are used to acquire large areas, while the camera inclination allows the possibility of capturing more detail for 3d reconstruction (Rossi, et al., 2017). Tilt camera can be set to 70° for good quality 3d reconstruction.

Strip path in acquisition mission can be applied both in horizontal (the case of maps) and vertical (e.g. to scan a façade) (Figure 94).

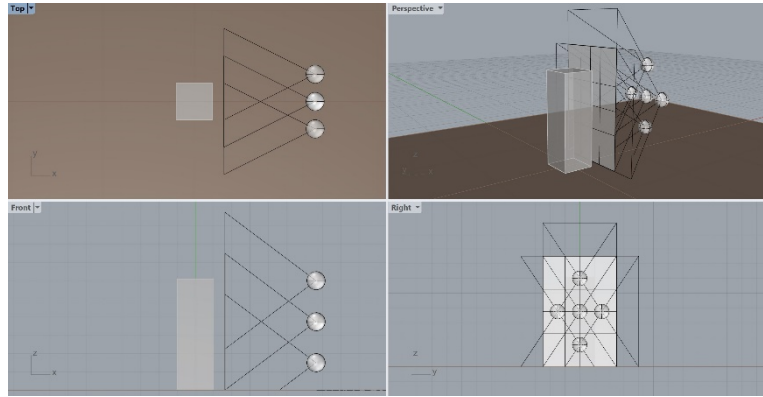


Figure 93 – Façade scanning using strip path

For sloping terrain, to maintain constant GSD parameter, the UAV must follow terrain slope (Figure 95).

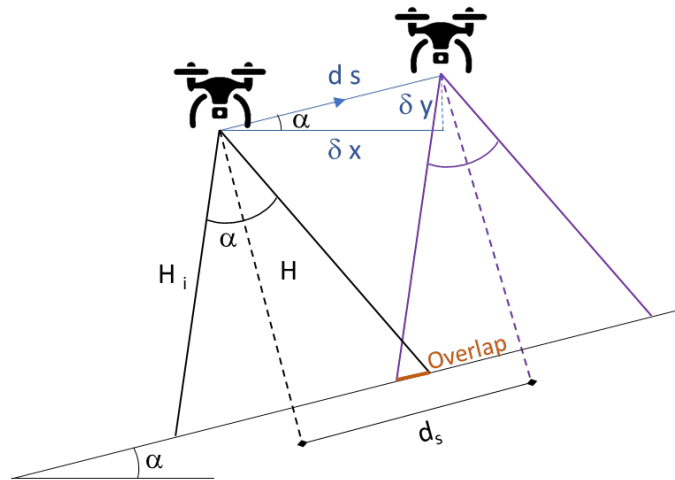


Figure 94 - Image overlap in sloping ground

For a sloping terrain with α inclination UAV position between two consecutive shoots is calculated as in Equation 7.

$$\Delta_x = d_s \cdot \cos \alpha$$

$$\Delta_y = d_s \cdot \sin \alpha$$

Equation 8 - UAV Δx and Δy in sloping terrain

Initial altitude height is calculated as in

$$H_i = \frac{H}{\cos \alpha}$$

Equation 9 - Initial UAV height for sloping terrain

In mission executed using **circular path** (Figure 96), the UAV execute a route moving around a defined Point Of Interest (POI). This route is indicated to acquire 3d information to obtain a complete 3d reconstruction of the object. The use of this type of mission in the case of large object such as bridges and viaducts with high vertical envelope, perfect fits the acquisition need.

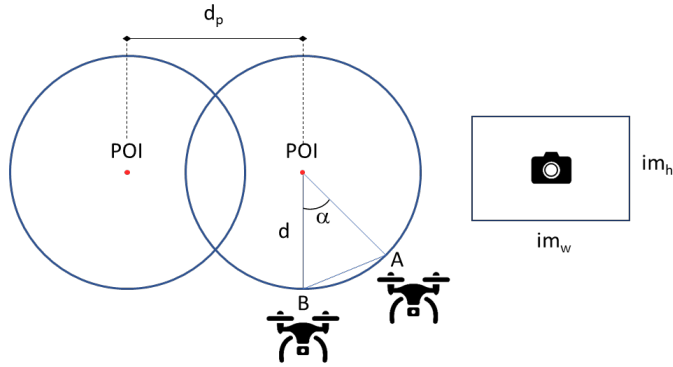


Figure 95 - Circular path for 3d acquisition

AB is calculated using the circular segment equation (Equation 9):

$$AB = 2d \sin (\alpha/2)$$

$$S = R \cdot \alpha$$

Equation 10 – Circular segment equation

The distance AB can be imposed equal to $d_{s\ transv}$ of considering d as the perpendicular distance from the object, overestimating the overlap. These parameters allows the definition of angle α between two consecutive positions of the UAV for shoots, for an assigned overlap (Equation 10) (Figure 97):

$$\alpha = 2 \arcsin [d_{s\ transv}/(2 \cdot d)]$$

Equation 11 – Angle between two consecutive position of UAV

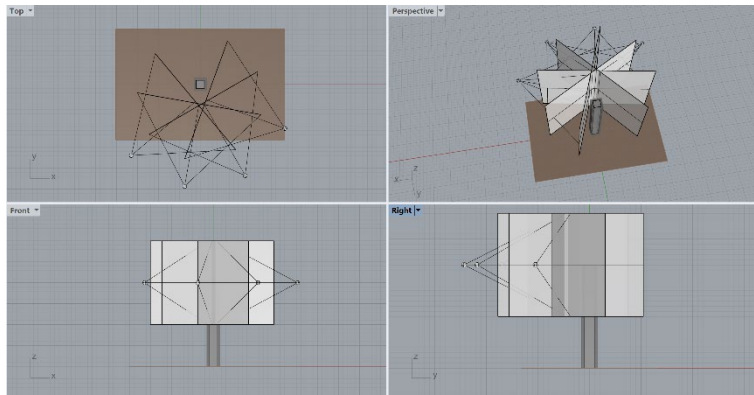


Figure 96 - Camera position for circular path acquisition

The distance d_p between two POI for fixed overlap area between two consecutive circles is calculated in Equation 11:

$$d_p = 2d \cdot (1 - \text{Overlap}_p)$$

Equation 12 – Angle between two consecutive position of UAV

The overlap between two consecutive circular paths can be set from 20 to 40% considering the field of view and the area covered from every image.

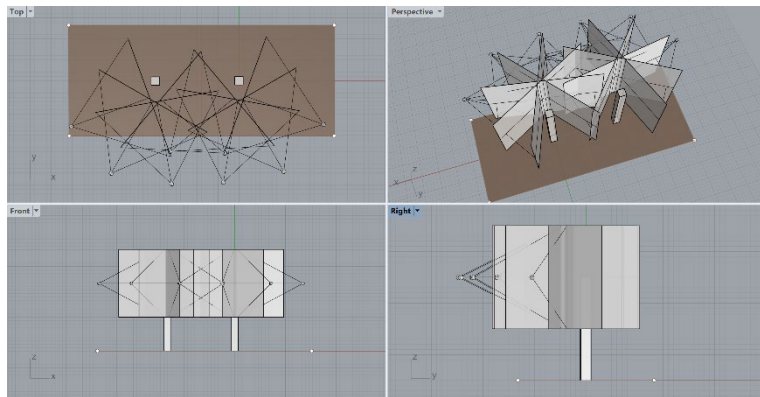


Figure 97 - Overlap between circle path for 3d acquisition

The tilt angle in every shoot is used to point the camera on the structure to be acquired. Moreover flight at a different height with different tilt angle angles (45° and 30°), allows accurate details acquisition as represented in Figure 99.

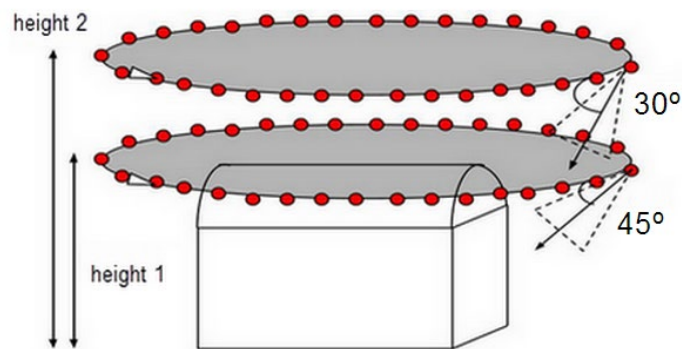


Figure 98 - Circular mission
Source: Pix4d

Waypoint navigation also allows the possibility to set specific camera parameters (e.g. tilt angle) for each photo, enable dynamic capture during acquisition phase.

Bridges and viaducts, as complex structure, presents specific problems in acquisition phases (no GPS signal under the deck, the prohibition of flying on the street for legal reason, presence of confined spaces), for this reason, a specific mission path and procedure is presented. According to the area and environment complexity and specific

characteristics of bridge's structure, the acquisition phase can be splitted into two phases:

- **Mission plan for pre-acquisition of the area (optional):**
acquisition of the area using strip path upon the viaduct (excluding the area on the street) for the first reconstruction of a low detail 3d model and digital elevation model;
- **Mission plan with a semi-circular path for structure acquisition:**
combined semi-circular mission from both sides of the bridge as specified in Figure 100 and Figure 101.

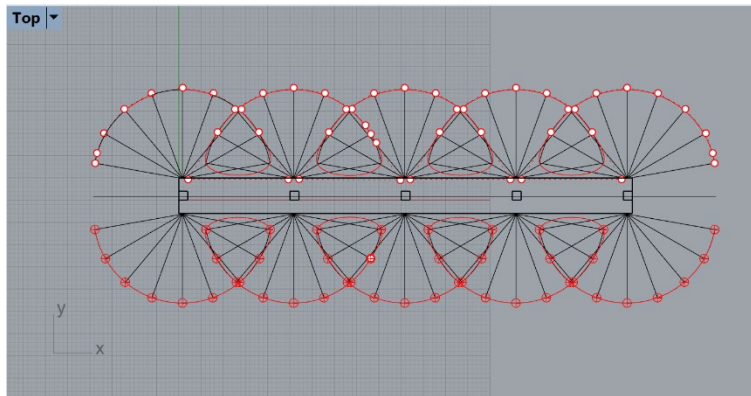


Figure 99 - Semi-circular path for 3d acquisition

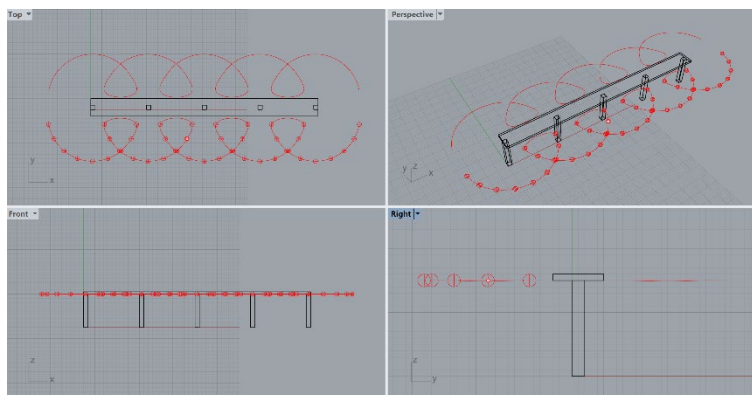


Figure 100 - Mission path for 3d acquisition of bridge

At least 3 flight (over the superstructure level, at superstructure level and under the superstructure level as indicated in Figure 102) with this path, at different height with specific tilt camera inclination to centre structure, are necessary for 3d acquisition. This methodology avoids the problem of weak GPS signal under the bridge using negative tilt inclination of the camera, allowing the possibility to capture detail under the deck.

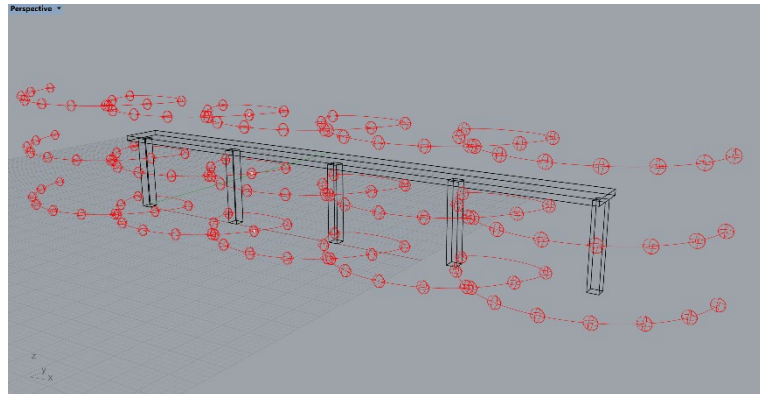


Figure 101 - Flight height for 3d acquisition

In the case of a complex environment, with the presence of vegetation or other obstacles, the use of UAV equipped with several sensors for collision avoidance is necessary.

Various open-source and commercial software available can be used to control the UAV in manual mission or waypoint automated mission setting up the flight plan. While manual mode and waypoint navigation with strip path or circular path for 3d acquisition all available in different software (Pix4d, DroneDeploy, Altizure, DJI Ground Station, Skycatch) but working in 2d space, the possibility to set-up a flight plan in the 3d space it is not yet available. The described procedure with specific flight plan in the 3d space for bridge 3d reconstruction is based on the use of Litchi software (VC Technology Ltd, London), that allows the set-up of 3d flight plan based on waypoint navigation, controlling specific settings as tilt camera and action to be executed. Also, the possibility to setup POI for the perfect navigation, fit with the developed methodologies (Figure 103). The platform also gives the

possibility to import surveyed 3d model or DEM (Digital Elevation Model) to set up a precise flight plan based on real elevation data.

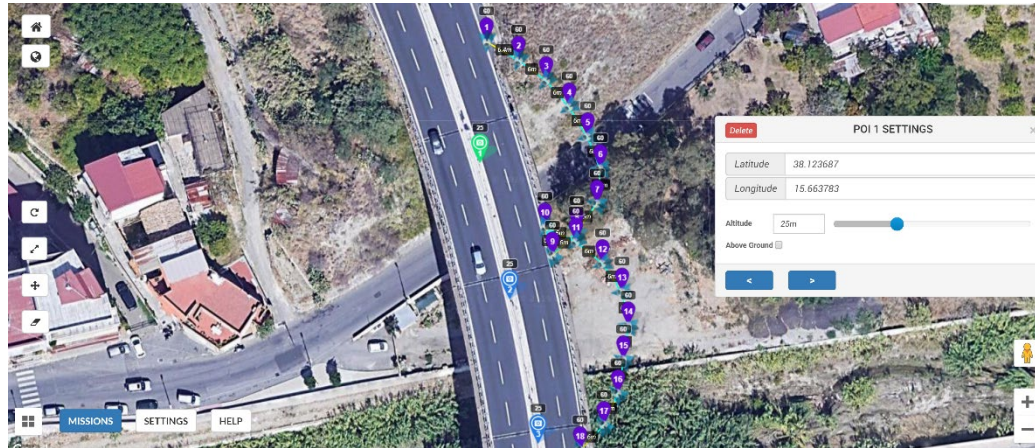


Figure 102 - Mission hub for mission 3d flight plan, Litchi platform

The mission route allows the UAV to operate in the 3d space as shown in Figure 104.

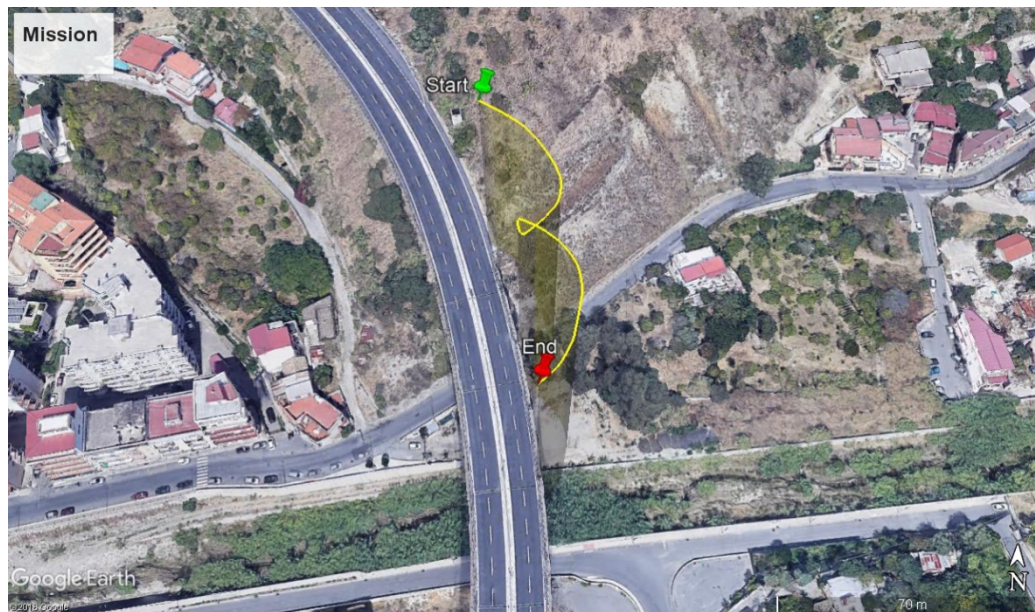


Figure 103 - 3d mission visualization

Also, the definition of the mission plan and the possibility to save the flight log ensures the repeatability of the operation during the time, enabling *continuous monitoring* on regular time-basis and the creation of a database to track changes (e.g. damages after an extraordinary event or after maintenance).

3 b. Georeferencing: As discussed in the previous chapter the SFM-MVS process needs coordinates to locate and scale the project in the real world to obtain a *scaled, oriented and geolocalised* model. The reconstruction without any geo-referred data or GCP can lead to a

model with distortion. The use of built-in UAV GPS is possible if the GPS refresh rate is superior to the shooting interval. Instead, for the use of Ground Control Point, these should be homogeneously distributed with a minimum of 4 GCP, to ensure the quality of georeferencing (James et al., 2017, Chiang et al., 2012). The influence of Ground Control Point on survey, compared with the in-built GPS is analysed in (Putch, 2017). A series of photogrammetric survey and analytical measurements have been carried out using different UAV model with and without control points, concluding that ground control points improved mapping accuracy 10x with an average error of 1 cm. In conclusion, if the project requires highly consistent rates of accuracy or should mission-critical determination need to be made from the dataset, GCP should be used. Moreover, in the GCP alignment process, the centre of marker is selected manually or automatically, but the image resolution it's affected by altitude. Accuracy will no matter if it's possible to precisely identify the target centre, but it's important to take into consideration and adjust the flight altitude to achieve a desired resolution that will allow to properly and confidently identify the GCP target within the processed map.

5.1.2 Data Elaboration

The elaboration phase can be divided into different steps:

4. *Data optimisation*

The acquired data (frame from videos, or images) must be optimized before the 3d reconstruction workflow. The optimisation process on raw data is executed on images parameter to highlight details and maximizing the number of key points (performing SIFT algorithm) for each photo. The following parameters must be optimised:

- With balance to obtain a neutral tone
- exposition to cancel overexposure zone and underexposure
- contrast
- light, shadow, white and black lowering light and increasing the black to highlight shadows
- clarity as a measure of the localised contrast must be increased over the middle
- vividness to act only on less saturated colours, saturation on all colours

5. *SFM-MVS algorithms for the generation of 3d point cloud*

Processed images, with geo-referenced information (from GCP or onboard RTK-GPS), are then used as input for the generation of the 3d geo-referenced point cloud through SFM-MVS algorithms, as previously discussed in chapter 3.

6. Image analysis for point cloud segmentation

In order to identify the different structural part of the bridge, point cloud classification must be performed, splitting terrain and structural sub-system (such as a pier, pier cap, deck and cable). The starting point of this process is the identification of the structure on the image dataset performed using image segmentation algorithms based on machine learning, as described in chapter 3. The classified dataset (image with alpha masks applied according to structural parts, as shown in Figure 104) it is used to select points in the 3d point cloud inside or outside the alpha mask, using Agisoft Metashape (Agisoft LLC, Russia).

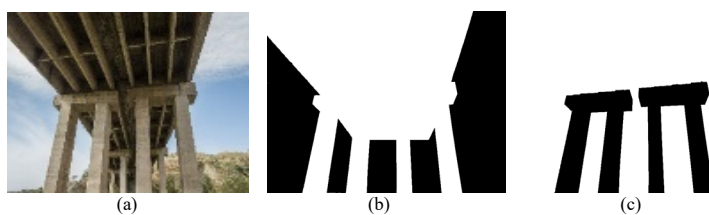


Figure 104 - UAV image segmentation

The output of this process, thanks to the application of the 2d masks on the 3d model, is a classified measurable 3d point cloud of the object.

7. Image analysis for cracks and deterioration

The application of machine learning algorithms can be used to identify standard defects and deterioration on the acquired image, and through masks, the position of these defects in the 3d model.

5.1.3 Feature extraction

8. Orthophoto, section and prospects

The standard output of the survey that can be extracted from the 3d point cloud and meshes are orthophoto, section and prospects of the bridges. The obtained results can be used for blueprint's comparison.

9. Extraction of structure geometrical characteristics

The extraction of the relevant information such as geometry from the surveyed model is performed using a semi-automated methodology. The developed procedure (synthesized in Figure 105) extracts the shape from the segmented structural parts and automatically insert the data into a pre-defined spreadsheet. The structural parts already classified are transformed from point cloud into a 3d mesh object using Screened Poisson Surface Reconstruction (Kazhdan & Hoppe, 2013). The automated transcription is performed using a simple User Interface (UI), and data swapping (point 4) used to avoid non-compatibility of extraction algorithms with Visual Basic Marco.

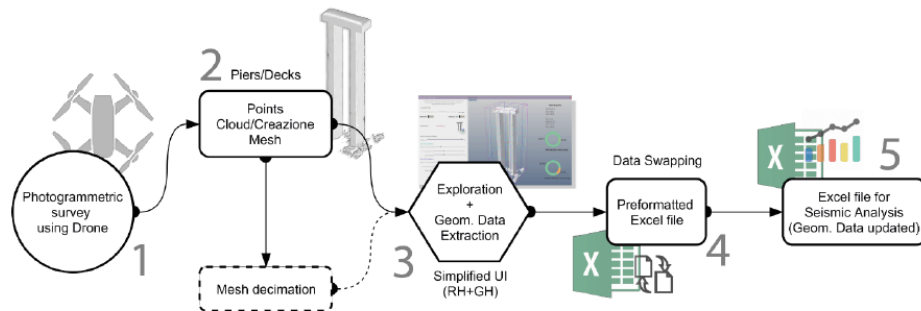


Figure 105 - Extraction of geometrical features

The extraction (point 3, Figure 106) is performed using Rhinoceros and Grasshopper (McNeel, North America) with the visual code represented in Figure 107.

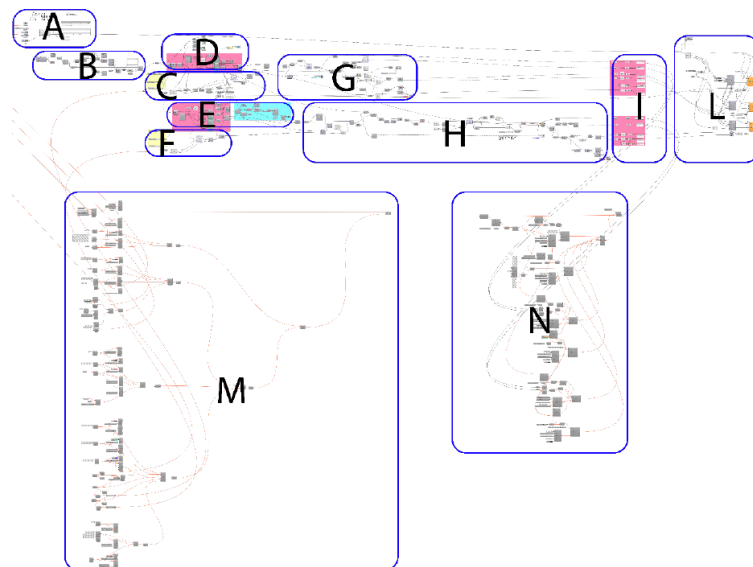


Figure 106 - Grasshopper algorithm for feature extraction

All the components are programmed ad-hoc.

The basic principle used is the definition of two cut-plane XY and YZ to define the structure resistant section. Block A is used to load the mesh into the workflow. B block is used to discretise the object and automatically orient the dominant axis according to z-axis. The bounding box, as volumetric element around the object, is created to intersect cut-plane inside the box and the object. In C,D,E,F block the cut-planes are setting up in XY and YZ. Through the block C and F the user can define the position of the cutting plan in % compared with height, offset distance from cutting-plane and a total number of cutting plane as shown in Figure 108.

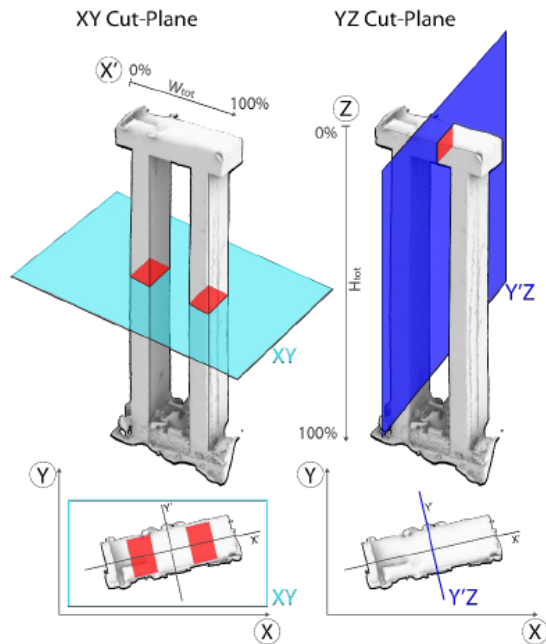


Figure 107 – Cut plane for geometry extraction

Block G and H are used to extract the closed polyline that defines the perimeter. A preventive verification of the planarity and closure of the polyline is executed. If the polyline is not close, the algorithm will approximate the closure. Block M and N are used to generate the UI and return extracted data to the user. Geometrical feature confirmed by the user is then automatically uploaded on a spreadsheet.

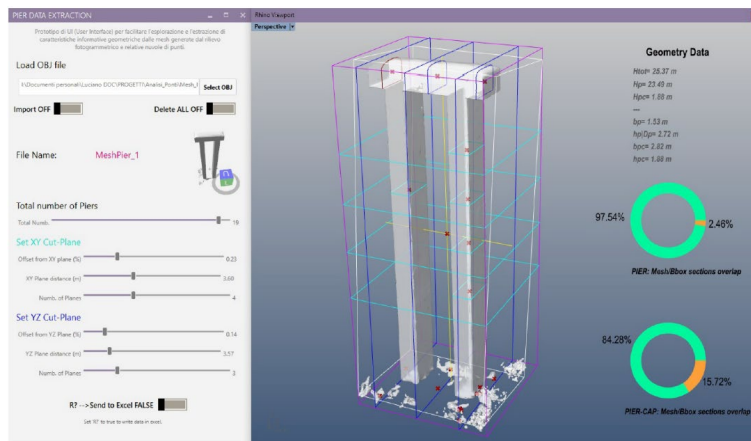


Figure 108 - Simplified UI for extraction of geometrical features

10. 3d inspection and measurable model on a web-based platform

The reconstructed 3d point clouds are enormous data and information difficult to manage and share (Wimmer et al., 2006, Scheiblauer et al., 2014). To enable a simple and effective visualisation, the possibility of analysing and inspecting the surveyed assets with a collaborative approach, a web-based framework was used. The platform for

visualising and share the information are fundamental in the survey process (Eschmann & Wundsam, 2017). Potree (Schuetz, 2016) is a free open-source WebGL based point cloud renderer for large point clouds and 3d meshes, developed at the Institute of Computer Graphics and Algorithms, TU Wien. This platform allows the online visualisation and sharing of classified 3d point cloud, converted into a light HTML file using Lastool (Hug, Krzystek, & Fuchs, 2012) and also 3d mesh. The 3d object must be uploaded on a dedicated web server and shared online using the web viewer (Figure 110).



Figure 109 - Web-interface for visualization and collaborative inspection

Moreover, the online platform allows different interaction and measurements to gather information from the uploaded model such as measurements, cross-sections, annotation, download and mesh visualisation.

5.2 Application to Annunziata viaduct, Reggio Calabria

Annunziata viaduct (38.123295 N, 15.663884 E) is a highway bridge located on the A2 “Autostrada del Mediterraneo” in the city of Reggio Calabria, Italy (Figure 110). The infrastructure, part of the A2 highway and managed by a public-private company, ANAS S.p.A, is located in the south of Italy and for this reason exposed to high seismic risk according to Italian INGV (National Institute of Geophysics and Volcanology). The strategic position makes this viaduct fundamental for the entire highway, linking north and south part of the city, allowing circulation of vehicle and truck out-side of the city. In case of collapse the entire highway will be interrupted with high risk and consequence on vehicle circulation and emergency response.

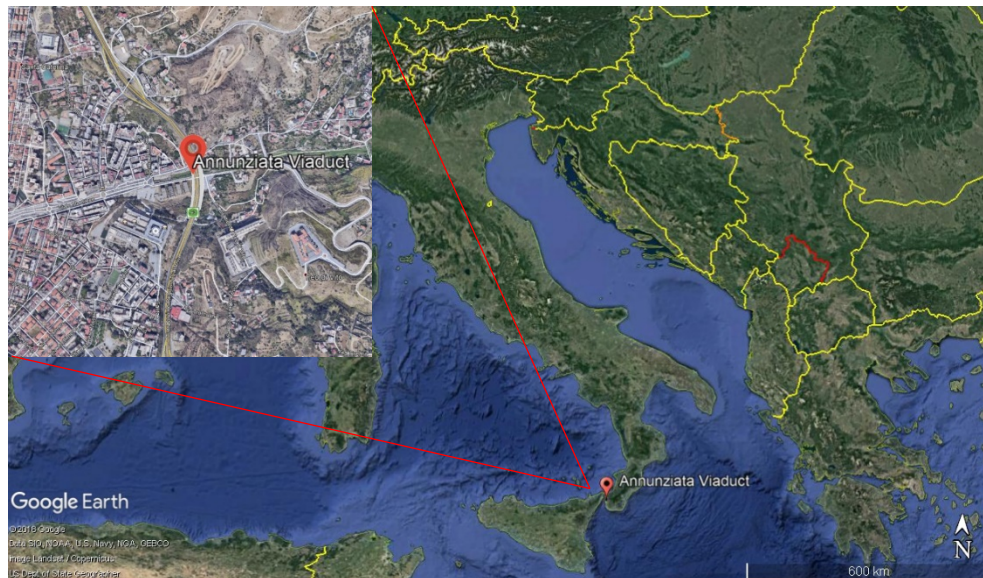


Figure 110 - Localization of Annunziata Viaduct, A2 Highway, Reggio Calabria, Italy

The viaduct, designed on 1970 and constructed from 1968 and 1980 upon the “Annunziata” river, is a simply supported, beam viaduct made of pre-stressed reinforced concrete with 9 short-spans of 27 m, and a total length of 254 m (in curve). Curvature radius is 150 m, and the medium height of the bridge is 25 m a.g.l. The viaduct was chosen for its simple structure and characteristics (Figure 112).



Figure 111 - Aerial view of Highway viaduct Annunziata, Reggio Calabria, Italy

The viaduct deck is composed of a standard module of 29 m with 4 beams and 3 crosses in pre-stressed reinforced concrete (Figure 113).



Figure 112 - Viaduct deck, down view

The two decks (one per each direction) are sustained by a couple of piers with a common foundation (Figure 114). Piers are made of rectangular section of 2,50 m x 1,60 m and pier cap dimensions are 8 m x 3 m.



Figure 113 - Viaduct Piers, support (a) and foundation (b)

Right and top views of the viaduct with element name are represented in Figure 115 and Figure 116:

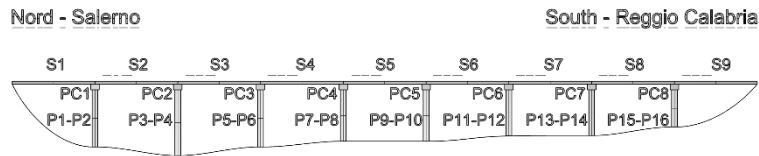


Figure 114 - Static scheme Annunziata viaduct

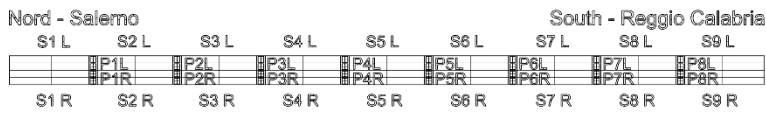


Figure 115 - Deck subdivision

For each direction (right and left) the viaduct is composed by a couple of piers, pier cap and standard deck element are synthesized in Figure 117.

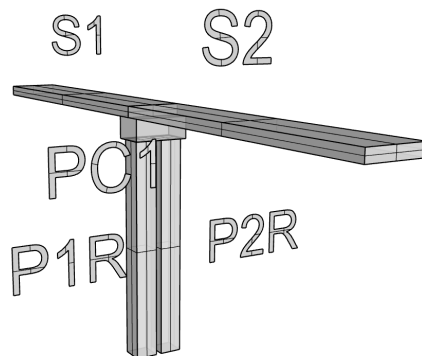


Figure 116 - Bridge elements

The structure elements are resumed in Table 12:

Span		Piers		Piers cap	
S1 Left	S1 right	P1-2 Left	P1-2 Right	PC1 Left	PC1 Right
S2 Left	S2 right	P3-4 Left	P3-4 right	PC2 Left	PC2 Right
S3 Left	S3 right	P5-6 Left	P5-6 right	PC3 Left	PC3 Right
S4 Left	S4 right	P7-8 Left	P7-8 right	PC4 Left	PC4 Right
S5 Left	S5 right	P9-10 Left	P9-10 right	PC5 Left	PC5 Right
S6 Left	S6 right	P11-12 Left	P11-12 right	PC6 Left	PC6 Right
S7 Left	S7 right	P13-14 Left	P13-14 right	PC7 Left	PC7 Right
S8 Left	S8 right	P15-16 Left	P15-16 right	PC8 Left	PC8 Right
S9 Left	S9 right				
Span = 18		Piers = 32		Pier cap = 16	
Tot number of element = 66					

Table 12 - Viaduct basic element

Several superficial cracks are visible on piers (Figure 118), as sign of lack of maintenance operations. Moreover, water infiltration from deck to piers, due to lack of adequate gutter, represents issue on the structure.



Figure 117 – Superficial cracks on piers (a,b)

Mechanical characteristics of materials obtained from the management company are resumed in Table 13:

Concrete Compression resistance [N/mm ²]	2,8
Steel Trazione resistance [N/mm ²]	258
Concrete elastic module [GPa]	5,7
Steel elastic module [GPa]	206

Table 13 - Material characteristics

5.2.1 “Annunziata” data acquisition

The aerial survey of the Annunziata Viaduct was executed in September 2018 in the early morning, with the cloudy weather condition and moderate operating temperature (18°C) to avoid direct sunlight in the acquired images and to optimise the dataset for the 3d reconstruction

process. The workflow for bridge aerial survey (Figure 88) was applied for the aerial survey plan, acquisition and elaboration process.

1. Definition of tasks, structure and area of interest

The objective of the mission was the complete acquisition of the Annunziata viaduct and the extraction of the structure geometry with centimetre accuracy. The acquired structure, a simply supported viaduct in the A2 highway and the related characteristics were explained in the previous paragraph.

Regulation in Italy, as previously explained, are emitted by “Ente Nazionale Aviazione Civile” (ENAC) and defined in “Regolamento Mezzi Aerei a Pilotaggio Remoto”. The EASA Drone Regulatory Framework, active in the European Union, is integrated into this national regulation. The city of Reggio Calabria is inside an ATZ (Aerodrome Traffic Zone) due to the presence of the Airport “Tito Minniti” near the city (Figure 119). As specified on the actual regulation UAV operation, with operating take-off mass less than 25 kg, into the ATZ is allowed in VLOS at the maximum flight height of 45 m AGL (Above Ground Level) or 45 m above the highest obstacle/infrastructure. Visual line of sight (VLOS) flight is allowed at a maximum distance of 200 m, with manual or automatic flight.

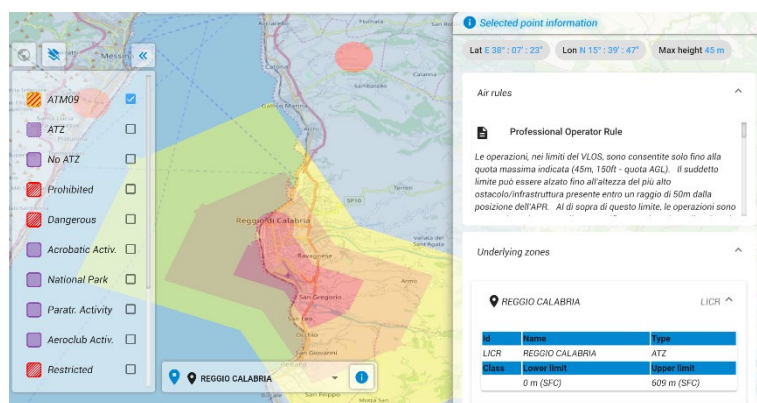


Figure 118 - Area of interest and regulation for ATZ zone, Source: D-flight (ENAC)

The environment around the viaduct is free, occupied by low altitude buildings and two cranes on the right side, and some vegetation on the right side (Figure 120). The presence of these obstacles was taken into consideration for the missions' flight plan. Considering that the viaduct height is 25 m, according to actual regulation and ATZ zone, maximum flight height is 80 m AGL.



Figure 119 - Obstacles and environment around Annunziata Viaduct

A virtual fence area around the object (Figure 121) was created to delimitate the operating airspace of the UAV and to allows the operation only inside this virtual 3d area. The take-off and landing point were set-up in the parking area near the bridge for safety and logistic reason.



Figure 120 - Virtual fence around Annunziata Viaduct for aerial survey

2. Definition of UAV type and payload

The aerial survey was performed using a commercial quadrotor UAV from DJI (DJI, Shenzhen, China), Mavic Pro, whose specs are summarised in Table 14. This model is a low-cost low-weight (700gr) and portable UAV that can be used to perform both manual and waypoint navigation to acquired photographic dataset.


	
Dimensions	83 x 83 x 198 mm
Weight	734 g
Max speed	65 km/h
Flight autonomy	27 min
Battery type. capacity	LiPo 3S – 3830 mAh
Maximum distance	13 km
Operating temperature	0° – 40° C
GNSS system	GPS/GLONASS
Flight accuracy	Vertical +/- 0,1 m Horizontal +/- 0,3 m

Table 14 - DJI Mavic Pro characteristics

Mavic Pro UAV has a fixed payload with Sony RGB camera sensor whose specs are reported in Table 15:

CAMERA SPECS	
Sensor	Sony 1/ 2.3'' CMOS
Lens	28 mm f/2.2
Real focal length	5 mm
Real sensor width	6.17 mm
Field Of View (FOV)	78,8°
Electronic Shutter Speed	8 s – 1/8000 s
ISO range	100-1600
Image resolution	12.35 MP
Image size	4000 x 3000
Geotagging	Internal built-in GPS

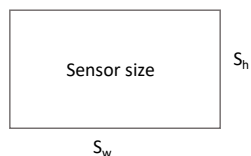
Table 15 - Payload camera sensor

The UAV has a built-in GPS used for position and geotag for images.

3. Flight Plan setup

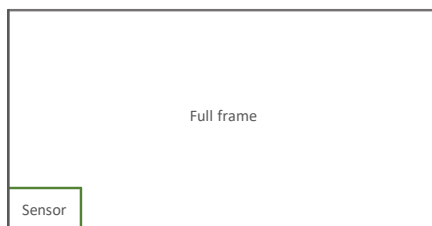
3a. The maximum flight distance (both perpendicular and vertical) to achieve centimetre level accuracy for the 3d model reconstruction, was set equal to 30 m. The GSD associated with the used RGB camera sensor and 30 m flight distance was calculated according to Equation 2 equal to 1 cm/pix.

CAMERA SENSOR



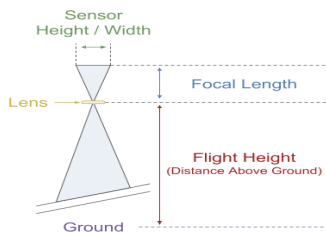
Sw = sensor width
Sh = sensor height
d = diagonal
cp = crop factor
Fr = focal length real
Fr 35eq = focal length 35mm equiv

Sw (mm)=	6,17
Sh (mm)=	4,55
d (mm)=	7,67
cf (crop factor)=	5,64
FR (mm) =	4,61
FR 35eq (mm) =	26,00



Full Frame (35mm)
Sw (mm)= 36
Sh (mm)= 24
d (mm)= 43,27

GSD Ground Sampling Distance



$$GSD_w = \frac{H \times S_w}{F_R \times im_w}$$

H = flight height
 S_w = Sensor width
 F_R = Focal Length
 im_w = image width

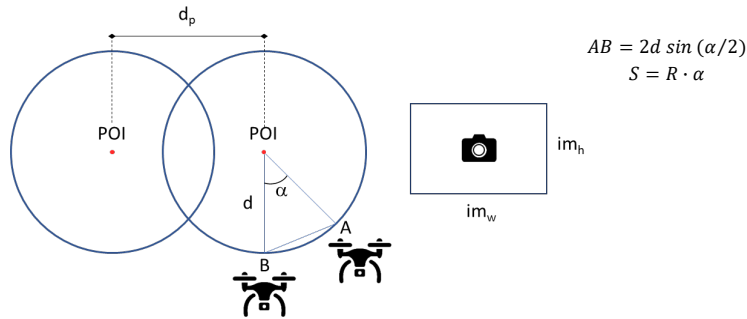
GSD required (cm/pixel)	1		
H max (m) =	30		
H (m) =	30		
GSD real (cm/pixel) =	1,0	Verified	
im w ground (m) =	39,94	perpendicular to UAV direction	$im_{w\ ground} = GSD \times im_w$
im H ground (m) =	29,95	On UAV direction	$im_{H\ ground} = GSD \times im_H$

Figure 121 – UAV sensors characteristics and GSD calculation

Waypoint navigation with the semi-circular path was planned and executed to acquire the entire photographic dataset, with an overlap of 90% between each photo and 30% from one circle to the subsequent as summarised in Figure 123.

Following the semi-circular path near the viaduct, six different missions (three for each side) were executed at different flight height (according to terrain slope variation) with different camera tilt angle, as summarised in Table 16.

CIRCULAR MISSION ACQUISITION



$$AB = 2d \sin(\alpha/2)$$

$$S = R \cdot \alpha$$

d from structure (m) = 30
 Overlap = 30% (suggested 20-40)
 d_p (m) = 42 distance between POI

GSD 1,0
 im_w ground (m) = 39,94 perpendicular to UAV direction
 im_h ground (m) = 29,95 On UAV direction

Fixed overlap

Transversal overlap = 90%
 $d_s T$ (m) = 3,99

α (°) = 7,63
 α (°) (approx) = 10 angle between photos

$$\alpha = 2 \arcsin [d_{s\,transv} / (2 \cdot d)]$$

Figure 122 – Circular mission settings for waypoint semi-circular path

Mission	Flight height	Camera tilt	UAV speed	Mission length
1 left	15	- 30 °	28 km/h	608 m
1 right	15	- 30 °	28 km/h	608 m
2 left	30	+ 10 °	28 km/h	618 m
2 right	30	+ 10 °	28 km/h	618 m
3 left	60	+ 60 °	28 km/h	620 m
3 right	60	+ 60 °	28 km/h	620 m

Table 16 - Missions detail

Litchi platform was used as mission planning, to set up the Point of interest, calculated as described, and set up the different waypoint and camera tilt angle at defined height AGL as in Figure 124.



Figure 123 - Semi-circular path with waypoint navigation, left side mission

The UAV route following the waypoint navigation as in the planned missions around the viaduct are visible in the 3d representation in Figure 125

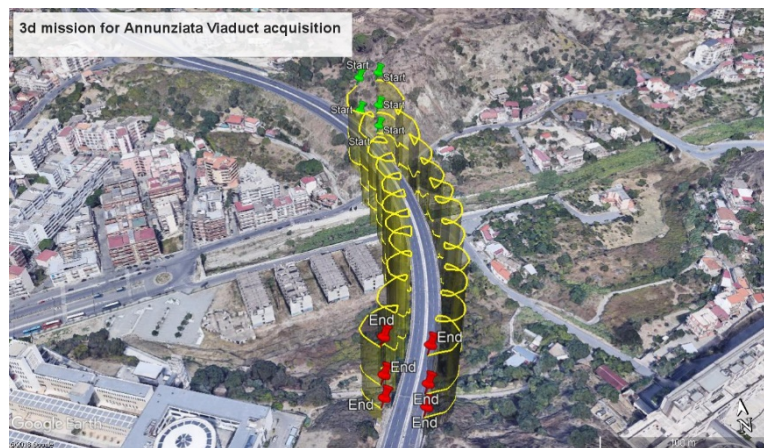


Figure 124 - 3d mission path

The acquired dataset is composed of 965 photos around the viaduct.

3b Georeferencing

To georeferencing the 3d model, different ground points were acquired using GEOMAX in WGS84 coordinate system, distributed on the plan as described in Figure 126 and summarised in Table 17:

Point n.	Latitude	Longitude	Altitude
1	38.123166	15.664129	48.039
2	38.123097	15.664128	48.224
3	38.121631	15.663419	68.445
4	38.123412	15.663525	54.120
5	38.123737	15.664095	58.325

Table 17 - Surveyed GCP with the position in WGS84

5.2.2 “Annunziata” viaduct data elaboration

4. Data optimisation

The entire acquired dataset was optimised enhancing shadows and reducing lights as described in the previous paragraph.

5. SFM-MVS algorithm

The dataset was elaborated using Agisoft Metashape (Agisoft LLC, Russia) applying the described SFM-MVS reconstruction algorithm to the photographic dataset: the obtained results are summarised in Figure 127 and Table 18.

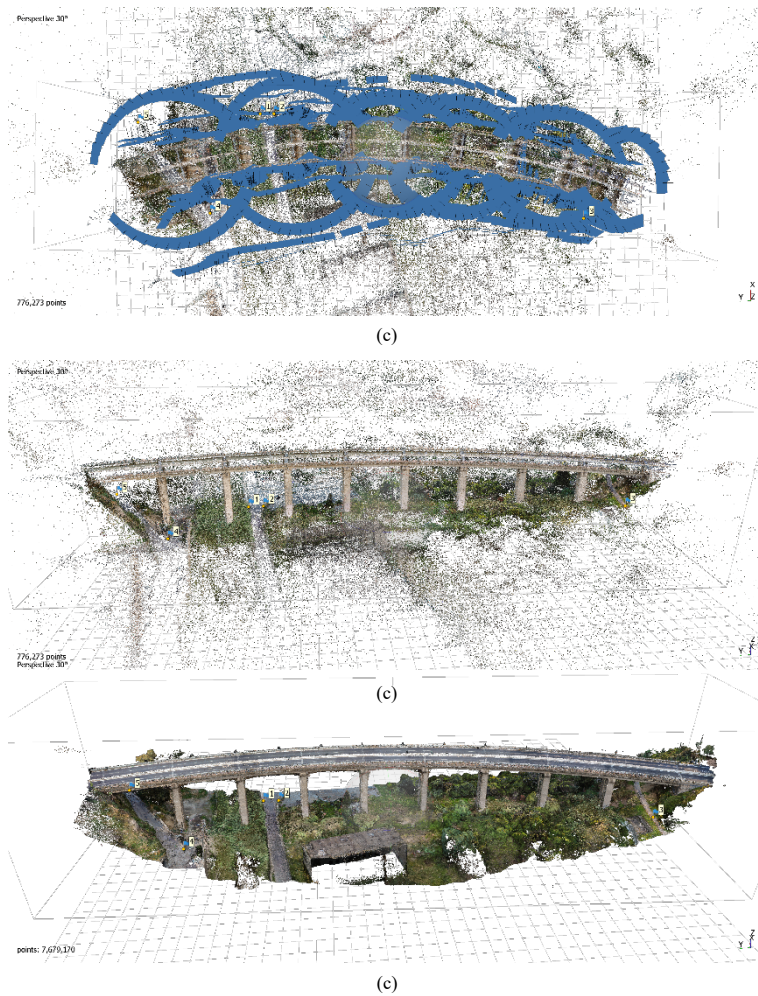


Figure 126 - SFM-MVS reconstruction (a) camera alignment, (b) sparse point cloud, (c) dense point cloud



Figure 125 - GCP position

Reconstruction process	Features
Photos alignment	965/965 aligned photos
Sparse point cloud	776.273 points
Dense Point cloud	7.679.170 points

Table 18 - SFM-MVS reconstruction detail

The acquired photos cover with sufficient overlap the entire area ensuring centimetre precision as shown in Figure 128

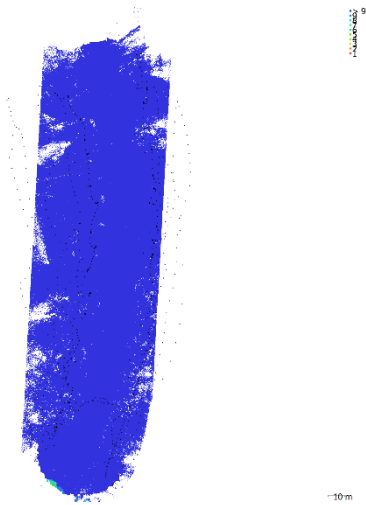


Figure 127 - Statistics camera coverage

6. Image instance segmentation for point cloud classification

To classify the obtained point cloud, the procedure using image segmentation was applied to the entire dataset. The training dataset of 15 images was used to train the neural network applying label to the images (Figure 129, Figure 130).

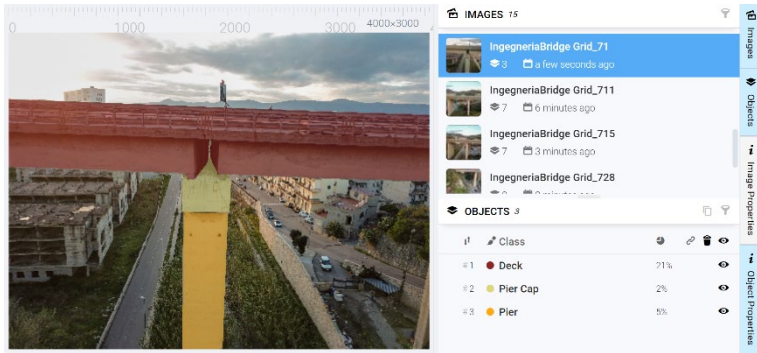


Figure 128 - Image labelling on web platform side view

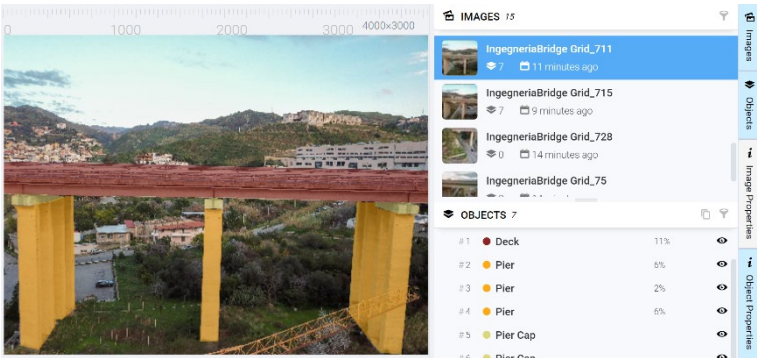


Figure 129 - Image labeling on web platform side overview

The augmented dataset composed of 330 images was used to train the neural network, also identifying the background.

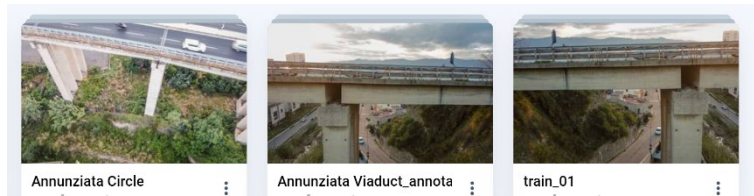


Figure 130 - Datasets for neural network training

The obtained point cloud classified with Ground (brown) Deck (purple) and piers (red) is represented in Figure 132.

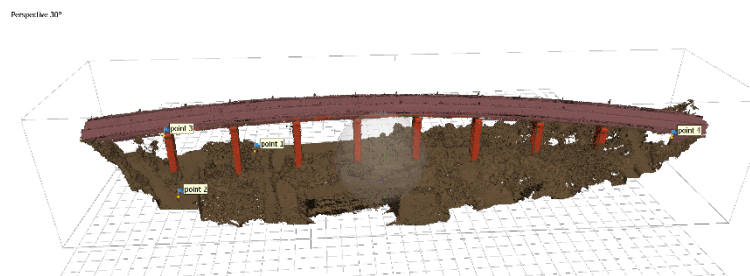


Figure 131 - Classified 3d point cloud with ground, piers and deck

5.2.3 “Annunziata” viaduct extraction and presentation

8. Orthophoto, section and prospects

The obtained orthophoto, DEM, section and prospects of the viaduct are represented in:

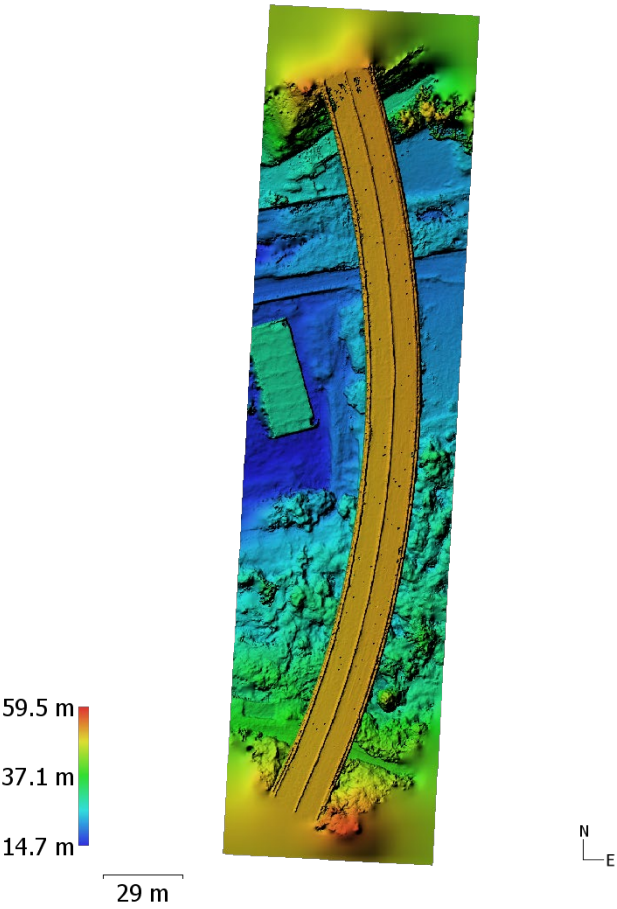


Figure 132 - DEM of the acquired area

9. Extraction of structure geometrical characteristics

The geometrical feature of the structure extracted using the procedure are summarised in the following images and table.

Deck

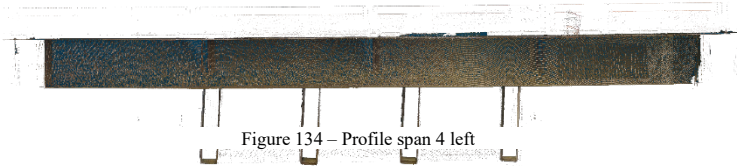


Figure 135 – Section Span 4 left



Deck dimensions are reported in Table 19:

Span n.		1	2	3	4	5	6	7	8	9
Lenght (m)		29	29	28,5	28,8	29	29	28,7	28,7	28
widht (m)		9,5	9,5	9,5	9,5	9,5	9,5	9,5	9,5	9,5

Base	base (m)	9,5	9,5	9,5	9,5	9,5	9,5	9,5	9,5	9,5
	height (m)	0,8	0,8	0,8	0,8	0,8	0,8	0,8	0,8	0,8
Beams	Lenght (m)	27	27	27	27	27	27	27	27	27
	base (m)	0,4	0,4	0,4	0,4	0,4	0,4	0,4	0,4	0,4
	height (m)	1,5	1,5	1,5	1,5	1,5	1,5	1,5	1,5	1,5
	n	4	4	4	4	4	4	4	4	4
Cross	Lenght (m)	6,5	6,5	6,5	6,5	6,5	6,5	6,5	6,5	6,5
	base (m)	0,2	0,2	0,2	0,2	0,2	0,2	0,2	0,2	0,2
	height (m)	1,5	1,5	1,5	1,5	1,5	1,5	1,5	1,5	1,5
	n	3	3	3	3	3	3	3	3	3

Table 19 - Span surveyed geometry

Piers

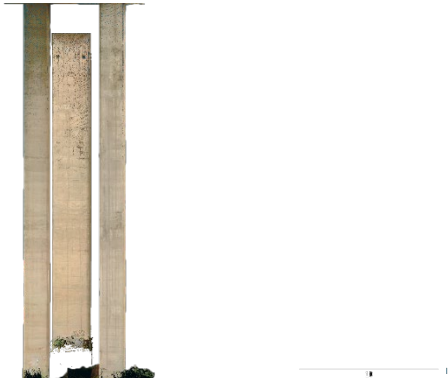


Figure 138 – Side view left, Piers 10 left

Figure 136 – Prospect of piers n.9-10 left



Figure 137 - Section piers 9-10 left

Pier dimensions are summarized in Table 20:

Pier	1	2	3	4	5	6	7	8
H (pier height) (m)	21	24	22	22	21	20	16	15

Geometry	R	R	R	R	R	R	R	R
h or D (m)	2,60	2,60	2,60	2,60	2,60	2,60	2,60	2,60
b (m)	1,50	1,50	1,50	1,50	1,50	1,50	1,50	1,50
c (m)	0,02	0,02	0,02	0,02	0,02	0,02	0,02	0,02

Table 20 - Pier dimensions, R = rectangular

Pier’s cap

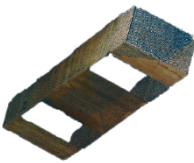


Figure 139 - Viaduct pier cap n.4 left

Pier cap dimensions are summarized in Table 21:

Pier cap	1	2	3	4	5	6	7	8
H pc (pier cap height) (m)	1,2	1,2	1,2	1,2	1,2	1,2	1,2	1,2

Geometry	R	R	R	R	R	R	R	R
h or D (m)	8,0	8,0	8,0	8,0	8,0	8,0	8,0	8,0
b (m)	2,5	2,5	2,5	2,5	2,5	2,5	2,5	2,5

Table 21 - Pier cap dimensions, R= rectangular

10. 3d inspectionable and measurable model on the web-based platform

The point cloud was uploaded on an interactive web platform for consultation and share (Figure 141).



Figure 140 - Point cloud visualization on online viewer

The web visualizer also allows the extraction of the section in CAD format, elevation model and profile (Figure 142).

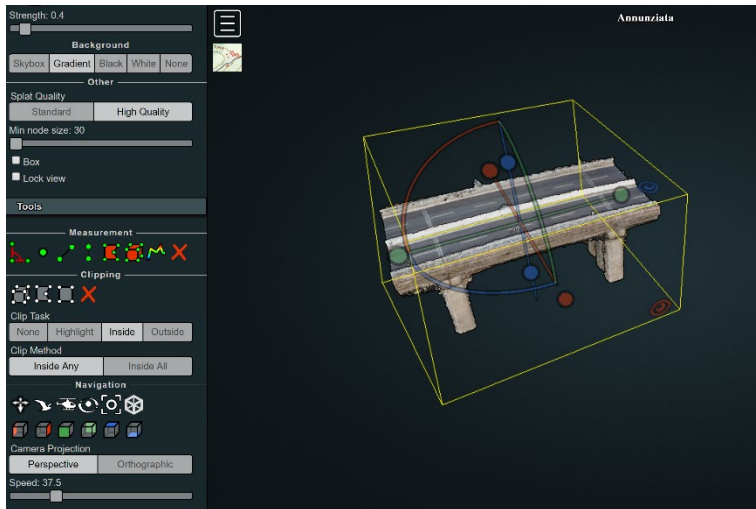


Figure 141 - Clipping box tool for feature extraction

5.3 Application to Musmeci bridge – Potenza

The bridge over Basento river (40.627313 N, 15.806557 E), also known as “Musmeci Bridge”, is located in south of Italy in Basilicata region, providing the primary access to the small hillside town of Potenza from the European route E 847, which runs along the banks of the Basento river connecting to the east (e.g., Apulia) and west (e.g., Campania) coasts (Figure 143).

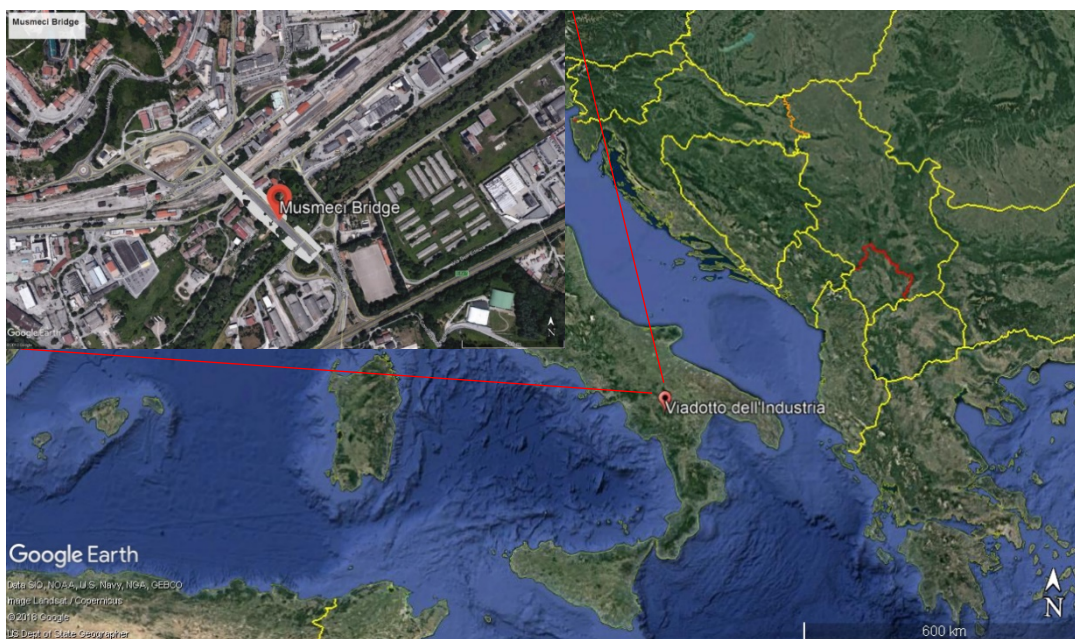


Figure 142 - Musmeci bridge overview

The bridge was designed by 87 Sergio Musmeci in the 1960s and represents a true work of art in RC which influenced the architectonic culture of the 20th century (Bavusi et al., 2011). The bridge is about 300m long and is composed of an RC box deck supported by a continuous double-curvature shell of the same material (Figure 143). The shell, that forms four equal spans of 69:20 m each has a thickness of 0:30 m and it is characterised by deeper ribs at both sides (i.e., lateral boundaries). It bears the bridge deck by means of 16 pairs of supports that are placed at equal intervals of 17:30m along the longitudinal axis and 12:00m transversally.

The RC shell is reinforced with two grids located in the intrados and extrados with the same concrete cover. In the original design, the RC shell should have supported a pedestrian crossing (made of a system of stairs and railings) located between the deck and the shell. Unfortunately, this pedestrian crossing was never realized even if the crossing on foot on the RC shell is still easy given the relative low curvature of the shell in the longitudinal direction.

At the two extremities of the bridge, the RC shell is connected to the abutments along its entire width, while it joins the intermediate foundations at 4 points placed at the vertices of a square of side 10.40m, positioned between each pair of contiguous spans. Each of the intermediate footings is made by four plinths, each supported by 4 RC piles of diameter 1m (Figure 145).

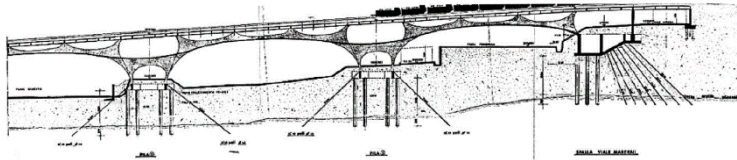


Figure 143 - Final design of the deck and foundations



Figure 144 - Musmeci bridge location

The gravity abutments are subjected to the horizontal thrust of the RC shell and are founded on 15 RC piles of diameter 1m, integrated with 144 steel piles (Figure 144). The deck is 16 m wide, for four traffic lanes, and has a five-cell RC boxed cross-section with elongated elliptical shape, 1.50m deep. It has an approximately constant longitudinal slope of 4 %. It consists of a Gerber beam with joints placed at 5,17 m from the midspan and from the centre between two consecutive spans. Accordingly, drop-ins have a length of 10,38 m, while cantilevered beams, of total length 24,22 m, have equal overhangings 3,46 m long. The analysis of the form of the bridge over the Basento river requires an accurate geometric three-dimensional (3D) model of the RC shell supporting the bridge deck. Lasers scan survey represents the most accurate and diffused technique for 3D geometric reconstruction. The main drawbacks of using laser scanners are related to: (i) expensive cost of the equipment, (ii) long time required for the survey and for data acquisition and (iii) time-consuming post-processing analysis. To obtain refined 3D models overcoming these drawbacks the discussed methodology for aerial survey with the use of Unmanned Aerial Vehicle (UAV) was performed.

In this case study, a refined 3D model of the first span (Figure 146) of the RC shell of the bridge over the Basento river was reconstructed. In a first step (data acquisition), a commercial UAV was employed to obtain a complete photographic dataset from different points of view. In a second step (3D reconstruction), an accurate geometric 3D model of the bridge was reconstructed. Finally, the so-obtained geometric 3D model has been compared with the designed geometry of the model. These phases are described below in full detail.

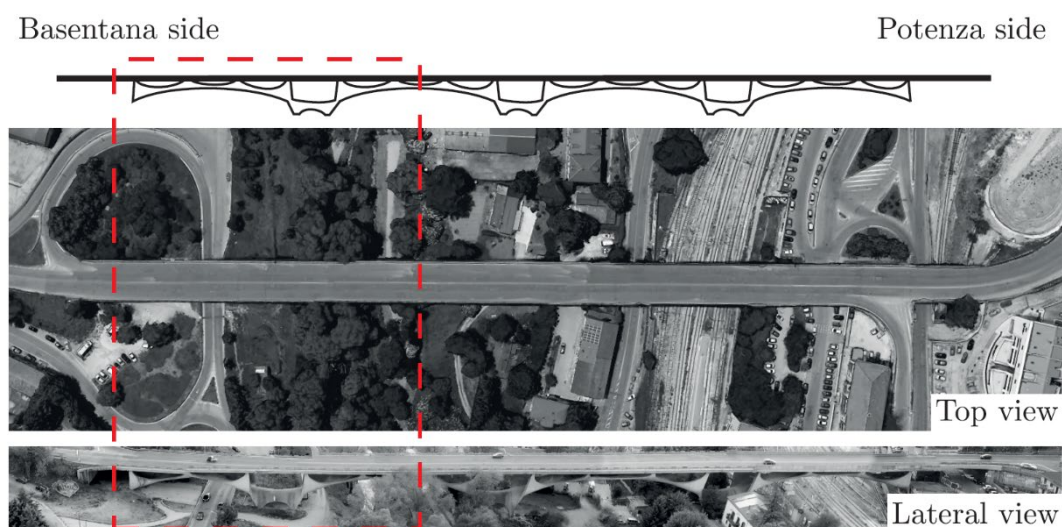


Figure 145 - Location and general arrangement of the bridge over Basento river (Potenza, Italy). The red dashed rectangle shows the region of the photographic aerial survey (i.e., first span).

5.4.1 “Musmeci Bridge” data acquisition

1. Definition of tasks, structure and area of interest

The object of the mission was the 3d reconstruction of the first span of the Musmeci bridge with centimeter accuracy. The airspace around the bridge, according to actual regulation and map, is free without any restriction (Figure 147).



Figure 146 - Regulation and flight restriction around Musmeci bridge

The left side of the bridge is covered by vegetation and trees. The virtual fence was defined to delimitate the operating airspace around the object and take-off and landing point was set in the right side parking area (Figure 148).



Figure 147 - Musmeci bridge virtual fence, take-off and landing point

2. Definition of UAV type and payload

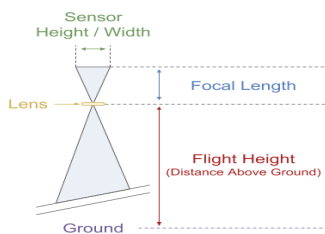
The aerial photographic survey was performed by using a commercial UAV DJI Mavic Pro (DJI, Shenzhen, China). The summary of the UAV characteristics and camera installed on the device are reported in Table 14 and Table 15. The built-in GPS allowed for controlling the UAV and obtaining camera positions.

3. Flight Plan setup

Recurrence and symmetry of the structure allowed for restricting the area of interest of the survey to the first span of the bridge (Figure 145), to have adequate clearance from vegetation and artificial obstacles.

To achieve centimetre accuracy (Lourenço & Figueiras, 2002), the maximum flight distance was set equal to 30 m. The GSD associated with the RGB camera sensor and 30 m flight distance was calculated according to Equation 1 (Figure 148).

GSD Ground Sampling Distance



$$GSD_w = \frac{H \times S_w}{F_R \times im_w}$$

$$\begin{aligned} H &= \text{flight height} \\ S_w &= \text{Sensor width} \\ F_R &= \text{Focal Length} \\ im_w &= \text{image width} \end{aligned}$$

GSD required (cm/pixel) 1

H max (m) = 30

H (m) = 30

GSD real (cm/pixel) = 1,0

im w ground (m) = 39,94

im H ground (m) = 29,95

Verified

perpendicular to UAV direction

On UAV direction

$$im_{w \text{ ground}} = GSD \times im_w$$

$$im_{H \text{ ground}} = GSD \times im_H$$

Figure 148 – UAV sensors characteristics and GSD calculation

Overlap was set equal to 80% by assigning proper image acquisition rate.

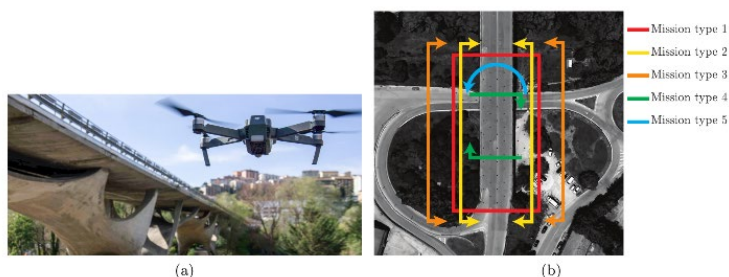


Figure 149 - (a) UAV in operating conditions near the bridge; (b) Path of the different missions executed

Flight missions were planned in semicircular waypoint mode from the two side of the bridge, and in manual mode (due to the complex bridge shape) inside the bridge (Figure 150) to acquire the internal geometry by employing the commercial software Litchi (VC Technology Ltd, London). The overall aerial survey was performed on an area of about 2.500 m, scanned in 38 min of effective flight. The acquired dataset consists of a total of 677 high-resolution photos corresponding to about 4 GB of data. The location of the camera poses is shown in Figure 151 together with a 3D model of the bridge.

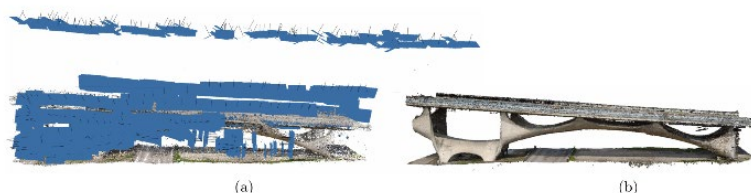


Figure 150 - (a) Camera poses, (b) 3d model of the bridge

3b. Georeferencing

Known measures of the bridge, obtained using a laser distance meter, have been used to calibrate the scale of the 3D model.

5.4.2 “Musmeci bridge” data elaboration

The photographic dataset acquired during the survey has been used as input of the 3D reconstruction process. This process was carried out in the photogrammetry software Metashape (Agisoft LLC, St. Petersburg, Russia) based on the MVS-MVS algorithms.

First, a sparse point cloud (301.035 points) has been obtained. Then, based on the estimated camera positions, spatial depth information for each camera has been calculated in order to obtain a dense point cloud (67.632.880 points). Subsequently, using the Poisson disk algorithm

(Criniere et al., 2016) implemented in MeshLab (Corsini et al., 2012), the dense point cloud was preliminarily simplified by uniformly decimating the number of points; then, the screened Poisson surface reconstruction algorithm was used to build a triangulated mesh of 12.953.842 elements.

5.4.3 “Musmeci bridge” feature extraction and presentation

Finally, given the complexity and irregularity of the surface mesh, a parametrisation of the geometry was carried out by using the 3D computer graphics software Rhinoceros v6 (Robert McNeel & Associates, Seattle, Washington, USA) together with the Mesh2Surface (KVS OOD, Blagoevgrad, Bulgaria). The 3D object was used to create curve-based free-form surfaces (i.e., a continuous surface) tailored on the original mesh surface Figure 151. The curve-based free-form surfaces used for the intrados and the extrados of the RC shell were obtained from a curve network of 7×24 parts. The reconstruction was done under real-time control by minimising the deviation between the original surface and the curve-based free-form surfaces. This operation allowed us to obtain two simple curve-based surfaces (intrados and the extrados) by reducing the acquisition error and defying the final 3D reconstructed model shows the comparison between the designed and the surveyed geometries. The designed surface represents the mid-surface of the RC shell. It has been obtained from the original blueprints by Musmeci, which are stored at the MAXXI (National Museum of the 21st Century Arts) in Rome.



Figure 151 – (a) 3d mesh reconstruction surface applied on upper and down sides
(b) 3d reconstructed model

As shown in Figure 153, the designed and the surveyed geometries are quite similar with some small differences between the foundation supports. The result is quite interesting and confirms that the actual geometry is quite in agreement with the blueprints indications although the realisation of this complicated geometry was done using a hand-crafted scaffolding system.

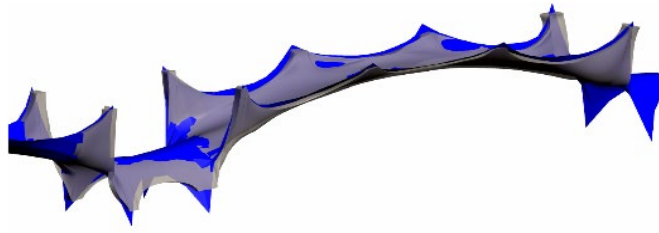


Figure 152 - 3d model with designed (blue surface) and surveyed geometry (transparent white solid)

References

- Bavusi, M., Soldovieri, F., Di Napoli, R., Loperte, A., Di Cesare, A., Carlo Ponzio, F., & Lapenna, V. (2011). Ground penetrating radar and microwave tomography 3D applications for the deck evaluation of the Musmeci bridge in Potenza, Italy. *Journal of Geophysics and Engineering*, 8(3), 33–46. <https://doi.org/10.1088/1742-2132/8/3/S04>
- Chen, S., Truong-Hong, L., Laefer, D., & Mangina, E. (2018). Automated Bridge Deck Evaluation through UAV Derived Point Cloud, (September). Retrieved from <https://archive.nyu.edu/handle/2451/43478>
- Chiang, K. W., Tsai, M. L., & Chu, C. H. (2012). The development of an UAV borne direct georeferenced photogrammetric platform for ground control point free applications. *Sensors (Switzerland)*, 12(7), 9161–9180. <https://doi.org/10.3390/s120709161>
- Corsini, M., Cignoni, P., & Scopigno, R. (2012). Efficient and Flexible Sampling with Blue Noise Properties of Triangular Meshes. *IEEE Transaction on Visualization and Computer Graphics*, 1–12.
- Criniere, A., Dumoulin, J., & Mevel, L. (2016). Heat transfer 1D modeling for Non Destructive Testing and Structural Health Monitoring for civil engineering structures improved by GPGPU. *8th European Workshop on Structural Health Monitoring, EWSHM 2016*, 2.
- Eschmann, C., & Wundsam, T. (2017). Web-Based Georeferenced 3D Inspection and Monitoring of Bridges with Unmanned Aircraft Systems. *Journal of Surveying Engineering*, 143(3), 04017003. [https://doi.org/10.1061/\(ASCE\)SU.1943-5428.0000221](https://doi.org/10.1061/(ASCE)SU.1943-5428.0000221)
- Escobar-Wolf, R., Oommen, T., Brooks, C. N., Dobson, R. J., & Ahlborn, T. M. (2018). Unmanned Aerial Vehicle (UAV)-Based Assessment of Concrete Bridge Deck Delamination Using Thermal and Visible Camera Sensors: A Preliminary Analysis. *Research in Nondestructive Evaluation*, 29(4), 183–198. <https://doi.org/10.1080/09349847.2017.1304597>
- Hackl, J., Adey, B. T., Woźniak, M., & Schümperlin, O. (2018). Use of Unmanned Aerial Vehicle Photogrammetry to Obtain Topographical Information to Improve Bridge Risk Assessment. *Journal of Infrastructure Systems*, 24(1), 04017041. [https://doi.org/10.1061/\(ASCE\)IS.1943-555X.0000393](https://doi.org/10.1061/(ASCE)IS.1943-555X.0000393)
- Hallermann, N., & Morgenthal, G. (2014). Visual inspection strategies for large bridges using Unmanned Aerial Vehicles (UAV). *Bridge Maintenance, Safety, Management and Life Extension*, (July), 661–667. <https://doi.org/10.1201/b17063-96>
- Hallermann, N., Taraben, J., & Morgenthal, G. (2018). BIM related workflow for an image-based deformation monitoring of bridges, (October).
- Ham, Y., Han, K. K., Lin, J. J., & Golparvar-Fard, M. (2016). Visual monitoring of civil infrastructure systems via camera-equipped Unmanned Aerial Vehicles (UAVs): a review of related works. *Visualization in Engineering*, 4(1), 1–8. <https://doi.org/10.1186/s40327-015-0029-z>
- Hug, C., Krzystek, P., & Fuchs, W. (2012). Advanced Lidar data processing with Lastools. *International Society for Photogrammetry and Remote Sensing (ISPRS)*, (July), 12–23.

- James, M. R., Robson, S., d'Oleire-Oltmanns, S., & Niethammer, U. (2017). Optimising UAV topographic surveys processed with structure-from-motion: Ground control quality, quantity and bundle adjustment. *Geomorphology*, 280, 51–66. <https://doi.org/10.1016/j.geomorph.2016.11.021>
- Kazhdan, M., & Hoppe, H. (2013). Screened poisson surface reconstruction. *ACM Transactions on Graphics*, 32(3), 1–13. <https://doi.org/10.1145/2487228.2487237>
- Khaloo, A., Lattanzi, D., Cunningham, K., Dell'Andrea, R., & Riley, M. (2018). Unmanned aerial vehicle inspection of the Placer River Trail Bridge through image-based 3D modelling. *Structure and Infrastructure Engineering*, 14(1), 124–136. <https://doi.org/10.1080/15732479.2017.1330891>
- Lourenço, P. B., & Figueiras, J. A. (2002). Solution for the Design of Reinforced Concrete Plates and Shells. *Journal of Structural Engineering*, 121(5), 815–823. [https://doi.org/10.1061/\(asce\)0733-9445\(1995\)121:5\(815\)](https://doi.org/10.1061/(asce)0733-9445(1995)121:5(815))
- Lovelace, B. (2015). Unmanned Aerial Vehicle Bridge Inspection Demonstration Project, (July), 214. <https://doi.org/10.1016/j.ceramint.2011.07.049>
- Morgenthal, G., & Hallermann, N. (2014). Quality Assessment of Unmanned Aerial Vehicle (UAV) Based Visual Inspection of Structures. *Advances in Structural Engineering*, 17(3), 289–302. <https://doi.org/10.1260/1369-4332.17.3.289>
- Putch, A. (2017). *Linear Measurement Accuracy of DJI Drone Platforms and Photogrammetry*.
- Rossi, P., Mancini, F., Dubbini, M., Mazzone, F., & Capra, A. (2017). Combining nadir and oblique uav imagery to reconstruct quarry topography: Methodology and feasibility analysis. *European Journal of Remote Sensing*, 50(1), 211–221. <https://doi.org/10.1080/22797254.2017.1313097>
- Scheiblauer, C., der Arbeit, V., Wimmer, M., Gervautz, M., gang Knecht, W.-, Marek, S., ... Arian, M. (2014). Interactions with Gigantic Point Clouds, 2014. Retrieved from <https://www.cg.tuwien.ac.at/research/publications/2014/scheiblauer-thesis/scheiblauer-thesis-thesis.pdf>
- Schuetz, M. (2016). Potree: Rendering Large Point Clouds in Web Browsers, 84.
- Wimmer, M., & Scheiblauer, C. (2006). Instant points: Fast rendering of unprocessed point clouds. *Proceedings Symposium on Point-Based Graphics 2006*, 129–136.
- Yang, C. H., Tsai, M. H., Kang, S. C., & Hung, C. Y. (2018). UAV path planning method for digital terrain model reconstruction – A debris fan example. *Automation in Construction*, 93(April), 214–230. <https://doi.org/10.1016/j.autcon.2018.05.024>
- Yoon, H., Shin, J., & Spencer, B. F. (2018). Structural Displacement Measurement Using an Unmanned Aerial System. *Computer-Aided Civil and Infrastructure Engineering*, 33(3), 183–192. <https://doi.org/10.1111/mice.12338>

6. Structural Application: rapid Seismic Risk assessment and form efficiency assessment

In this chapter, two methodologies are introduced for the rapid seismic risk assessment of simply supported bridges and form efficiency assessment of arch bridges. The major damages and cause of collapse for concrete bridges, inducted from earthquake forces, are presented. Starting from the acquired bridges geometry through aerial survey, presented in the previous chapter, two different case studies are presented: the rapid seismic risk assessment of a simply supported bridge, the Annunziata Viaduct and the form efficiency assessment of an arch bridge located in Potenza, Musmeci bridge.

6.1 Rapid seismic risk assessment

Major damages on reinforced concrete bridges can be divided, as briefly summarized in chap.4, according to superstructure (deck) and substructure (piers).

Decks major cause of collapses is due to cinematic design error such as:

- hammering between adjacent spans and
- deck losses of support.

Under seismic loads, inadequate support length frequently brings to direct collapse, as shown in Figure 154:



Figure 153 - Cypress Viaduct Loma Prieta earthquake, USA



Figure 154 – Nishinomiya-ko viaduct collapse, Hyogo-Ken Nanbu earthquake Japan

In the substructures, piers damages are generally due to:

- flexural ductility's defects
- shear resistance defects.
- Inadequate design of column/beam joints (Figure 156)



Figure 155 - Frame pier collapse, Shinkansen Viaduct, Kobe

Generally, collapse is caused by a sequence of fails, such as flexural stress (Figure 157), insufficient boundary's restriction and reduction of shear resistance.



Figure 156 - Collapse for flexural ductility depletion, Gothic Avenue Viaduct, California

The probability of complete structural collapse due to loss of balance associated with this fails is very high. In the case of frame pier, the design column/beams are fundamental in structural resistance.

The presented methodology allows the evaluation of the seismic risk using geometrical data obtained from the aerial survey. Safety evaluation is conducted using linear structural analysis with punctual verification in critical parts. Generally, the contribution of the deck is negligible in the overlap seismic response of the structure. Bridge piers, abutments and bearings are instead considered as critical components affecting the system's seismic performance: for this reason, the investigations are concentrated on the substructure (piers and abutment) and on the structural joints.

To perform the risk assessment and evaluate the safety condition of the bridge the following parameters are necessary:

- Geometry of the bridge, from the UAV aerial survey
- Structural details, obtainable from the blueprints or from investigation. The design process can be also simulated according to law and regulation used to design the structure; moreover, structural details can be extracted according to the different typology of structural elements used in the design derived from the standardized abacus.
- Material mechanical characteristics: Piers and abutments must be investigated while the deck is enough to observe a good state of conservation. Mechanical characteristics could be also supposed from the age of construction and the state of preservation.
- Geotechnical site characterization: obtainable from the site-specific characteristics or with the specific investigation.

Input parameters	Source
Geometry	UAV aerial survey
Structural details	Blueprint or simulated project
Material mechanical characteristics	Investigation or hypothesis
Geotechnical characterization	Obtainable from the site

Table 22 - Input parameters for rapid seismic risk assessment

Three different levels of knowledge are defined in NTC 2018:

- LC1: limited knowledge
- LC2: adequate knowledge
- LC3: accurate knowledge

The use of the level of knowledge is linked with the strategic importance of the construction; the analysis of existing bridges must be conducted with LC3 level of knowledge except for exceptional case in which LC2 can be adopted. In-situ investigation can be conducted according to the required level of knowledge or to verify the existing information's (such as blueprint, design specification).

LC	Geometry	Structural Detail	Material propriety	FC
LC1	From partial or complete original blueprint	From incomplete blueprint	From incomplete blueprint	
LC2	From original blueprint with limited or extended survey	From incomplete blueprint with limited or extended in-situ investigation	From blueprint or from original materials certificate specification with limited or extended in-situ investigation	1.20
LC3	limited or extended survey	From complete blueprint with limited or extended in-situ investigation	From original materials certificate or from blueprint specification with extended in-situ investigation	1.00

Table 23 – Details in Level of knowledge

The medium mechanical characteristics of the materials must be considered for the structural analysis. For network analysis, LC1 level can be used for the first-level analysis.

6.1.1 Verification format

According to limit state design (LSD) also known as load and resistance factor design (LRFD), the limit state is defined as a condition of a structure beyond which it no longer fulfils the relevant design criteria. NTC 2018 defines two limit state categories: Exercises limit state (SLE) and Ultimate Limit State (SLU) with two sub-limit states for each category.

Exercise Limit State (SLE) is characterised by local damages that reduce the structural durability and efficiency, displacement and deformation that can limit the use and efficiency of construction in terms of non-structural elements and plants.

- **Operativity Limit State (SLO):** the damage after the seismic event should not compromise the regular asset functionality.
- **Damage Limit State (SLD):** the construction suffers damage that does not compromise resistance and stiffness for both vertical and horizontal seismic loads. The structure is regularly usable.

Ultimate Limit State (SLU) is characterised by losses of structure equilibrium, excessive displacement and deformation, reaching of the maximum structural capacity in foundation, joints and terrain and structural instability. The two limit states belong to this category are defined as:

- **Life safeguard limit state (SLV):** the construction preserves resistance and stiffness for vertical loads and a safety margin for horizontal seismic loads
- **Collapse limit state (SLC):** the construction preserves a safety margin for vertical seismic loads and an exiguous safety margin for collapse for and a safety margin for horizontal seismic loads.

On existing bridges and viaducts, the verifications are executed in both longitudinal and orthogonal direction and with two Limit state configurations, one for Exercise Limit state (SLD) and one for Ultimate Limit State (SLC):.

- **Longitudinal direction SLD**
- **Longitudinal direction SLC**
- **Orthogonal direction SLD**
- **Orthogonal direction SLC**

Assuming D_x and D_y the quantity derived from the demand model analysis (displacement, rotation or shear) in the two main flexural planes of an element, and C_x and C_y as the correspondent capacity, the verification is executed satisfying equation (1):

$$\sqrt{\left(\frac{D_x}{C_x}\right)^2 + \left(\frac{D_y}{C_y}\right)^2} \leq 1 \quad (13)$$

Two types of verifications are executed:

1. **Flexural** is made in terms of displacement at the pier top
2. **Shear** in terms of force at the base of the pier

Analysis and structural model

The considered structural model must replicate the structure's actual state in a simplified form, to verify the critical components under seismic loads. For the global structural analysis pier and abutments are considered as interlocking joints.

In Italy simply supported bridge on unique piers represents the standard and most diffused statics scheme for bridge and viaduct (Pinto et al., 2009). For this type of bridges, a specific simplified analysis, that represents a good compromise in terms of simplicity and accuracy, is presented. The adopted structural model is composed by a vertical shelf with the distributed mass along the height on which pier cap and deck weigh. In transversal direction each pier can be considered as a simple independent oscillator, while in longitudinal direction the system can be considered with one degree of freedom. The methodology consists in the application of a static non-linear and simplified analysis where the force-displacement relationship at the top of the shelf is calculated using the moment-bending relationship.

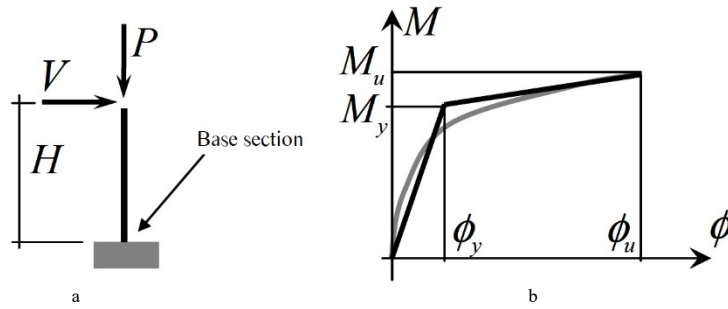


Figure 157 – (a) Simplified static scheme and (b) moment bending relationship

Piers effective mass at the top is calculated, for constant section, from the sum of 30% of pier's mass and pier cap mass. For each pier, the mass is calculated using equation (13):

$$m = 0,3 m_{pier} + m_{pier\ cap} + m_{deck} \quad (14)$$

For the analysis in the transversal direction, effective mass' height is calculated using (14):

$$H_{eff\ tras} \cong [(0,3 m_{pier} + m_{pier\ cap})H_p + m_{deck} H_{deck}]/m \quad (15)$$

For the analysis in the longitudinal direction, effective mass height is equal to the distance from the top of the foundation to the support plane.

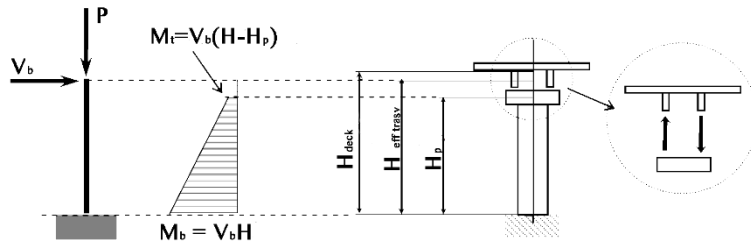


Figure 158 - Static scheme and height of bridge's piers

The moment-bending relationship (Figure 158) is calculated for standardised section (Figure 160) according to (Petrone & Monti, 2019) using equation (15) yielding bending and equation (16) yielding moment:

$$\phi_y = \frac{\varepsilon_y}{d} \frac{1}{1 - \xi_y} \quad (16)$$

$$M_y = m_y b d^2 f_c \quad (17)$$

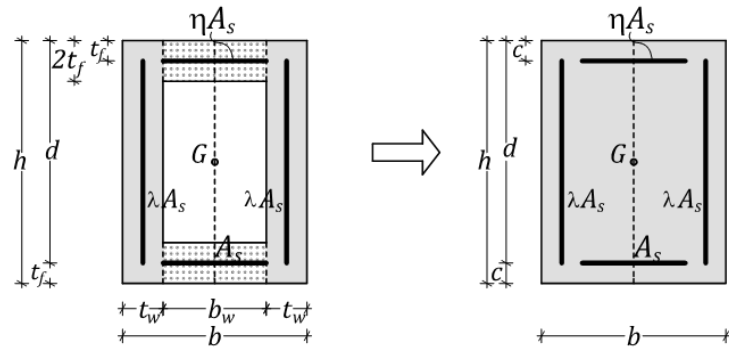


Figure 159 - Sections geometrical features

The term m_y is calculated according to equation (17), while ξ_y calculated according to equation (18)

$$\begin{aligned}
 m_y = & \frac{1}{2} \bar{\epsilon}^2 \left(\frac{\xi_y}{1 - \xi_y} \right)^2 \xi_y \left[(1 + \tau_f) - 2\nu_1 \xi_y \right] + \\
 & - \frac{1}{2} \bar{\epsilon}^2 \left(\frac{\xi_y}{1 - \xi_y} \right)^2 \beta_2 \beta_w \left(\xi_y - 2\tau_f \right) \left[(1 + \tau_f) - 4\tau_f - 2\nu_1 (\xi_y - 2\tau_f) \right] + \\
 & + \frac{1}{2} \mu_s (1 - \tau_f) \left(1 + \eta \frac{\xi_y - \tau_f}{1 - \xi_y} \right) + \\
 & + \frac{1}{2} \frac{\lambda \mu_s}{1 - \tau_f} \left\{ \frac{(\xi_y - \tau_f)^2}{1 - \xi_y} \left[(1 - \tau_f) - \frac{2}{3} (\xi_y - \tau_f) \right] + (1 - \xi_y) \left[(1 - \tau_f) - \frac{2}{3} (1 - \xi_y) \right] \right\}
 \end{aligned} \quad (18)$$

$$\xi_y = \frac{p + \mu_s [1 + \lambda + \tau_f (\eta + \lambda)]}{2p + \mu_s [2 + \eta + 3\lambda + \tau_f (\eta + \lambda)]} \quad (19)$$

Ultimate blending (19) and Ultimate moment (20) are calculated from the following equations:

$$\phi_u = \frac{\epsilon_{cu}}{d} \frac{1}{\xi_u} \quad (20)$$

$$M_u = m_u b d^2 f_c \quad (21)$$

The term m_u is calculated according to (21), with ξ_u calculated according to equation (22) :

$$\begin{aligned}
m_u = & \beta_1 \xi_u \left[\frac{1}{2} (1 + \tau_f) - v_1 \xi_u \right] + \\
& - \beta_2 \beta_w \left\langle \xi_u - 2\tau_f \right\rangle \left[\frac{1}{2} (1 + \tau_f) - 2\tau_f - v_1 (\xi_u - 2\tau_f) \right] + \\
& + \mu_s \frac{1}{2} (1 - \tau_f) (\eta + 1) + \\
& + \frac{2\lambda \mu_s}{1 - \tau_f} \left\{ \left(\xi_u - \tau_f \right) \left[\frac{1}{2} (\xi_u - \tau_f) - \frac{2}{3} \bar{\epsilon} \xi_u \right] + (1 - \xi_u) \left[\frac{1}{2} (1 - \xi_u) - \frac{2}{3} \bar{\epsilon} \xi_u \right] \right\}
\end{aligned} \tag{22}$$

$$\xi_u = \frac{p - 2\beta_2 \beta_w \tau_f + \mu_s \left(1 - \eta + 2\lambda \frac{1 + \tau_f}{1 - \tau_f} \right)}{\beta_1 - \beta_2 \beta_w + \frac{4\lambda \mu_s}{1 - \tau_f}} \tag{23}$$

6.1.2 Capacity Model

1) Flexural at piers top – maximum displacement

Displacement at pier's top is calculated using equation (25):

$$\delta_y = 1/v \varphi_y H^2 / 3 \tag{24}$$

Total displacement in the longitudinal direction is calculated from equation (25) with the contribution of plastic rotation in the plasticised zone at the pier's base (26); the term $l_p = 0.10 H_p$ (Pinto et al., 2009).

$$\delta_u = \delta_y + (\varphi_u - \varphi_y) l_p (H - l_p / 2) \tag{25}$$

In the transversal direction the elastic period of the pier is calculated using equation:

$$T = 2\pi \sqrt{m_i / k} = 2\pi \sqrt{m_i \delta_y / V_y} \tag{26}$$

2) Pier shear

Pier shear resistance is calculated using equation (28)

$$\begin{aligned}
V_R = & \frac{1}{\gamma_{el}} \left\{ \frac{b - x}{2L_{Vr}} \min(N; 0.55 A_c f_c) + \left(1 - 0.05 \min(5; \mu_{\Delta, pl}) \right) \times \right. \\
& \times \left[0.16 \max(0.5; 100 \rho_{tot}) \left(1 - 0.16 \min\left(5; \frac{L_{Vr}}{b} \right) \right) \sqrt{f_c} A_c \right] + V_w \left. \right\}
\end{aligned} \tag{27}$$

the term $\mu_{\Delta,pl} = \theta / \theta_y - 1$ represent the plastic contribution of the required element ductility.

6..1.3 Demand Model

Seismic hazard is based on the horizontal and vertical elastic response spectrum as defined in Italian NTC (“Norme tecniche per le Costruzioni” 2018 (Ministero delle Infrastrutture e dei Trasporti, 2018) and Eurocode 8 (Holst et al., 2011).

Infrastructure has different levels of anti-seismic protection according to their relevance to respect safety condition and design resistance even after the seismic event, according to the principles behind national and international regulations. Safety is defined by the association of a performance expectation (limit state) with a defined seismic intensity level characterised by exceeded probability (P_{VR}) in a defined time interval (Life of the structure V_R). The return period of a seismic event with a defined seismic intensity is calculated according (29):

$$T_R = -V_R / \ln(1 - P_{VR}) \quad (28)$$

The design life of the structure (V_R) is defined in the actual European and Italian regulations, according to (12):

$$V_R = C_u \cdot V_n \quad (29)$$

The terms C_u represent the class of use (Table 24) while V_N represents the Nominal life (Table 25).

Class of use	I	II	III	IV
C_u	0.7	1.0	1.5	2.0

Table 24 - Class of use (Italian NTC 2018)

Type of construction	Provisory	Ordinary	Strategic
V_N	≤ 10	≤ 50	≤ 100

Table 25 - Nominal life

The maximum exceeded probability of a seismic event in the Nominal life of a structure according to the considered limit state is defined as P_{VR} .

P_{VR} values associated with a correspondent limit states are summarised in Table 26.

Limit state	Serviceability		Ultimate	
	SLO	SLD	SLV	SLC
P_{VR}	81 %	63 %	10 %	50 %

Table 26 – Return period for different limit state

For the existing strategic bridges and bridges (class of use III and IV) the verification of the complete service after a seismic event is mandatory. Serviceability is ensured by Damage Limit State (SLD) associated with $P_{VR} = 63\%$.

The demand model is represented by the Seismic hazard in a site as both vertical and horizontal loads on a structure. The seismic hazard is characterized for each limit state (P_{VR} value) and defined with the elastic load spectrum in terms of the horizontal acceleration. Load spectrum is a function of local parameters such as:

- a_g maximum horizontal acceleration on the site
- F_0 maximum amplification factor of the horizontal spectrum
- T_C^* period in correspondence of the constant velocity phase of the horizontal spectrum

These terms are defined in NTC2018 (Ministero delle Infrastrutture e dei Trasporti, 2018). Seismic hazard is defined by the three components x, y and z described as acceleration response elastic spectrum, displacement response elastic spectrum and historical series of seismic motion. Figure 157 represents the elastic spectrum for horizontal components with the analytic expression for every segment.

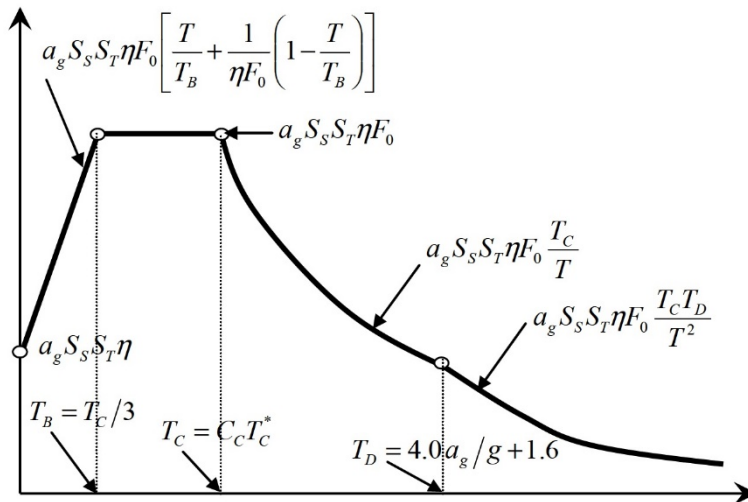


Figure 160 - Elastic spectrum in Horizontal acceleration

S_s , C_C S_T are calculated according to local terrain condition and defined in NTC 2018. Vertical components have the same parameters while F_0 is substitute as in (31):

$$F_V = 1,35 * F_0 \sqrt{A_g/g} \quad (30)$$

The vertical component must be considered for the joint verification and on pre-compressed deck but can be ignored for the bridges' pier verification.

1) Flexural at piers top – displacement demand

The maximum displacement at the top of the pier is calculated from the displacement elastic spectrum equation (32) in the two directions:

$$\begin{aligned} \delta_{max} &= S_{De}(T) & T \geq T_c \text{ o } q^* \leq 1 \\ \delta_{max} &= S_{De}(T)/q^* [1 + (q^* - 1) T_c/T] & T \geq T_c \text{ o } q^* \leq 1 \end{aligned} \quad (31)$$

Loads q^* is calculated using equation (33), with V_y equal to M_y/H_p

$$q^* = m S_e(T) / V_y \quad (32)$$

2) Shear demand (at base)

Shear force is calculated from the following equation (34):

$$V_y = m S_{De}(T) \quad (33)$$

Where T is the pier's period.

6.2 Seismic risk assessment of Annunziata Bridges

The **demand model** is evaluated using the site-specific characteristics (soil, topography), class of use and nominal life:

1. DEMAND MODEL

SITE CHARACTERISTICS - Hazard

Selection for Municipality

Selection for Coordinates

Longitude Latitude

Selection for Municipality

Region Calabria Province Reggio Calabria Municipality Reggio di Calabria

Longitude 15,662100 Latitude 38,111500

Life cycle and Use

Nominal life VN = 100 anni

Class of use IV

Use coeff. CU = 2,00

Nominal life VR = 200 anni

Soil type and topography

Vs,30 m/s	Soil	Topograp.	Terrain
300	C	T1	NO

Figure 161 - Demand model, site characteristics and life cycle

The resulting spectrum in terms of both horizontal acceleration and horizontal displacement are represented respectively in Figure 163 and Figure 164:

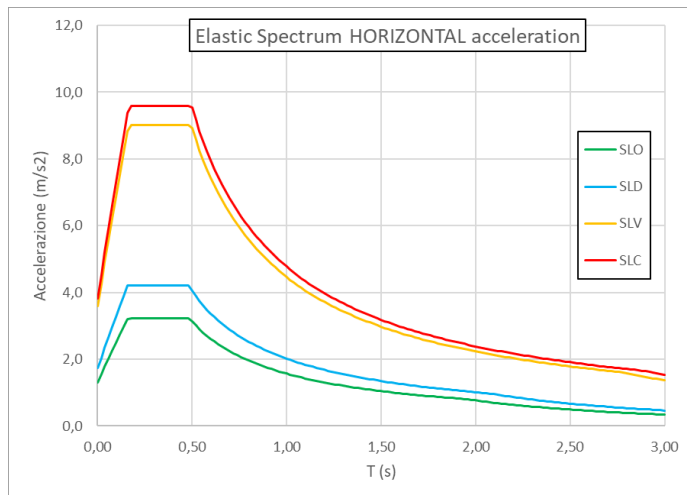


Figure 162 - Elastic spectrum for horizontal acceleration

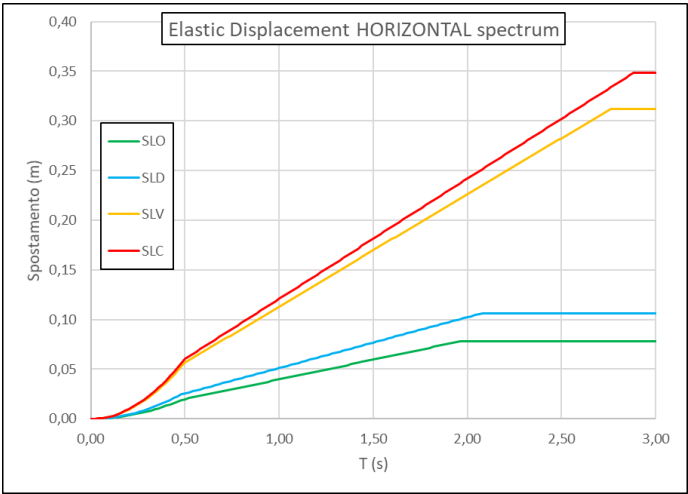


Figure 163 - Elastic displacement horizontal spectrum

Displacement in horizontal and vertical is represented in Figure 165 and Figure 166

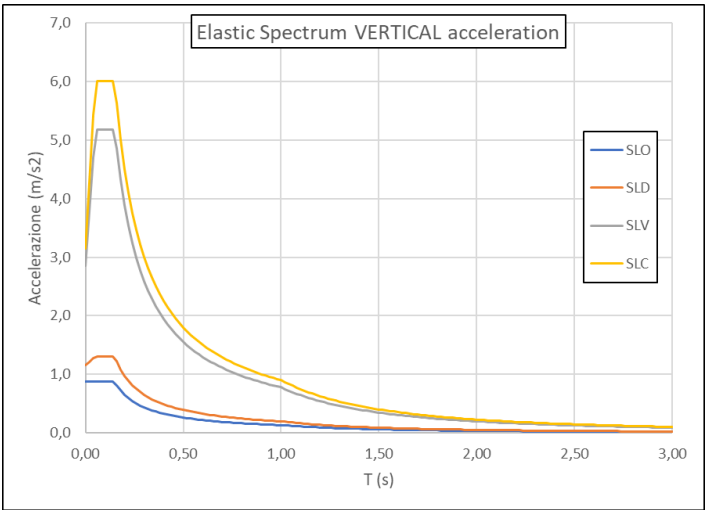


Figure 164 - Elastic displacement spectrum

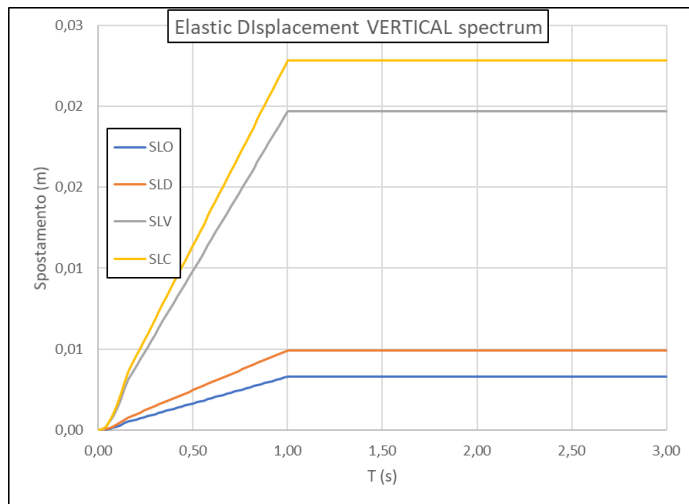


Figure 165 - Elastic spectrum vertical acceleration

The geometrical feature extracted in chapter 5 is used to extract the simplified geometrical model of bridge Figure 167.

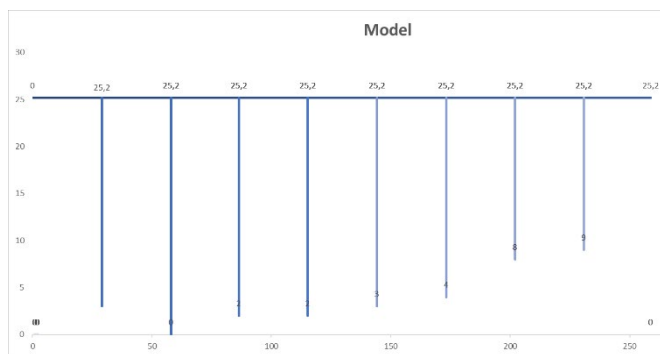


Figure 166 - Bridge simplified geometrical model

For each pier's the moment-blending relationship was evaluated using equation (15) (16) (19) (20) and are presented in Figure 168 and Figure 169.

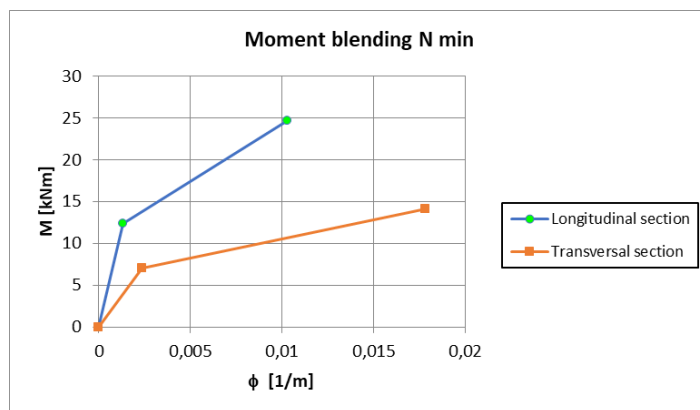


Figure 167 - Moment blending relationship for pier section

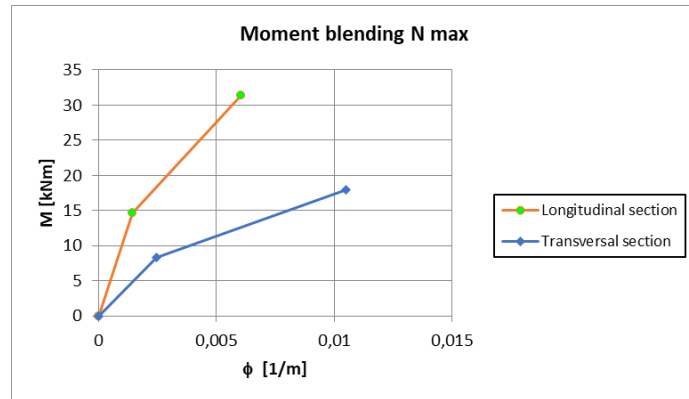


Figure 168 - Moment blending relationship for pier section

The comparison of the demand and capacity model was calculated using equation (12).

6.3 Form efficiency evaluation of Musmeci Bridge

The evaluation of the form efficiency of the structure of Musmeci Bridge and the comparison with the surveyed model (described in chapter 5), was realised using the Force Density Method.

The Force Density Method (FDM) was first proposed by (Schek, 1974) for the form-finding of cable networks in the same years in which the bridge over Basento river was erected. According to the original formulation, the FDM amounts to obtain the shape of a network subjected to given nodal forces in which a so-called force density is assigned to each branch. This quantity is defined as the ratio between the axial force and the length of each branch and, although unusual, it was used since 1921 as a component of the geometric stiffness matrix (Eriksson & Tibert, 2006). However, the length of bar elements is initially unknown; hence the assignment of the so-called force densities is not straightforward, especially if one recalls that the final shape of the structure depends upon the input values of the force densities.

The generalisation of the FDM to membranes subjected to isotropic stress states is described in (Maurin & Motro, 1998), which substituted the concept of force density by that of membrane stress density. However, as discussed in Musmeci [57], the supporting shell was demanded to have a higher bending along the transversal direction, mainly for usability reasons to provide a surface that can be easily crossed by walking. Hence, its shape was designed by assuming the compressed membrane be subjected to a different value of compressive stresses along the longitudinal and transversal directions. For this reason, it is useful to employ a further generalisation of the FDM that allows for assigning non-isotropic surface stress densities (Pauletti & Pimenta, 2008).

One of the advantages of employing this last version of the FDM is that it is formulated by considering the concept of natural force density, which derives its name from the natural quadratic strain or Green strain. Thanks to this approach, one can directly assign the working axial force or membrane stresses in place of the force/stress densities. Actually, force/stress densities are evaluated as a function of the reference (initial) configuration of the network and of the prescribed value of natural force or membrane second Piola-Kirchhoff stress.

Hence, the FDM analysis amounts to assigning a reference configuration and the working axial forces and membrane stresses of bar and membrane elements. Then set of nodal equilibrium equations is assembled and solved for the unknown positions of free nodes and reactions of restrained nodes. Thus, the viable configuration of the model is computed explicitly by solving a linear system of equations.

In (Marmo et al., 2019), the formulations of the bar and triangular membrane elements and the basic equations underlying the FDM analysis are briefly recalled. In this application, bar elements are used

to model the ribs placed at the boundary of the RC shell, while membrane elements are used to model the interior of the structure.

6.3.1 Description of the FDM mesh

In order to reduce the size of the problem to be solved by employing the FDM, recurrence and symmetry of the structure can be invoked to model only one-sixteenth of the entire membrane. Such a portion of the structure corresponds to half a span along the longitudinal direction by half the width along the transversal direction Figure 170 (a). Moreover, the slope will be neglected in the numerical analyses according to what was done by Musmeci during the design process.

Let us consider a right-handed reference system (x, y, z) with x -axis parallel to the deck, the y -axis orthogonal to it and the z -axis in the vertically upward direction (Figure 170).

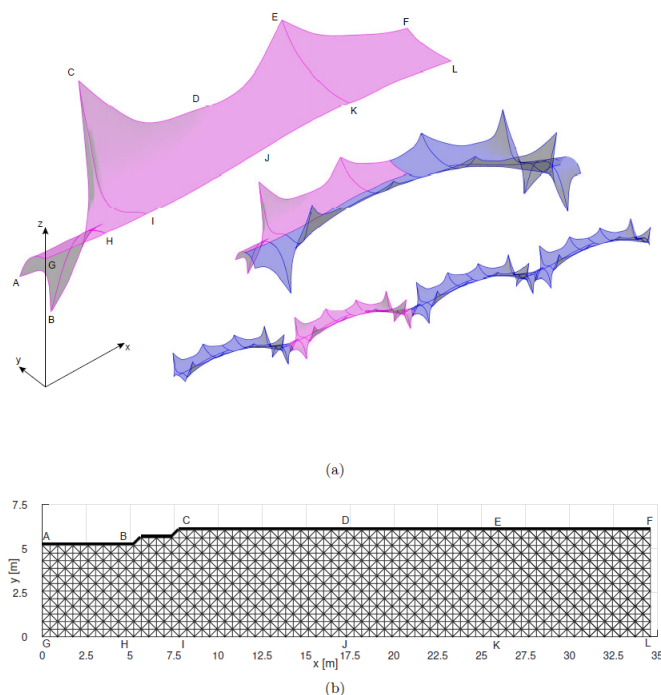


Figure 169 - FDM model of one-quarter span of the RC membrane: (a) schematic view of the modelled portion of the bridge and (b) reference configuration composed of membrane (thin lines) and bar (thick lines) elements.

The reference configuration of the FDM model is input by defining a grid of nodes equally spaced at distance of 0.4325 m along both the transversal and longitudinal axes of the bridge. Such a distance corresponds to one quarter the grid spacing of 1.73 m that was employed initially by Musmeci for his numerical solution. Nodes of such a grid of vertices are then connected by triangular elements and bar elements Figure 170 (b) to model the shell and boundary ribs, respectively.

Letters (from A to L) in Figure 170 indicate twelve significant nodes of the model. In particular, B represents the node where the membrane touches the foundation; hence its position is fully restrained to have coordinates (5:20; 5:20; 0) m. Nodes C and E are those where the membrane meets the bridge deck, hence only their horizontal coordinates (i.e., x and y) are exceeded, C (8:65; 6:00) m and E (25:95; 6:00) m, while they are loaded by a vertical force equal to the load transmitted to these points by the deck, $f_zC = f_zE = 3250$ kN

Additional significant nodes are placed along the edge of the bridge, namely point A, representing the midpoints between two consecutive supports of the membrane, point D representing the tip of the concavity between C and E, and point F, placed at the centre of the central concavity of each span. The entire boundary A-F of the model is free, with the mentioned exceptions of nodes B, C and E. Finally, nodes G, H, I, J, K and L are placed along the central axis of the shell and have the same longitudinal abscissas of the points A, B, C, D, E and F, respectively.

Symmetry constraints are applied along the boundaries A-G, G-L and F-L. In particular, x coordinates of the nodes laying along the edges A-G and F-L are fixed to the values $x = 0.00$ m and $x = 34.60$ m, respectively. This implies that reactions at these nodes are parallel to x. Similarly, nodes laying on the edge G-L are restrained to have fixed y coordinate equal to 0.00 m so that nodal reactions are parallel to y. Reactions of the nodes pertaining to the mentioned edges represent normal thrust transmitted to the adjacent portion of the structure, beyond

the symmetry planes. Actually, because of symmetry, no tangential stresses are expected at these points.

6.3.2 Effect of the prescribed forces and stresses on the FDM solution

The viable configuration of a FDM model depends upon the prescribed values of force/stress densities assigned to each element. This allows designers to find different structural forms corresponding to the desired distribution of internal forces. Hence, a series of preliminary numerical analyses have been carried out for the bridge. In these analyses, prescribed values of axial forces and stresses within bar and triangular membrane elements have been varied in order to show how the shape of the supporting membrane of the bridge is influenced by the design assumptions.

In particular, two different cases are analysed: (i) viable configurations obtained by assigning the vertical forces at nodes C and E and (ii) viable configurations obtained by assigning the vertical positions of nodes C and E. The two cases are reported in Figure 172 and Figure 171, respectively.

In these plots, the red surfaces represent the computed viable configurations, while the transparent white surfaces are the surveyed shell mid-surface. In both cases, results relevant to the cases in which the transversal and longitudinal membrane stresses, namely N_x and N_y , are assumed to be equal (Figure 172 a and Figure 171 a) or to have different values (Figure 172 b and Figure 171 b), are reported. In all these cases, an axial force $P = 400$ kN is applied to all bar elements.

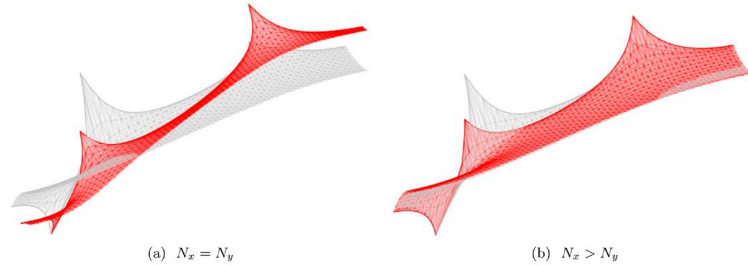


Figure 171 - Viable configurations for different assigned stress densities given the vertical downward force in nodes C and E, $fz_C=fz_E=3250$ kN, ($P=400$ kN): (a) $N_x=1000$ kN/m, $N_y=1000$ kN/m, $z_C=8.74$ m, $z_E=17.59$ m; (b) $N_x=1800$ kN/m, $N_y=200$ kN/m, $z_C=10.02$ m, $z_E=16.60$ m.

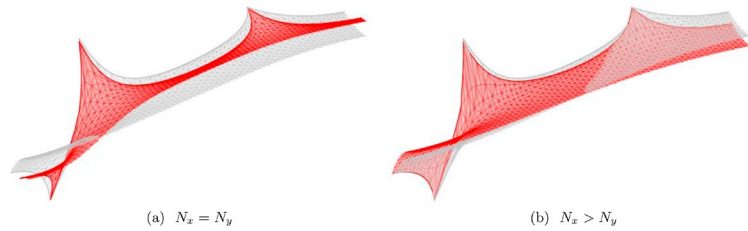


Figure 170 - Viable configurations for different assigned stress densities given the location of the points C and E, $z_C=z_E=14.00$ m, ($P=400$ kN): (a) $N_x=1000$ kN/m, $N_y=1000$ kN/m, $fz_C=7593$ kN, $fz_E=1402$ kN; (b) $N_x=1800$ kN/m, $N_y=200$ kN/m, $fz_C=5758$ kN, $fz_E=2006$ kN.

In the first case (Figure 172), a downward vertical force has been applied to both nodes C and E, $fz_C = fz_E = 3250$ kN, and their horizontal positions have been set to C (8.65, 6.00) m and E (25.95, 6.00) m. These figures show that both the shape of the viable configuration and the vertical position of the nodes C and E modify as a function of the considered design assumptions. Quote values computed for the two reported solutions are given within the caption of the Figure. Recalling

that these points are required to have a fixed quote equal to 14.00 m, both these viable configurations are unfeasible.

In the second case (Figure 171), nodes C and E have been assumed to have a fixed vertical position ($z_C = z_E = 14.00$ m), similar to what has been done by (Magrone et al., 2016). Corresponding viable configurations are reported in Fig. 13 for different assigned stress densities. However, being the position of the nodes C and E fully constrained, the vertical forces transferred from the deck to the shell cannot be assigned and must be evaluated a posteriori as restraint reactions. Their values are reported within the caption of the figure and are sensibly different from the ones actually applied to these

nodes, which are both equal to 3250 kN.

Concluding, both approaches, corresponding to assigned vertical forces or assigned vertical positions of the nodes C and E, produce forms that do not correspond to the actual form and equilibrium of the shell. Hence, the vertical positions of nodes C and E (z_C and z_E) shall be left unknown to have full control of the actual forces that load the shell. This represents what was done by Musmeci on the neoprene sheet experiment using iron wires and pulleys, and what physically happens on the bridge due to the particular configuration of the joints along the deck.

For this reason, an iterative procedure has been used in which both the position and the forces applied to the structure are controlled. This procedure is described in the following Section and amounts to set tentative values of force/stress and verifying that the viable configuration is sufficiently close to the actual shape of the RC shell.

6.3.3 Iterative procedure and comparison between shell geometries

As shown above, no forces and stresses can be assigned in advance to the elements of the reference configuration, rather it is imposed the final configuration of the membrane to fit, as accurately as possible, the surveyed shape of the RC shell. Within this procedure, forces and stresses are determined iteratively by comparing the viable configuration with the actual shape of the membrane. To this end, the significant twelve points A-L listed above are selected as a reference for

estimating the distance between the computed and the actual shape of the membrane.

At each iteration, experimental values of forces and stresses are estimated, and the corresponding viable configuration of the shell is determined by the FDM. Then, the standard deviation of the distances between the positions of selected reference points pertaining to the viable and surveyed configurations is computed. The standard deviation is chosen as the objective function to be minimized by employing an optimisation algorithm based on the interior point method (Altman & Gondzio, 1999).

In order to reduce the number of unknowns, forces and stresses assigned to each element are computed by linearly interpolating the values attained at the reference points A-L. Hence, unknown parameters of the analysis are represented by these values, only. Since Musmeci [57] does not refer to any variation of stresses along the transversal direction of the bridge, the distribution of stress densities is kept constant along this direction. Hence, only six pairs of longitudinal and transversal membrane stress values are chosen as unknown parameters, corresponding to the membrane stresses assigned to the six alignments

A-G, B-H, C-I, D-J, E-K and F-L. Similarly, forces assigned to bar elements are computed by interpolating the six values assigned to the points A, B, C, D, E and F. In conclusion, the total number of unknown bar forces and membrane stresses amount to only eighteen values.

After applying such an iterative procedure, the viable configuration reported in Figure 173 is obtained. Within the same Figure, the position of the reference points A-L is shown by blue circles. This first comparison shows that the computed geometry of the membrane is very close to the points chosen as a reference.

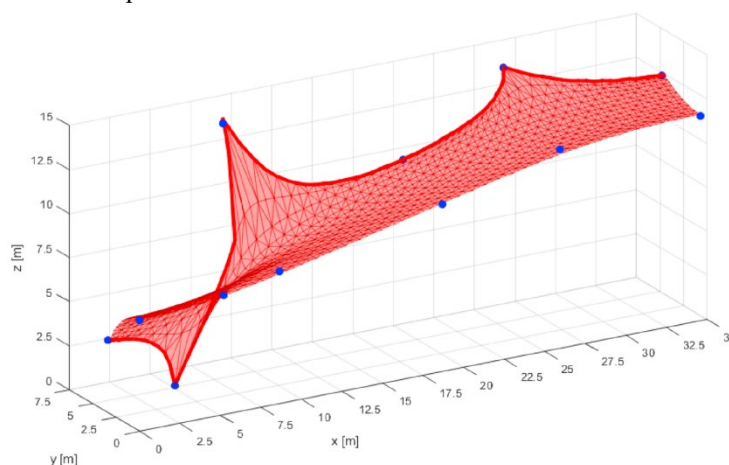


Figure 172 - Viable configuration and reference points

The corresponding eighteen values of forces/stresses are reported in Table 26. Recall that these values are those identified by the iterative application of the FDM and do not correspond to the Cauchy stresses within the membrane since the problem is expressed in terms of second Piola-Kirchhoff stress tensor. However, recall also that, the neoprene sheet experiment allowed Musmeci to estimate longitudinal axial stresses of 1800 kN/m and transversal stresses varying between 100 kN/m and 200 kN/m. These values are quite similar, yet slightly lower, than those reported in Table 27.

Alignment	x [m]	P [kN]	Nx [kN=m]	Ny [kN=m]
A-G	0	2300	1800	450
B_H	5,19	0	1700	270
C-I	8,65	0	2000	130
D-J	18,7	0	2150	100
E-K	25,95	2000	2400	400
F-L	34,60	5000	2400	400

Table 27 - Final values of forces and stresses employed for evaluating force/stress densities

The superposition between the viable configuration and the designed one is reported in Figure 174 where the modelled quarter span of the structure has been replicated and reflected about the symmetry planes

to extend the comparison to a region that is larger than one entire span of the bridge. Such a comparison shows that the two surfaces have negligible differences.

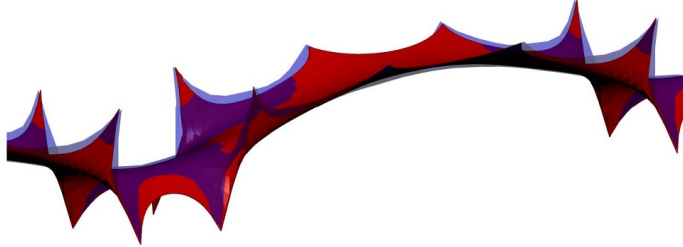


Figure 173 - Viable configuration (red surface) and designed geometry (transparent blue surface)

In this regard, it should be recalled that the viable configuration obtained by our iterative implementation of the FDM has been computed by taking as reference the position of a few points of the UAV survey; hence, a more significant comparison is the one that takes as reference the surveyed geometry of the shell. Such a comparison is reported in Figure 175 showing that high agreement between the computed and the surveyed geometries is achieved. Relative differences $\Delta^A_B = (z_a - z_b)/z_{ref}$ between the quotes of reference points belonging to the viable (z_v), surveyed (z_s) and design (z_D) geometries of the shell are summarised in Table 28.

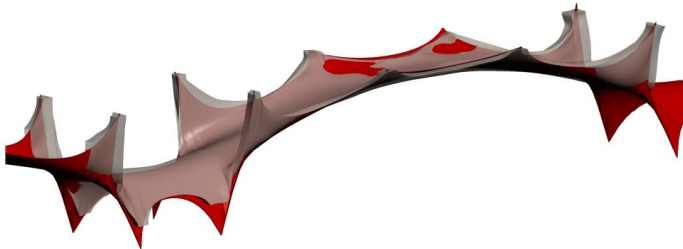


Figure 174 - Viable configuration (red surface) and surveyed geometry (transparent white solid)

These differences are scaled by the average quote of the entire shell, which is $z_{ref}=7$ m, in order to make the relative error independent from the scale of the structural model. The relative differences relevant to the viable form (first row of Table 28) are always below 4% and lower than those associated with the other two comparisons. Hence, the convergence of the iterative procedure to a feasible configuration that agrees with the objective form is confirmed.

	A	B	C	D	E	F	G	H	I	J	K	L
Δ^S_V	0.000	0.000	-0.035	-0.017	-0.010	-0.022	-0.003	0.007	0.017	-0.009	0.038	-0.013
Δ^P_V	0.014	0.000	-0.048	0.020	-0.023	-0.094	-0.031	-0.019	-0.040	-0.064	0.077	-0.068
Δ^P_S	0.014	0.000	-0.013	0.036	-0.013	-0.071	-0.028	-0.026	-0.060	-0.056	-0.017	-0.056

Table 28 - Quote differences $\Delta^A_B = (z_A - z_B)/z_{ref}$ between corresponding points of the viable (z_v), surveyed (z_s) and design (z_D) geometries of the shell.

References

- Altman, A., & Gondzio, J. (1999). Regularized symmetric indefinite systems in interior point methods for linear and quadratic optimization. *Optimization Methods and Software*, 11(1–4), 275–302. <https://doi.org/10.1080/10556789908805754>
- Eriksson, A., & Tibert, A. G. (2006). Redundant and force-differentiated systems in engineering and nature. *Computer Methods in Applied Mechanics and Engineering*, 195(41), 5437–5453. <https://doi.org/https://doi.org/10.1016/j.cma.2005.11.007>
- Holst, J. M. F. G., Rotter, J. M., Calladine, C. R., Eoin Dunphy, NORM, E. S. N. E. Euro., DNV, ... Starnes, J. H. (2011). Eurocode 8 Part 2: Design of structure for earthquake resistance: Bridges. *Journal of Constructional Steel Research*, 54(2), 18–20. <https://doi.org/10.2514/2.2772>
- Magrone, P., Tomasello, G., Adriaenssens, S. M., Gabriele, S., & Varano, V. (2016, January 1). Revisiting the form finding techniques of Sergio Musmeci . (P. J. S. Cruz, Ed.), *The Bridge over the Basento River* . CRC Press/Balkema . Retrieved from <http://www.scopus.com/inward/record.url?scp=85015053450&partnerID=8YFLogxK>
- Marmo, F., Demartino, C., Candela, G., Sulpizio, C., Briseghella, B., Spagnuolo, R., ... Rosati, L. (2019). On the form of the Musmeci ' s bridge over the Basento river. *Engineering Structures*, 191(April), 658–673. <https://doi.org/10.1016/j.engstruct.2019.04.069>
- Maurin, B., & Motro, R. (1998). The surface stress density method as a form-finding tool for tensile membranes. *Engineering Structures*, 20(8), 712–719. [https://doi.org/https://doi.org/10.1016/S0141-0296\(97\)00108-9](https://doi.org/https://doi.org/10.1016/S0141-0296(97)00108-9)
- Ministero delle Infrastrutture e dei Trasporti. (2018). Aggiornamento delle “Norme Tecniche per le Costruzioni” - NTC 2018, 1–198.
- Pauletti, R. M. O., & Pimenta, P. M. (2008). The natural force density method for the shape finding of taut structures. *Computer Methods in Applied Mechanics and Engineering*, 197(49), 4419–4428. <https://doi.org/https://doi.org/10.1016/j.cma.2008.05.017>
- Petrone, F., & Monti, G. (2019). Unified code-compliant equations for bending and ductility capacity of full and hollow rectangular RC sections. *Engineering Structures*, 183(June 2018), 805–815. <https://doi.org/10.1016/j.engstruct.2018.12.082>
- Pinto, P. E., Franchin, P., & Lupoi, A. (2009). Valutazione e consolidamento dei ponti esistenti in zona sismica, 7.
- Schek, H.-J. (1974). The force density method for form finding and computation of general networks. *Computer Methods in Applied Mechanics and Engineering*, 3(1), 115–134. [https://doi.org/https://doi.org/10.1016/0045-7825\(74\)90045-0](https://doi.org/https://doi.org/10.1016/0045-7825(74)90045-0)

7. Conclusion and perspectives

In this work, a methodology for the aerial survey, acquisition of geometrical feature of bridges and viaducts using UAV and aerial photogrammetry was presented. The state of the art of survey and computer vision techniques for photogrammetric 3d reconstruction was described. Bridges represent the most critical part of an infrastructure network and need ordinary and extraordinary maintenance. Western countries have to face this massive problem of verifying and guaranteeing the performance of more than 50 years bridge to ensure regular operation and safety.

The complete workflow from the image and topographic data, to automatic extraction of structural geometric information, was used to quickly obtain, starting from few geometrical data, the fragility curve of bridges in order to verify the seismic response. To verify the proposed procedure two case studies, of two different bridges structural typology, were presented: a simply supported bridges, to verify the seismic response (the common typology in Italian infrastructure network) and arch bridge to verify its form efficiency.

The originality of the proposed methodology consists in the new application of the UAV in a complete workflow, in order to perform a rapid seismic risk assessment of bridges with limited information about the structure (e.g. in the case of missing blueprints). Merely starting from the age of construction and the obtained geometrical feature it is possible to achieve the first level of knowledge of the bridge's condition. Nowadays, as already discussed, infrastructure maintenance is a huge problem in western countries, and the possibility to gather an adequate level of knowledge of the bridges and viaduct structure represents a key point in the analysis, especially at a network level. Time and cost to acquire the necessary information are crucial factor in network analysis and this methodology, compared as discussed with traditional survey, drastically reduce the survey's time using relative low-cost equipment (as UAV). Moreover, with the standardise procedure, UAV pilot can perform the data acquisition on field (reducing costs of intervention), and the technician can analyse the data in the infrastructure control room. Also, real-time video transmission gives the possibility to perform remote inspection as a first-level analysis, without going on field. The standardise workflow allows the possibility to create a digital database and representation of the bridges and infrastructure on a Gis (Geographic Information System) also with the time dimension. The possibility to perform the planned flight and repeat future flight on the same path/trajectory, and to perform the inspection on a regular fixed time is also useful for the creation of a dynamic database with the same point of view.

The actual limitation in the application of the UAV aerial survey is represented by the incomplete and fragmented regulation (that should be unified in Europe in 2022 as presented) and in minor part the needs to refine the UAV autonomous navigation systems and makes this available at industrial/commercial level. Regulation, in this case, is fundamental to enable the full potential and application of this technology.

All these factors, makes this methodology, once overcome the actual limitation in terms of regulation and technical refinement, the perfect workflow for a massive amount of data and network application.

The main stakeholders for this methodology are represented by the infrastructure management company, both public and private that are interested in reducing time and cost of the intervention and needs to perform continuous monitoring and control to ensure a good level of knowledge of the structure. The use of the UAV system, in the future integrated into a mobile control room, will be useful to gather data and transmit these data in real-time in the control center.

Actually, experimentation is ongoing in Italy with one of the major private infrastructures managing company, and the final results will be object of future scientific research.

Improvements in the workflow are related to two different points: from one hand the improvements in terms of hardware in the UAV with autonomous navigation systems based on computer vision systems (Figure 175) and the integration in complete system drone-in-a-box solutions (Figure 176). The navigation systems will enable the possibility to follow precisely flight plan even in complex environment with the presence of vegetation and obstacles.

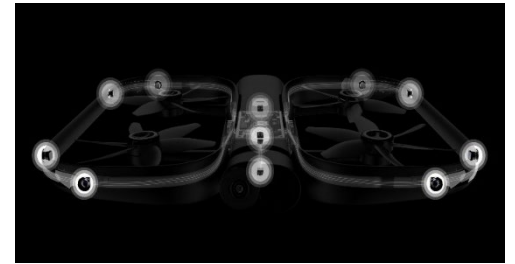


Figure 175 - Skydio autonomous UAV navigation based on Computer Vision Algorithms (source: Skydio)



Figure 176 - Airobotics hangar base for drone automation, Source Airobotics

From the other hand, the improvements in computer vision techniques can speed up the elaboration of the 3d model and the relative semantic point cloud segmentation. Also, the possibility to use real-time SFM-MVS to create a point cloud of the surveyed asset will reduce the time of the operation allowing the verification directly on field.

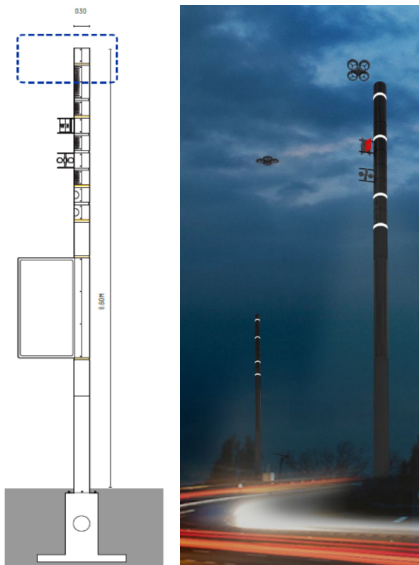


Figure 177 – Distributed drone base on Smart Road
(source: Anas)

Future perspectives, as a consequence of technological advancements, will allow the use of autonomous solutions (actually in experimentation or preliminary design) distributed on an infrastructure network to perform autonomous and remote monitoring and inspections (Figure 177, Figure 178).

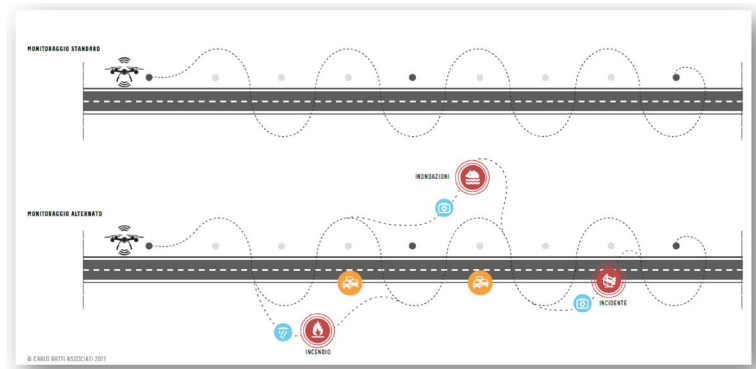


Figure 178 - Anas smart road drone stations on infrastructure